INTERFACE ENGINEERING STRATEGIES TO INDUCE MULTIFUNCTIONALITY IN CONVENTIONAL CARBON FIBER/EPOXY COMPOSITES

Doctoral Thesis

by

"ANKIT CHAUHAN"

(2017MEZ0004)

DEPARTMENT OF MECHANICAL ENGINEERING

INDIAN INSTITUTE OF TECHNOLOGY ROPAR

April, 2024

INTERFACE ENGINEERING STRATEGIES TO INDUCE MULTIFUNCTIONALITY IN CONVENTIONAL CARBON FIBER/EPOXY COMPOSITES

A Thesis Submitted
In Partial Fulfilment of the Requirements
for the Degree of

DOCTOR OF PHILOSOPHY

by

“ANKIT CHAUHAN”

(2017MEZ0004)

DEPARTMENT OF MECHANICAL ENGINEERING

INDIAN INSTITUTE OF TECHNOLOGY ROPAR

April, 2024

Ankit Chauhan: Interface engineering strategies to induce multifunctionality in conventional carbon fiber/epoxy composites

This thesis is dedicated to the energy

that bestowed me through these years

INDIAN INSTITUTE OF TECHNOLOGY ROPAR

CERTIFICATE

This is to certify that the thesis entitled "*Interface engineering strategies to induce multifunctionality in conventional carbon fiber/epoxy composites*" submitted by Ankit Chauhan to the Department of Mechanical Engineering, Indian Institute of Technology Ropar for the award of the degree of Doctor of Philosophy is a record of bona fide research work carried out by him under our supervision.

The thesis has reached the standards fulfilling the requirements of the regulations relating to the degree. The work contained in this thesis has not been submitted to any other university or institute for the award of any degree or diploma.

Dr. Prabhat K. Agnihotri

Associate Professor,

Department of Mechanical Engineering

Indian Institute of Technology Ropar, India

INDIAN INSTITUTE OF TECHNOLOGY ROPAR

CANDIDATE'S DECLARATION

I, **Ankit Chauhan**, hereby declare that the work presented in the thesis, entitled "**Interface engineering strategies to induce multifunctionality in conventional carbon fiber/epoxy composites**" in partial fulfilment of the requirements for the award of the degree of **Doctor of Philosophy** and submitted to the Department of Mechanical Engineering, Indian Institute of Technology Ropar is an authentic record of my research work carried out by me under the supervision of Dr. Prabhat K. Agnihotri.

The matter presented in this thesis has not been submitted elsewhere for the award of any other degree of this Institute or any other University/Institute.

Ankit C

ANKIT CHAUHAN

Date:

(Signature of the candidate)

This is to certify that the above statement made by the candidate is correct to the best of my knowledge.

Dr. PRABHAT K. AGNIHOTRI

Supervisor

Department of Mechanical Engineering

Indian Institute of Technology Ropar

ACKNOWLEDGEMENTS

I would like to express my deepest gratitude to my supervisor Dr. Prabhat K. Agnihotri, for his invaluable guidance and encouragement throughout this research work. I thank him for bestowing overwhelming trust, cultivating independent thinking, and having time for those long research-related discussions whenever needed, despite their busy schedule. Their work ethics, sincerity, and humbleness will always be a source of inspiration throughout my life.

I warmly thank my Doctoral Committee members, Prof. Navin Kumar, Dr. Srikant Sekhar Padhee, Dr. T J Dhilip Kumar, and Dr. Naveen James for continuously monitoring the progress of work and providing valuable suggestions and encouragement. I would like to thank Dr. T J Dhilip and Dr. Avijit Goswami for sharing HPC facilities to perform MD simulations and providing the functionalized carbon fibers. I am thankful to Dr. Vishwajeet Mehandia for allowing me to perform the viscosity measurements. Moreover, I would like to extend my thanks for the invaluable guidance, in-depth suggestions, and sharing of knowledge to Prof. Sumit Basu (IIT Kanpur) and Prof. Nandini Gupta (IIT Kanpur). I am very thankful to the Indian Institute of Technology Ropar for providing the necessary infrastructure and financial support. I am also thankful to the Ministry of Human Resources and Development, Government of India, for providing the scholarship to conduct this research work.

I thank my colleagues, who have supported my work and stimulated my interest in research in various ways: Dr. Harpreet Singh Bedi, Dr. Beant Kaur Billing, Dr. Viney Ghai, Dr. Jasdeep Bhinder, Dr. Ankit Baranwal, Dr. Vishal Agarwal, Mr. Sudhendu Nath Tiwari, Mr. Vinay Kumar, Mr. Shiva Bansal, Mr. Devnarayan Dhiwar, Mr. Vaibhav Gupta, and Mr. Prakash Kumar. I like to thank my friends Neha Mehani, Vansha Kher, Aman Arora, Ridhima Verma, Radhika Raina, Gagan, and Prasoon Raj for their constant support and for making my time at IIT Ropar a truly memorable experience.

Finally, my deepest gratitude goes to my family for their constant love, patience, and support through all these years.

ABSTRACT

Carbon fiber reinforced plastics composites (CFRPs) are widely used in structural and space applications due to their superior properties such as high specific strength, high specific stiffness, good corrosion resistance, and low maintenance cost. However, the anisotropy in their average mechanical, electrical, and thermal properties poses a difficult challenge in designing CFRPs for next-generation advanced applications. Moreover, in most advanced structural applications, composites are no longer required as load-bearing members alone. For example, they should be able to resist lightning strikes and dissipate thermal energy in various applications. Thus, the CFRPs are expected to perform more functions than just bearing the structural loads. This necessitates inducing multifunctional characteristics in CFRPs. The key to achieving multifunctionality is to improve the electrical and thermal conductivities while maintaining the mechanical properties of conventional CFRPs.

The average mechanical, thermal, and electrical properties of CFRPs depend on their constituents i.e. carbon fiber and polymer matrix (epoxy here). Since, carbon fibers are usually good conductors, the poor electrical and thermal properties of CFRPs are primarily due to the insulating nature of the epoxy matrix and interfacial thermal and electrical resistance at the fiber/matrix interface. Among several possible strategies, chemical modification of fiber surface is a well-proved approach to improve the interfacial properties in CFRPs. Molecular dynamics (MD) is a suitable tool to probe the interface and hence qualitatively as well as quantitatively reveal the molecular level mechanisms that operate at the fiber/matrix interface. This will help in identifying suitable strategies to optimally functionalize the carbon fiber/epoxy interface. The present thesis aims to propose suitable design and fabrication routes to process multifunctional CFRPs for advanced structural applications.

To achieve the objectives, MD simulations are performed to investigate the effect of functionalization on the interfacial thermal conductivity of carbon fiber/epoxy composites. Various functional groups, including small ones like carboxylic and amine as well as larger ones like aniline, single-chain para-amine surface grafted molecules (SGM), and double-chain meta-amine SGM are attached to the carbon fiber surface. The degree of functionalization is varied to gain insights into the underlying mechanisms that govern interfacial thermal conductivity. MD simulations show that suitable functionalization increases the interfacial thermal conductivity $\left(K_{\mathrm{i}}^{\mathrm{f}}\right)$ by up to ~ 25 times. A relatively higher improvement in interfacial thermal conductivity is observed with larger functional groups. This is due to the fact that larger molecules exhibit more

vigorous fluctuations in their end-to-end distances. Also, K_i^f does not seem to depend strongly on the degree of functionalization (*f*) beyond 5% *f* in most cases. An exception is, single-chain para-amine SGM which shows increasing improvement with *f*.

Next, MD simulations are carried out to explore whether same functional group would be effective in increasing interfacial shear response in carbon fiber/epoxy system. To this end, microbond test is modelled in MD simulations. MD simulations predict that functionalization of carbon fiber may lead to ~ 12 times improvement in interfacial shear strength (IFSS) as compared to unfunctionalized carbon fiber/epoxy composite. Moreover, large functional groups are more effective in improving the IFSS. The interfacial failure mechanics seem to depend on the length of the functional group. The failure in carbon fiber with an aniline functionalized carbon fiber/epoxy system is confined to epoxy molecules only. Breaking of bonds within the functional groups is recorded in case of single-chain para-amine and double-chain meta-amine SGM functionalized carbon fiber/epoxy system.

In the next part, an experimental investigation is carried out to find the electrical percolation threshold of multi-walled carbon nanotubes (CNTs) in the CNT modified epoxy (CNT/Ep) nanocomposites. Varying concentration of CNTs filler (0.5 – 3 wt.%) is used to fabricate the CNT/Ep nanocomposites. The percolation threshold is found to be 0.1 wt.%. A sudden jump in the electrical conductivity by factor of ~ 10^9 at 0.1 wt.% CNT as compared to neat epoxy (Ep) suggests the formation of a percolating network of CNTs within the epoxy. Fracture toughness tests reveal that the maximum improvement is obtained at 1 wt. % CNTs which is 61% higher as compared to neat epoxy. This suggests that 1 wt.% CNTs are optimum to improve the electrical and mechanical properties of CNT/Ep nanocomposites.

To verify the predictions from MD simulations, an optimum aniline functional group that allows only cohesive failure in epoxy is synthesized. Later, carbon fiber surface is functionalized with the aniline. Microbond tests are performed to evaluate the interfacial shear strength (IFSS) of the fiber/matrix interface as a function of fiber (unfunctionalized and functionalized) and matrix (Ep and CNT/Ep) combinations. Functionalization of carbon fiber with anilines shows IFSS of 37.6 ± 3.3 MPa which is 149% higher as compared to unfunctionalized carbon fiber (15.1 ± 1.7 MPa). Moreover, the IFSS of the aniline functionalized carbon fiber/CNT/Ep system is found to be higher than the aniline functionalized carbon fiber/Ep composites. Fractography analysis of tested samples shows that different failure mechanisms operate in unfunctionalized and functionalized carbon fiber/epoxy composites. Moreover, the strengthening of epoxy due to the addition of CNTs helps in improving the IFSS in CNT/Ep composites. It is envisaged that

harnessing the synergistic effects of carbon fiber functionalization and CNTs modified epoxy should provide multifunctionality to conventional carbon fiber reinforced plastics (CFRPs) with enhanced thermal, electrical, and mechanical properties for structural applications.

Keywords: Carbon fiber, epoxy, interfacial thermal conductivity, functional group, functionalization, molecular dynamics simulation, carbon nanotubes, electrical conductivity, fracture toughness, interfacial shear strength, microbond test, composite.

Content

LIST OF TABLES

LIST OF FIGURES

ABBREVIATIONS

CFRPs	Carbon fiber reinforced plastics composites
MD	Molecular dynamics
SGM	Surface grafted molecules
CNTs	Carbon nanotubes
wt. %	Weight percentage
IFSS	Interfacial shear strength
FRP	Fiber-reinforced plastics
EPON862	Diglycidyl ether of bisphenol F
DETDA	Diethyl toluene diamine
MWCNTs	Multi-walled carbon nanotubes
TGA	Thermogravimetric
XPS	X-ray Photoelectron spectroscopy
NMR	Nuclear magnetic resonance
LAMMPS	Large-scale Atomic/Molecular Massively Parallel Simulator
PCFF	Polymer consistent force field
PBC	Periodic boundary conditions
PPPM	Particle-particle-particle mesh
NVT	Constant number of particles, volume, and temperature
NPT	Constant number of particles, pressure, and temperature
NVE	Constant number of particles, volume, and energy
CF	Carbon fiber
ReaxFF	Reactive force field
S-SGM	Single-chain para-amine SGM
D-SGM	Double-chain meta-amine SGM
Ep	Neat epoxy
CNT/Ep	Carbon nanotube modified epoxy
SENB	Single-edge-notch bending

SYMBOLS

$K_{\mathrm{i}}^{\mathrm{f}}$	Interfacial thermal conductivity with functionalization
f	Degree of functionalization
K_{i}	Interfacial thermal conductivity without functionalization
τ_{IFSS}	Interfacial shear strength
L_{x}	Length in *X*-direction
L_{y}	Length in *Y*-direction
T	Temperature
t	Time
r_{c}	Cutoff distance
R1	Reactive atom of EPON862
R2	Reactive atom of DETDA/functional group
Q_{added}	Heat added to the hot slab
Q_{removed}	Heat removed from the old slab
q_{z}	Heat flux in the *Z*-direction
Q	Heat
A	Cross-sectional area
T_{j}	Average temperature of slab *j*
τ	Total time of MD simulation
N_{s}	number of atoms in the slab *j*
k_{B}	Boltzmann constant
m_l	Atomic mass of atom l
v_l	Instantaneous velocity of atom l
T_{ij}	$T_{\mathrm{j}} - T_{\mathrm{i}}$
Z_{23}	$Z_{\mathrm{i}} - Z_{\mathrm{i}}$
K_{cf}	Thermal conductivity of carbon fiber
K_{ep}	Thermal conductivity of epoxy
N_{g}	Number of graphene layers
K	Thermal conductivity
$X_{(\mathrm{i})}$	End-to-end vector
MSD	Mean squared displacement
t_1	Thickness of the unconstrained (or mobile) epoxy region

t_2	Thickness of the constrained (or fix) epoxy region
l_e	Embedded length
$\dot{u_X}$	Constant velocity
u_x	Pullout displacement in *X*-direction
$F_X(u_X)$	Force required to pull the fiber at u_X
$E(u_X)$	Total potential energy of the system at u_X
$E(0)$	Total potential energy of the system before pullout of fiber
ΔE_{vdW}	Change in van der Waals energy
ΔE	$E(u_X) - E(0)$
ΔE_{ref}	Pull-out energy for the reference case (epoxy/graphene system without functionalization)
ΔE_{amine}	Pull-out energy for the amine
$\Delta E_{aniline}$	Pull-out energy for the aniline
ΔE_{S-SGM}	Pull-out energy for the S-SGM
ΔE_{D-SGM}	Pull-out energy for the D-SGM
ΔE_{func}	Pull-out energy for the functionalized system
η	Viscosity
$\dot{\gamma}$	Shear rate
σ_{DC}	Direct current electrical conductivity
R	DC electrical resistance
B	thickness
K_{IC}	Critical stress intensity factor
W	Width
L	Length
S	Span length
a_n	Notched length
a_r	Natural crack length
a	Summation of notched and natural crack length
F_Q	Critical Load
δ	Chemical shifts
J	Coupling constants
s	Singlet
d	Doublet
F_{max}	Maximum debond force obtained during the microbond test

d	Diameter of carbon fiber

Chapter 1: Introduction

1.1 Multifunctional composites

Multifunctional composites are a class of composite materials that are designed to perform additional functions other than their primary role. For example, advanced structural applications necessitate composites to have non-structural functions such as energy storage, thermal management, lightning strike protection, and electromagnetic interference shielding, in addition to their role as a load bearing member [1–10]. They are being developed to reduce redundancy between subcomponents and functions and to improve the performance and efficiency of the overall system. Fiber-reinforced plastics (FRP) outperform traditional metallic materials due to their low weight, high modulus-to-weight ratio, high strength-to-weight ratio, and good corrosion resistance. These outstanding properties (see Table 1.1) make FRPs a substitute for metals in structural applications such as aerospace, space, automotive, etc. Among the FRPs, carbon fiber reinforced plastics (CFRPs) are preferred where performance and low weight are the primary concerns, not the cost. In today's Formula 1 race cars, CFRPs are extensively used in key components including the body, gearbox, chassis, interior, and suspension. For various sporting goods athletic shoes, tennis rackets, racing bicycles, or snow skis, CFRPs are used to make components as they provide better maneuvering and high speed due to their low weight, vibration damping, and high flexibility. Very low thermal coefficients of CFRPs provide thermal stability over a wide range of temperatures ranging from -100^{o}C to 100^{o}C in designing structures for space applications like space telescopes, satellites, spacecraft, etc [11]. The major structural applications of FRP are related to the commercial and military aircraft. With the usage of CFRPs nearly 5 – 6% in the 1980s, CFRPs contribute more than 50% by weight at present in both two major airplane manufacturers Boeing and Airbus (see Fig. 1.1) [12].

Table 1.1. Tensile properties of composites and metallic materials [11].

Material	Density, (g/cm^3)	Specific modulus, (10^6 m)	Specific tensile strength, (10^3 m)
High-modulus carbon fiber-epoxy matrix (unidirectional)	1.63	13.44	77.5
Boron fiber-6061 Al alloy matrix (annealed)	2.35	9.54	48.1
High-strength carbon fiber-epoxy matrix (unidirectional)	1.55	9.06	101.9
Kevlar 49 fiber-epoxy matrix (unidirectional)	1.38	5.6	101.8
Carbon fiber-epoxy matrix (quasi-isotropic)	1.55	2.99	38
SAE 1010 steel (cold-worked)	7.87	2.68	4.72
AISI 4340 steel (quenched and tempered)	7.87	2.68	22.3
6061-T6 aluminium alloy	2.7	2.6	11.7
7178-T6 aluminium alloy	2.7	2.6	22.9
INCO 718 nickel alloy (aged)	8.2	2.57	17.4
I7-7 PH stainless steel (aged)	7.87	2.54	21
Ti-6Al-4V titanium alloy (aged)	4.43	2.53	26.9
E-glass fiber-epoxy matrix (unidirectional)	1.85	2.16	53.2

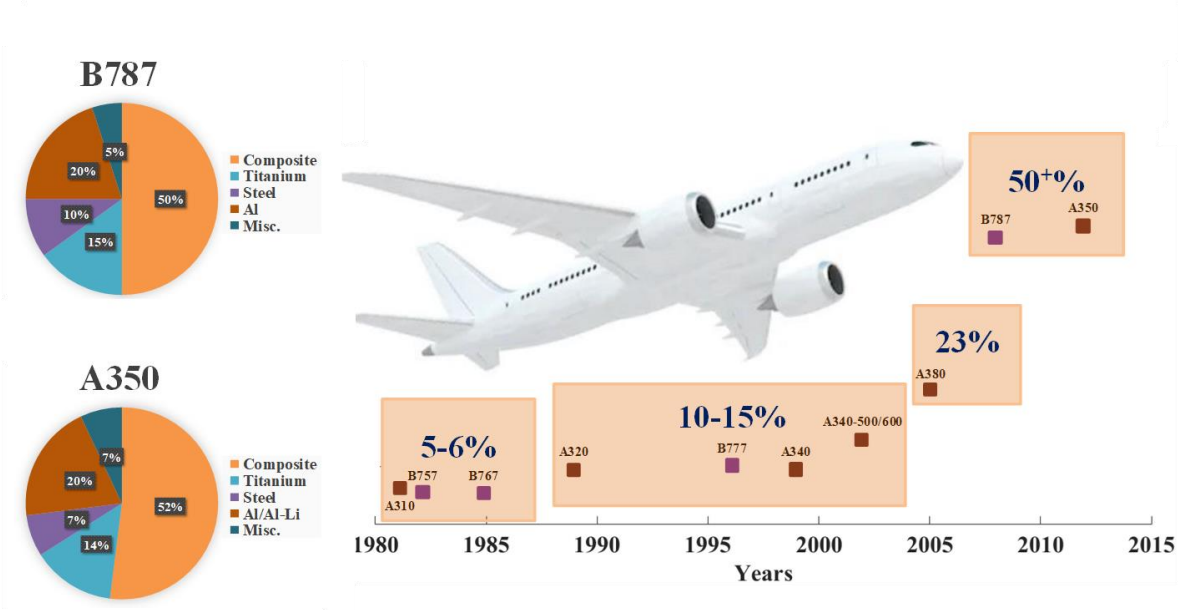

Figure 1.1. History of carbon fiber reinforced plastics (CFRPs) used by weight in major two airplane manufacturers Boeing and Airbus [13].

In advanced applications, CFRPs are expected to perform more functions other than bearing the structural loads alone. Composites must be able to resist lightning strikes, harmful electromagnetic radiation and dissipate thermal energy [12,14–18]. For example, in the aerospace industry, the current protection system consists of metal mesh attached to carbon fiber-reinforced plastics which increases the overall weight of aircraft and decreases fuel efficiency. Also, these heavy metallic structures induce the stresses in composite and weaken the structure [19,20]. Removing the metallic part from structures require inducing multifunctional characteristics in conventional CFRPs. One key aspect of inducing multifunctionality is to improve the electrical and thermal conductivities while maintaining the mechanical properties of conventional CFRPs. The present thesis aims at devising strategies to achieve this objective through a combined numerical and experimental approach.

1.2 State of the art

The anisotropy in their average mechanical, electrical, and thermal properties pose a difficult challenge in designing CFRPs for next-generation advanced applications [3,6,21,22]. CFRPs properties are governed by its basic constituents (fiber and matrix) and the interface between the fiber and matrix [23]. Conventional CFRPs have better in-plane electrical conductivity ranges of ~10^3-10^4 S/m due to the dominating nature of carbon fibers while out-of-plane properties are governed by insulating polymer layer between the two laminas. This reduces the electrical conductivity by about 10^{-4} times and the out-of-plane electrical conductivity of CFRPs ranges

from ~0.1 – 6 S/m. Due to the dominating nature of the polymer, CFRPs also show poor out-of-plane thermal conductivity ~ 0.1 W/m/K which is significantly lower than their in-plane thermal conductivity ~10 W/m/K [12,14,17,18,20,24,25]. In addition, the high electrical and thermal resistance at the fiber/matrix interface (interfacial electrical and thermal resistance) also contributes to the poor out-of-plane electrical and thermal properties of CFRPs. The poor out-of-plane properties of CFRPs makes them vulnerable and susceptible to damage that may occur due to harmful electromagnetic radiation and lightning strike [16,26]. Consequently, significant efforts have been made to improve the electrical and thermal properties of CFRPs [12,14,15,17,18,20,24,25,27–31].

One promising approach is the utilization of conductive nanofillers like carbon black, graphene, graphite, carbon nanotubes (CNTs), and carbon nanofibers [32–34] as second reinforcing fillers in conventional FRPs. Among these, the addition of CNTs is preferred due to their large aspect ratio, ability to form percolating conductive pathways at low concentrations, and excellent combination of mechanical, electrical, and thermal properties. The CNTs are introduced as second fillers in conventional composites to process multiscale composites [1,24,35,36]. The CNT-based polymer matrix multiscale composites have been prepared using two strategies. In the first approach, the CNTs are dispersed in a polymer matrix and later this modified matrix is used with fiber to manufacture multiscale composites [27,30]. CNTs are either directly grown or deposited on the surface of the fiber in the second approach [36,37]. The CNT-grafted fiber is impregnated with polymer matrix to process multiscale composites [20,24]. The out-of-plane electrical conductivity of CFRPs has shown significant improvement of 32% – 292% [27,28,30] and 30% – 1400% [20,24,25,29] using two strategies respectively. The addition of CNTs results in out-of-plane electrical conductivity values of CFRPs ranging from 0.9 – 8.9 S/m. The through-thickness electrical conductivity of the order of 10 S/m is desirable in FRPs for electromagnetic interference (EMI) shielding applications [14]. An exceptional value of 75 S/m is achieved [29] while improvement in thermal conductivity (< 15%) and interlaminar shear strength (< 27%) are either not reported or low in most of the studies [20,24,25,27,29,30,36,38].

It is to be noted here that the dispersion of CNTs in the polymer matrix [39–42] (first approach) augments the mechanical properties to a larger extent relative to the grafting of CNT on the fiber fabric [43] (second approach). Moreover, CNT grafting has other issues such as it is very difficult to ensure uniform growth of CNTs on the entire fabric [4], and the sample size is limited by the size of the reactor. Therefore, CNT dispersion to modify polymer is preferred over CNT grafting on the fiber fabric in this thesis.

The surface of carbon fiber is inert and does not form any covalent bond with the matrix [44–46]. This results into the poor interfacial interaction between fiber and matrix which limits the thermal, electrical, and mechanical properties to achieve multifunctionality in CFRPs [47–50]. Various strategies such as dip coating [51,52], nanoparticle grafting [53–55], thermal treatment [56,57], plasma treatment [58,59], high-energy irradiation [60,61], matrix modification [55,62–64], sizing [52,62,65] and chemical modification [66–74] have been implemented to increase the interfacial interaction between fiber and matrix. Among these, chemical modifications have shown significant improvement in interfacial interaction due to the mechanical interlocking and covalent bonding between functionalized fiber and polymer [61,66,70,71]. Not only this, the presence of functional groups at the interface is beneficial to tailor the electromagnetic interference shielding properties of composites [75–77]. It is expected that the chemical functionalization of fiber surface may also decrease the interfacial electrical and thermal resistance in composites. This may improve the average electrical and thermal conductivity of CFRPs.

1.3 Issues and proposed solutions

It is evident from the above discussion that introducing conductive fillers such as CNTs into conventional CFRPs is an effective approach to enhance the mechanical, electrical, and thermal properties of CFRPs.

Carbon fiber coated with ~ 0.25 wt. % CNTs using electrophoretic deposition technique are used to fabricate CNT modified CFRPs. The out-of-plane electrical conductivity increases by 30% along with 27% improvement in the interlaminar shear strength after CNT coating on the fiber [24]. In another study, reduced graphene oxide (0.12 wt. %) is used to coat the carbon fiber enhances the out-of-plane electrical conductivity of composites by 350% while 14% improvement is reported in the interlaminar shear strength [78]. Kostopoulos et al. [30] modified matrix with 0.1%, 0.5%, and 1 wt. % CNTs to prepare the composites. The out-of-plane electrical conductivity increases by 126%, 199%, and 292% corresponding to 0.1%, 0.5%, and 1 wt. % CNTs while thermal conductivity is not reported. Carbon fiber grafted with CNTs (2.24 wt. %) shows the improvement in the out-of-plane electrical conductivity by 230% while out-of-plane thermal conductivity increases by only 15% [20]. It is interesting to note that the relative improvement in electrical conductivity in modified composites is significantly higher than the thermal conductivity even at low filler concentrations. The improvement in the electrical conductivity is attributed to the formation of electrical percolating pathways that help charges to flow from one end to the other end. However, the lack of a thermally conducting pathway limits

the enhancement in thermal conductivity of modified composite system. This also highlights the fact that different mechanisms are responsible for electrical and thermal conductivity in composites. Additions of CNTs in the range of 0.1 wt.% to 1 wt.% into epoxy enhances the electrical conductivity by 8 orders of magnitude but improves thermal conductivity by 11% only [79]. Higher filler loadings (50 – 70 wt.%) is required for significant improvement in thermal conductivity [79–81]. However, it leads to decrease in mechanical properties and loss of processability due to the higher resin viscosity at such filler concentrations [80,81]. The lower increase in thermal conductivity is mainly due to higher interfacial thermal resistance at filler/filler and filler/matrix that can be alleviated by replacing the van der Waals interaction by strong covalent bonds [82]. The out-of-plane thermal conductivity improves by 65% due to the formation of continuous thermal conductivity pathways in functionalized carbon fiber polymer composite [50]. Apart from experimental studies, numerical tools are also used to optimize the constitution of composites [83]. MD simulations have been performed to study the interfacial thermal properties in carbon nanotube [84,85] or graphene [86–88] reinforced polymers but limited to small molecules only like formyl, carboxyl, amine, hydroxy, fluorine etc. [84–88]. The effect of carbon fiber functionalization on the interfacial thermal conductivity in CFRPs using MD simulations is rather limited [89].

In addition to the improvement in thermal properties, the efficacy of fiber functionalization approach is governed by effectiveness of functional groups in load transfer at fiber/matrix interface. The load sharing occurs in the form of interfacial shear stresses which are normally evaluated in terms of interfacial shear strength (IFSS) of the composite [90,91]. The presence of strong covalent bond at fiber/matrix interface contributes towards the structural integrity of composites and improves the interfacial strength by ~172% [66,92,93]. Accordingly, effect of functional groups on the interfacial shear stress response in composites is studied using MD simulations [66,67,92,94–98]. However, most of the studies are limited to functional groups that do not react with polymer [94,96–98]. Recently, large molecules capable of forming covalent bond with epoxy are considered in MD simulations to predict the IFSS [66,67,95].

In spite of these advances, the interfacial failure mechanisms that act in unsized and functionalized carbon fiber/epoxy systems are not well understood. Which type of functional group, small or large is better suited and why? What is the optimum degree of functionalization (f)? How does the interfacial failure depend on the chemistry at the interface? Is it possible that certain functional groups may simultaneously enhance the interfacial strength as well as interfacial thermal and electrical conductivity? These are a few key questions that have motivated the research work carried out in this thesis. It is envisaged that this will help in identifying suitable

strategies to optimally functionalize the carbon fiber/epoxy interfaces.

The study of relevant literature shows that the dispersion of conducting fillers such as carbon black, graphene, graphite, carbon nanotubes (CNTs), and carbon nanofibers improves the electrical and thermal conductivity of epoxy. Among these, the addition of CNTs is preferred in this thesis due to their large aspect ratio, ability to form percolating conductive pathways at low concentrations, and excellent combination of mechanical, electrical, and thermal properties. It will be interesting to see if is it possible to harness the synergetic effects of carbon fiber functionalization and CNT modified epoxy to improve the thermal, electrical, and interfacial strength of conventional carbon fiber/epoxy composites.

1.4 Objectives

The present thesis aims to propose suitable design and fabrication routes to process multifunctional CFRPs for advanced structural applications (see Figure 1.2). The objectives of the present thesis are defined as,

1. To identify the optimum functional group and degree of functionalization (*f*) to improve the interfacial thermal conductivity (K_{i}) of carbon fiber/epoxy interface using molecular dynamic simulations.
2. To identify the optimum functional group and degree of functionalization (*f*) to improve the interfacial shear strength (τ_{IFSS}) of carbon fiber/epoxy interface using molecular dynamic simulations.
3. To improve the electrical and mechanical properties of epoxy using carbon nanotubes (CNTs).
4. To harness the synergetic effects of carbon fiber functionalization and CNT modified epoxy in CFRPs.

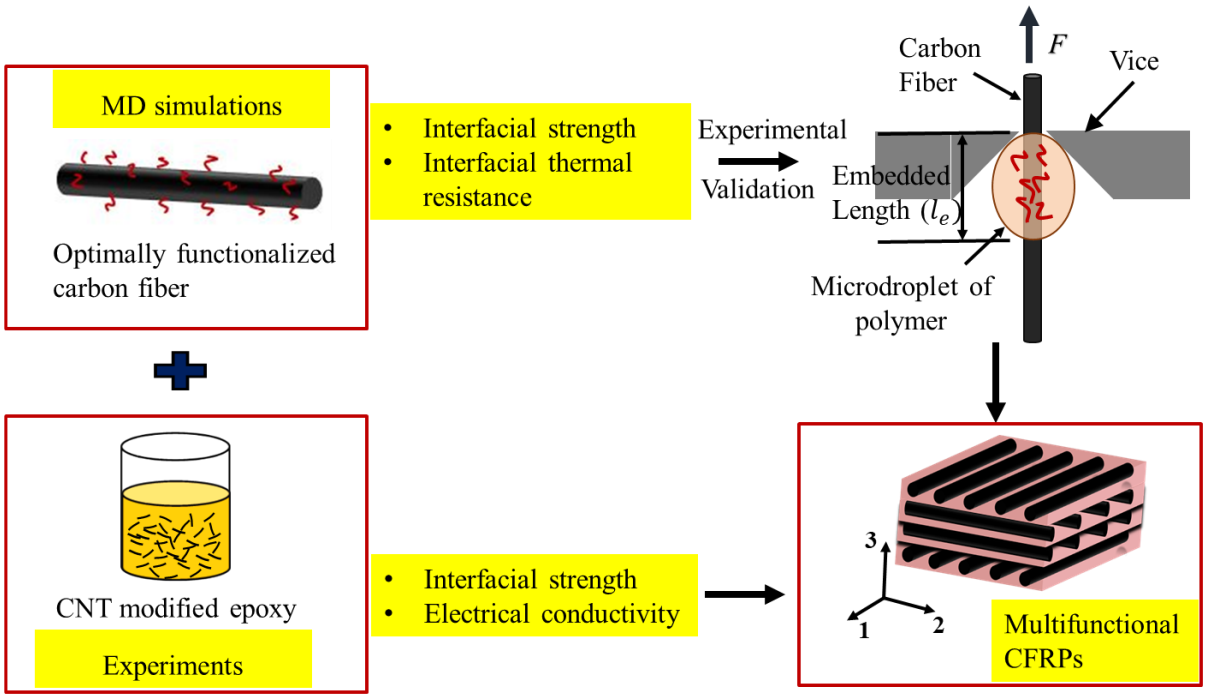

Figure 1.2. Steps followed to achieve the objectives of the present thesis.

1.5 Organization of the thesis

The research work performed in the present thesis is organized into seven chapters. A chapter-wise breakup of the thesis work is as follows,

Chapter 1: Introduction

Chapter 1 provides the introduction of composites for structural applications and the motivation of the present study. Subsequently, the need for multifunctionality in composites is explained. The state-of-the-art design and development strategies proposed in the literature for multifunctional composites are discussed. Based on the literature data, the research gaps are identified and the objectives of the present study are outlined.

Chapter 2: Materials and methods

Chapter 2 summarizes various materials, chemicals, processing routes, and characterization techniques used in the present study.

Chapter 3: Molecular dynamic study on modulating the interfacial thermal conductivity of carbon fiber/epoxy interfaces

The effect of functionalization on the interfacial thermal conductivity of carbon fiber/epoxy interfaces using molecular dynamics (MD) simulations is presented in **Chapter 3**. In MD simulations, while carbon fiber is modelled with 10 graphene layers, diglycidyl ether of bisphenol

F (EPON862) and diethyl toluene diamine (DETDA) are used as epoxy resin and the crosslinker respectively. Carbon fiber is functionalized with various chemical groups (carboxylic, amine, aniline, single-chain para-amine SGM, and double-chain meta-amine SGM). The degree of functionalization is varied to gain better insights into the underlying mechanisms that govern interfacial thermal conductivity. Based on the predictions of the MD simulations, the optimal functional group is identified to process CFRPs with improved thermal conductivity.

Chapter 4: Molecular dynamic study on modulating the interfacial interactions of carbon fiber/epoxy interfaces

Chapter 4 characterizes the effect of carbon fiber functionalization on the interfacial shear response of carbon fiber/epoxy composites. The MD model developed in Chapter 3 is extended to perform microbond MD simulations. Displacement boundary conditions are imposed to pullout graphene layer from epoxy matrix. The IFSS of carbon fiber/epoxy system is compared for unfunctionalized and functionalized cases. Chemical group that can simultaneously improve the interfacial thermal conductivity and interfacial strength are identified. It is observed that the type of interfacial failure strongly depends on the interfacial chemistry at graphene/epoxy interface.

Chapter 5: Study of electrical and mechanical properties of CNT/epoxy nanocomposites

Apart from thermal conductivity and interfacial strength, improving electrical conductivity of insulating epoxy matrix is another major objective of the present thesis. **Chapter 5** presents the percolation analysis of carbon nanotube (CNT) modified epoxy matrix. It is necessary to determine the optimum loading of CNTs as they tend to agglomerate at higher concentrations in epoxy. Moreover, the viscosity of epoxy increases with the addition of CNTs. This may lead to poor wetting of carbon fiber with epoxy and hence weaker properties of CFRPs. Optimum concentration of CNTs is obtained through rigorous electrical measurements, fracture testing, and viscosity measurements of CNT/epoxy nanocomposites.

Chapter 6: Synergetic effects of carbon fiber functionalization and CNT modified epoxy on the interfacial shear strength of carbon fiber/epoxy composites

The experimental verification of MD simulations predictions is carried out in **Chapter 6**. Microbond tests are performed for various fiber (functionalized and unfunctionalized) and matrix (neat epoxy and CNT modified epoxy) combinations. The IFSS of different material combinations is evaluated from the experimental data. The functionalization of carbon fiber indeed improves the interfacial shear strength of carbon fiber/epoxy composites. Moreover, the synergistic effects of fiber functionalization and matrix modification significantly improve the

interfacial strength of CFRPs. Fractography of tested samples reveals that the interfacial failure mechanisms vary with the interfacial chemistry in CFRPs.

Chapter 7: Conclusions and future scope

The key findings of the present study are summarized in **Chapter 7**. Possible future directions of the present work are also presented in this chapter.

Chapter 2: Materials and methods

2.1 Materials

The details and specifications of the materials used in the present thesis are described below.

2.1.1 Polymers

Epoxy is a thermoset polymer that consists of two parts: epoxy resin (EPOFINE – 556) and hardener (FINEHARD – 5200). The epoxy resin and hardener are purchased from the Fine Finish Organics Pvt. Ltd. The characteristics of epoxy is mentioned in Table 2.1.

Table 2.1. Characteristics of epoxy resin and hardener polymers.

Characteristic	Unit	Epoxy resin	Hardener
Density at 25 ^{o}C	g/cc	1.15 – 1.20	0.99 – 1.02
Flash point	^{o}C	> 200	> 120
Storage life	Years	1	1

2.1.2 Carbon nanotubes

Multi-walled carbon nanotubes (MWCNTs) (Product specification, CAS 308068-56-6) are purchased from Nano Research Elements, India. All the specifications of carbon nanotubes (CNTs) are listed in Table 2.2.

Table 2.2. Specifications of carbon nanotubes (CNTs).

Specifications	Unit	CNTs
Outer diameter	nm	10–30
Average length	µm	3–10
Specific surface area	m^2/g	200
Tap density	g/cm^3	0.28
True density	g/cm^3	2.1
Electrical conductivity	S/cm	> 100

Thermal conductivity	W/(m.K)	> 3000

2.1.3 Carbon fiber and chemicals

Carbon fibers (230 GSM, density 1.8 g/cc, average modulus 100 GPa) are purchased from Hindustan Technical Fabrics, India. Initially, carbon fibers have a sizing layer named as received carbon fiber. Carbon fibers are heated in the chemical vapour deposition at 650 ^{o}C for 15 minutes under inert nitrogen gas to complete removal of sizing named as unsized carbon fiber. All the chemicals are procured from TCI, India.

2.2 Sample preparation

In this section, the preparation of CNT/epoxy nanocomposites, aniline functionalized carbon fiber, and single fiber/matrix composite are discussed.

2.2.1 Preparation of nanocomposites

CNT/epoxy nanocomposites are prepared using different wt.% of CNTs i.e., 0.05, 0.1, 0.3, 0.5, 1,1.5, 2 and 3. For each type of nanocomposites, CNTs are dispersed into the epoxy resin and hardener in equal proportion (100:24) using an ultrasonic probe sonicator (750 W, 20 kHz, probe tip 13 mm, Cole-Parmer, USA) at 50% amplitude for 2 hours keeping maximum temperature less than 70 ^{o}C. Then, dispersed solutions are mixed using a glass rod and poured into the mold to prepare the CNT/epoxy nanocomposites followed by a curing cycle of 80 ^{o}C for 6 hours, 120 ^{o}C for 2 hours, and 160 ^{o}C for 6 hours.

2.2.2 Aniline functionalized carbon fiber

Firstly, the carbon fiber received from the manufacturer is heated at 600 ^{o}C for 15 minutes under inert argon gas in the chemical vapor deposition to remove the sizing layer to get graphite structure at the outer surface of the carbon fiber named unsized carbon fiber. One end of amine in benzene-1,4-diamine is protected with a trifluoroacetyl group followed by attachment of the synthesized functional group to form a covalent bond with unsized carbon fiber using a diazonium reaction. Later, the fiber is acidic washed to remove the trifluoroacetyl protected group to give free amine named aniline-carbon fiber.

2.2.3 Single fiber/matrix composite

Single fiber/matrix composite is prepared by pouring a drop of matrix onto a single carbon fiber filament extracted from a carbon fiber tow. As the drop makes contact with the fiber it

disintegrates into the multiple microdroplets. Thereafter, these microdroplets are subjected to a curing cycle of 80 ^{o}C for 6 hours, 120 ^{o}C for 2 hours, and 160 ^{o}C for 6 hours to prepare a single fiber/matrix composite.

2.3 Characterization

Electrical conductivity test to find the electrical percolation threshold for CNT/Ep nanocomposites is performed using IM3523 HIOKI LCR meter, Japan at a constant voltage of 2V using the two electrodes method. The viscosity behavior at different shear rates is done by using the rheometer (Anton Paar, MCR 702, Austria). Fracture toughness test is performed using single-edge-notch-bending (SENB) configuration under a three-point setup on a universal testing machine (Shimadzu Corp., Japan) as per ASTM D5045-14. Fractography analysis is carried out using field emission scanning electron microscopy (FESEM, JEOL, JSM-7610F, Japan). Thermogravimetric (TGA/DSC 1 STARe SYSTEM, Mettler Toledo), X-ray photoelectron spectroscopy (XPS, Excalab 250Xi, Thermo Fisher Scientific), and Nuclear magnetic resonance (NMR) spectra (JEOL JNM-ECS spectrometer, Japan) are the characterization techniques used in the present thesis.

Chapter 3: Molecular dynamic study on modulating the interfacial thermal conductivity of carbon fiber/epoxy interfaces

It is discussed in chapter 1 that the chemical modification of fiber surface is a promising approach to enhance the interfacial properties between the fiber and the polymer matrix. However, determining the 'right ligand' to achieve this objective is a difficult problem. In this chapter, molecular dynamics (MD) simulations are performed to characterize the effect of different chemical ligands on the interfacial thermal conductivity (K_i) of carbon fiber/epoxy composites. The carbon fiber is modeled as graphene layers, diglycidyl ether of bisphenol F (EPON862) and diethyl toluene diamine (DETDA) are used as epoxy and crosslinker in MD simulations. The carbon fiber is functionalized with different types of small (amine and carboxylic) and large (aniline, single-chain para-amine surface grafted molecules (SGM), and double-chain meta-amine SGM) functional groups with varying degrees of functionalization.

3.1 Introduction

Carbon fiber reinforced plastics composites (CFRPs) are increasingly used in aerospace and space applications due to their high specific strength, high specific stiffness, and good corrosion resistance [12,18,20]. However, the anisotropic nature of their average mechanical, electrical and thermal properties poses a difficult challenge in designing CFRPs for next-generation advanced space applications. While CFRPs have fiber-dominated better in-plane thermal conductivity of ~ 10 W/m.K, they have a very poor out-of-plane thermal conductivity of about ~ 1 W/m.K [14,15,18,20,31]. The lower out-of-plane thermal properties of CFRPs make them susceptible to damage due to inefficient heat dissipation under high thermal load.

The average thermal properties of CFRPs depend on their constituents (fiber and matrix) and the interface between the fiber and the polymer matrix [23]. While carbon fiber is thermally conductive, the insulating nature of the matrix is primarily responsible for the poor out-of-plane thermal conductivity of CFRPs. In addition, the high thermal resistance at the fiber/matrix interface also contributes to the poor out-of-plane thermal properties of CFRPs. Various nanofillers such as carbon nanotubes [99–101], graphene [79,102], and metallic nanoparticles [103–105] have been used to improve the thermal conductivity of the polymer matrix. Unfortunately, the addition of nanofillers introduces an interphase region at the nanofiller/matrix interface. This leads to a significant increase in interfacial thermal resistance and thus the relative

improvement in thermal properties of polymer matrix and CFRPs after the addition of nanofillers is less than expected. Alternate approaches to improve the average thermal properties of CFRPs by modifying the surface of the carbon fiber by desizing, dip coating, spray coating, chemical modification, high-energy irradiation, plasma treatment, and thermal treatment have also been explored [23,29,106,107]. Chemical modifications, namely the presence of functional groups such as hydroxyl, carboxyl, amines (as well as more specialized macromolecules like poly-*p*-phenylene benzobisoxazole, see [50]) are reported to reduce the interfacial thermal resistance [66,86,87,94,108–110]. Even though efforts have been made to functionalize fiber surfaces with different ligands (some of which are shown in Fig. 3.1), there are still many questions that remain. We attempt to rank a few functional groups based on their effectiveness in reducing the interfacial thermal resistance in a carbon-epoxy system.

Earlier, MD simulations have been used to study the interfacial thermal properties in carbon nanotube [84,85] or graphene [86–88] reinforced polymers. However, to the best of our knowledge very few reports on the effect of carbon fiber functionalization on the interfacial thermal conductivity in CFRPs using MD simulations exist [89]. To this end, we have considered various functional groups with varying chemical structure, backbone length and reactivity with epoxy, including small ones like carboxylic and amine as well as larger ones like aniline, single-chain para-amine surface grafted molecules (SGM), and double-chain meta-amine SGM. The degree of functionalization is also varied to gain better insights into the underlying mechanisms which govern interfacial thermal conductivity.

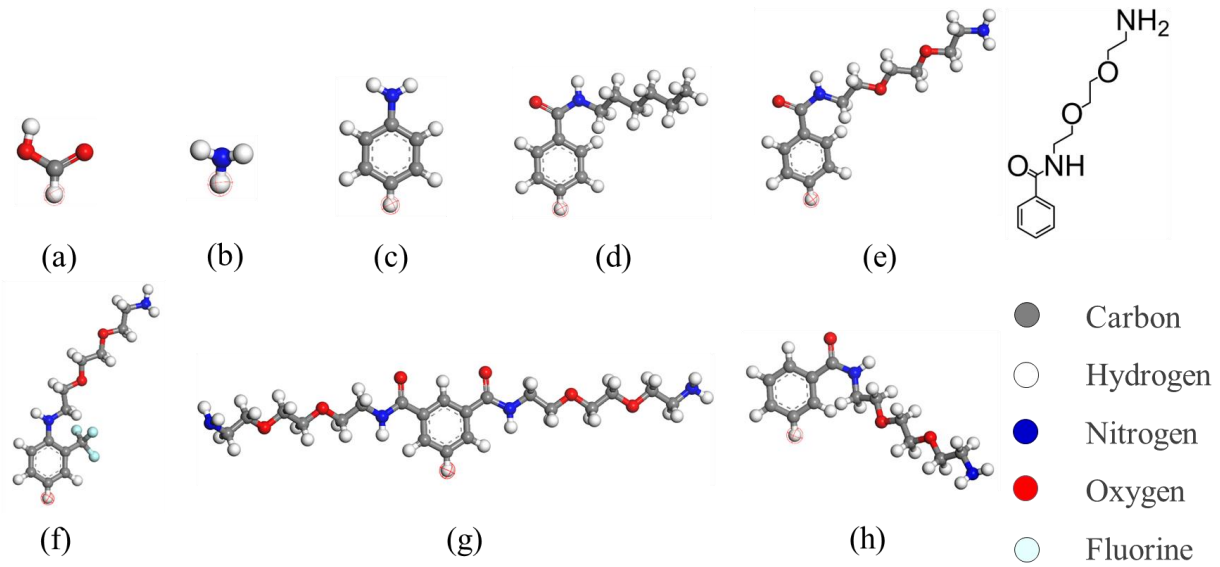

Figure 3.1. Chemical structure of commonly used functional groups (a) carboxyl, (b) amine, (c) aniline, (d) lipophilic amide, (e) single-chain para-amine, (f) single chain para-amine with meta

trifluoromethyl, (g) double-chain meta-amine, and (h) single chain meta-amine SGM [66,67,88,92,95]. (a) – (c), (e) and (g) are considered in our MD simulation.

3.2 Computational details

3.2.1 MD model

The initial atomistic model is prepared using Material studio 18.1 [111]. Subsequent MD simulations are performed using the Large-scale Atomic/Molecular Massively Parallel Simulator (LAMMPS) package [112]. Figure 3.2(a) schematically describes the numerical model of a single carbon fiber embedded in epoxy matrix used in MD simulations. To model the interface region between the fiber and epoxy, the model in Fig. 3.2(b) is used. Here, 10 graphene layers with a spacing of 3.35 Å [95] are placed in a simulation box with length of 148 Å in the *Z*-direction. Unless otherwise stated, the cross-sectional dimensions used are L_x = 38.4 Å and L_y = 39.4 Å.

The diglycidyl ether of bisphenol F (EPON862) and diethyl toluene diamine (DETDA) (Fig. 3.2(b)) represent the epoxy resin and crosslinker (curing agent) in the MD model. Using Amorphous Module in Material Studio 18.1, EPON862 and DETDA are packed in a stoichiometric ratio of 2:1 in the volume adjacent to the graphene layers at a density of 1.2 g/cm^3 the experimentally measured density of the polymer [113]. Figure 3.2(c) show a typical system after packing of epoxy in the simulation box.

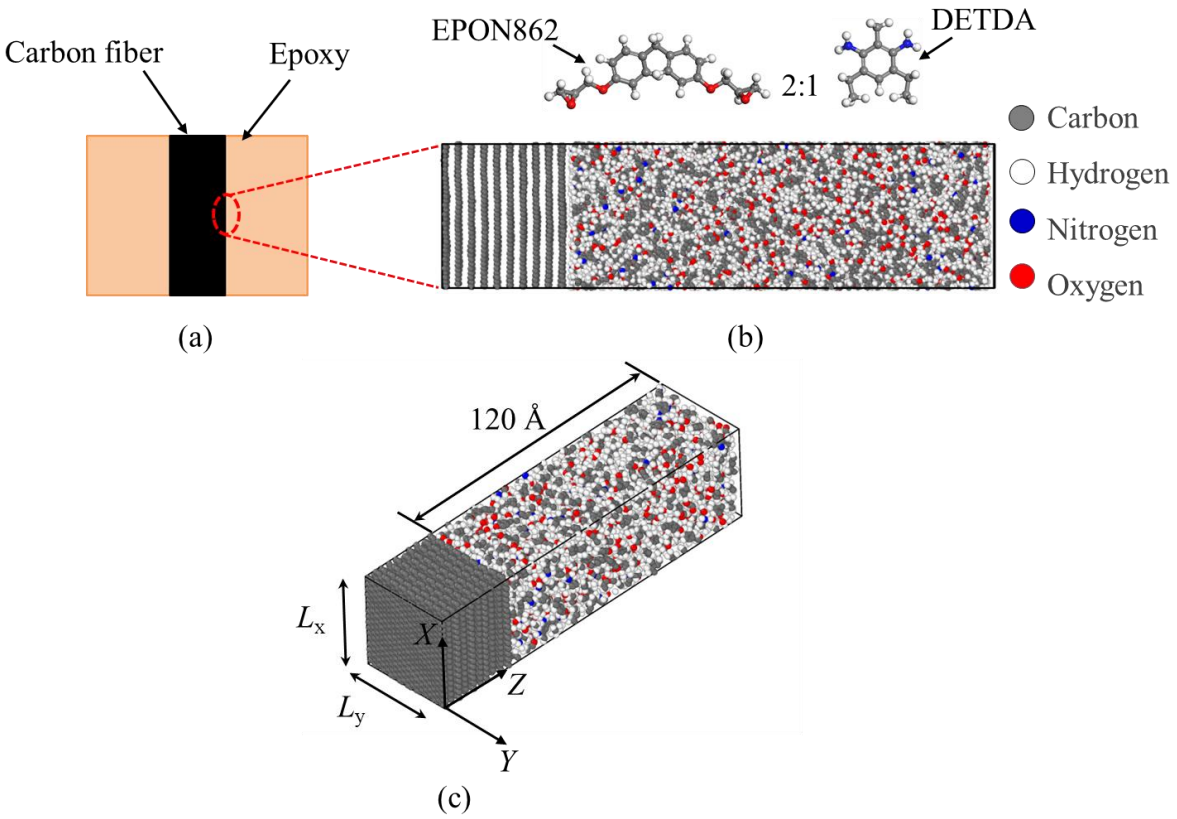

Figure 3.2. (a) Schematic of a single carbon fiber/epoxy composite. (b) Carbon/epoxy MD system where ten graphene layers are used to model the carbon fiber. Diglycidyl ether of bisphenol F (EPON862), and diethyl toluene diamine (DETDA) represent epoxy resin and crosslinker in MD simulations. Finally, a typical carbon/epoxy system is shown in (c).

3.2.2 MD simulation details

We have used the polymer consistent force field (PCFF) for all simulations conducted in LAMMPS [114]. Periodic boundary conditions (PBC) are implemented in all the directions of the simulation box. The temperature and pressure of the system are controlled via Nose-Hoover thermostat [115,116] and Berendsen barostat respectively[117]. A velocity-Verlet algorithm is implemented to integrate the equation of motion with a timestep of 1 fs. The cut-off for van der Waals interactions is taken as 10 Å and a 0.5 Å tail correction is applied to avoid the discontinuities in energy and pressure [118]. Particle-particle-particle mesh (PPPM) algorithm is implemented to include the long-range Coulomb interactions with energy accuracy of 0.001 Kcal/mol. All the MD simulations are performed using the Forcite module in Material Studio 18.1 unless specified otherwise.

After packing, the carbon/epoxy system will have overlapping atoms. To remove these unwanted interactions, energy minimization is carried out via a combination of steepest descent, adjusted

basis set Newton-Raphson, and quasi-Newton methods with an accuracy of 0.001 kcal/mol and 0.5 kcal/mol/Å in energy and force, respectively [119]. The systems are then subjected to anneal cycle with a timestep of 0.25 fs as shown in Fig. 3.3 to avoid the local inhomogeneity [119,120].

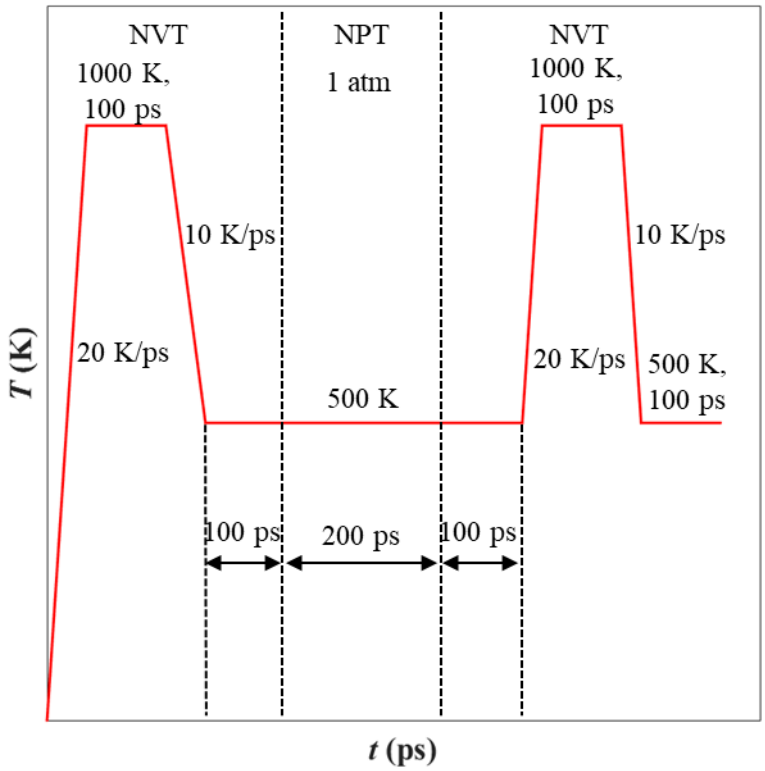

Figure 3.3. Temperature variation in the anneal cycle used to the carbon – epoxy systems.

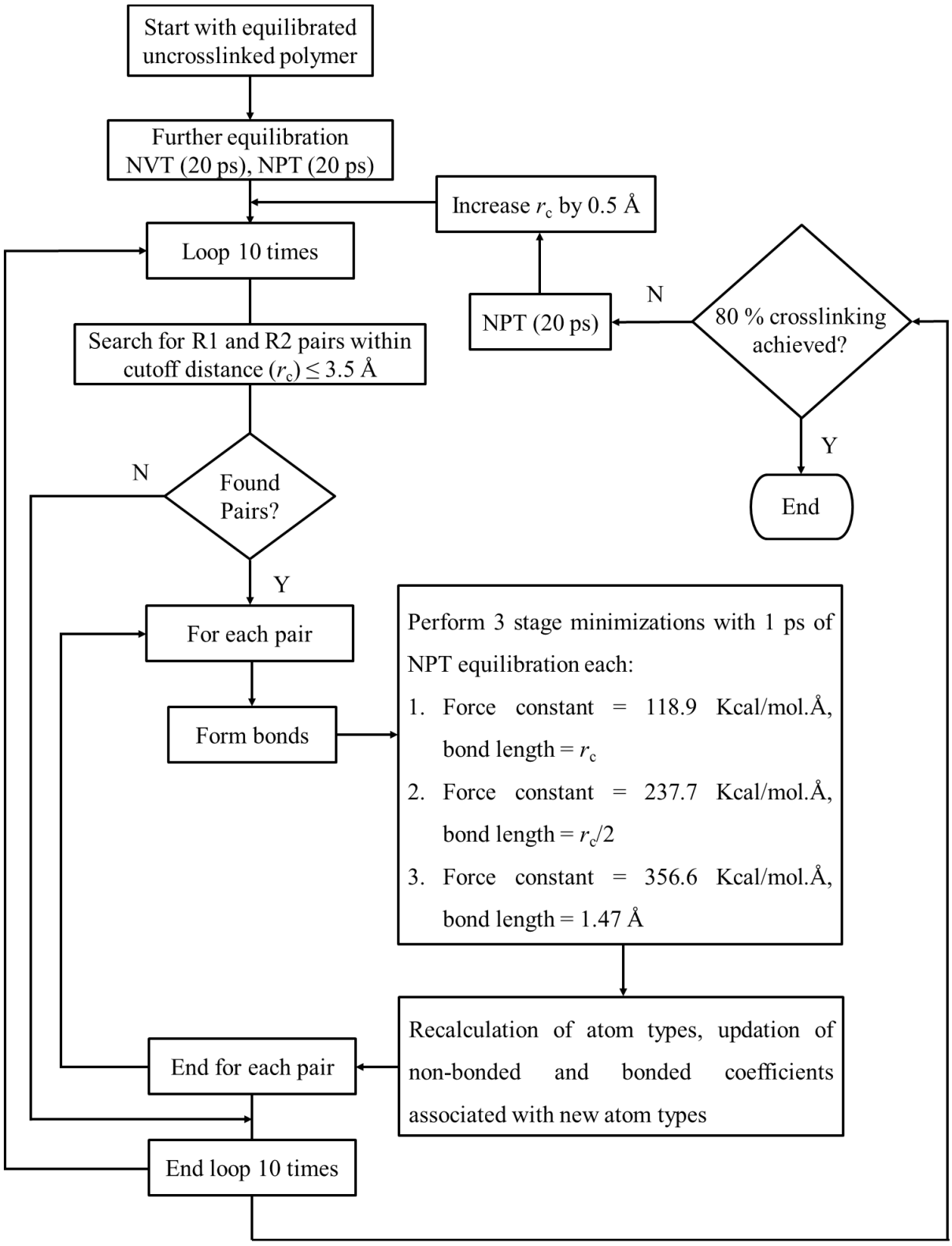

Figure 3.4. Flowchart describing the steps used in crosslinking of EPON862 and DETDA.

After annealing, crosslinking between EPON862 and DETDA molecules is allowed in MD simulations following the strategy depicted in Fig. 3.4. Note that, in case functional groups are attached to the graphene, R2 can be on the functional group as well. This is the atom that connects to the open epoxide ring in Figs. 3.5(b) and (c). In all functional groups shown in Fig. 3.1, R2 is

a nitrogen atom. The only exception is the carboxyl group, where R2 is an oxygen that is part of the hydroxyl group.

In all cases, reported here, 80% crosslinking is achieved. This also seems to be the extent of crosslinking achieved in thermoset over time [120]. After achieving 80% crosslinking, the MD system is further equilibrated under NPT ensemble for 500 ps at 300 K and 1 atm to attain the requisite density of 1.099 ± 0.002 g/cm^3.

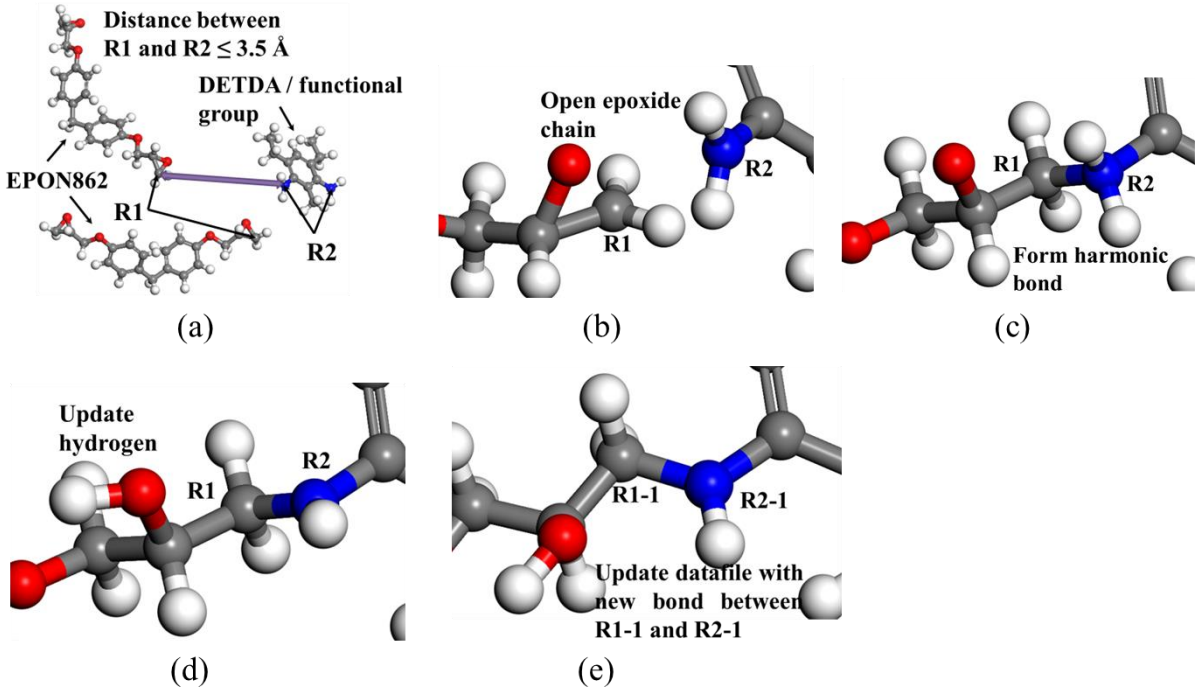

Figure 3.5. Different steps involved in crosslinking between EPON862 and DETDA.

3.2.3 Determining thermal conductivities

Figure 3.6 shows the methodology implemented to investigate thermal conductivities of the carbon/epoxy interface and bulk epoxy. Periodic boundary conditions are imposed in the *X* and *Y* directions only. Adiabatic slabs at both the ends of simulation box are created by insulating one graphene layer at each end as shown in Fig. 3.6. Thermal gradient across the length of the simulation box is defined by maintaining the temperature of hot slab (two graphene layers next to the insulated graphene layer) at 350 K and cold slab (a region of 5 Å width adjacent to the bin at the other end) at 250 K. The temperatures of the hot and cold slabs are kept constant by continuously adding and removing energy from them using Nose-Hoover thermostats. The rate of heat added to the hot slab Q_{added}, (removed from the cold slab $Q_{removed}$) in order to maintain its temperature constant, is monitored. At steady state, we should expect $Q_{added} = Q_{removed} = Q$. Consequently, the heat flux in the *Z*-direction is

$$q_z = \frac{Q}{A}, \tag{3.1}$$

where $A = L_x \times L_y$ is the cross-sectional area. An NVE ensemble is used for the rest of the system in the MD simulations.

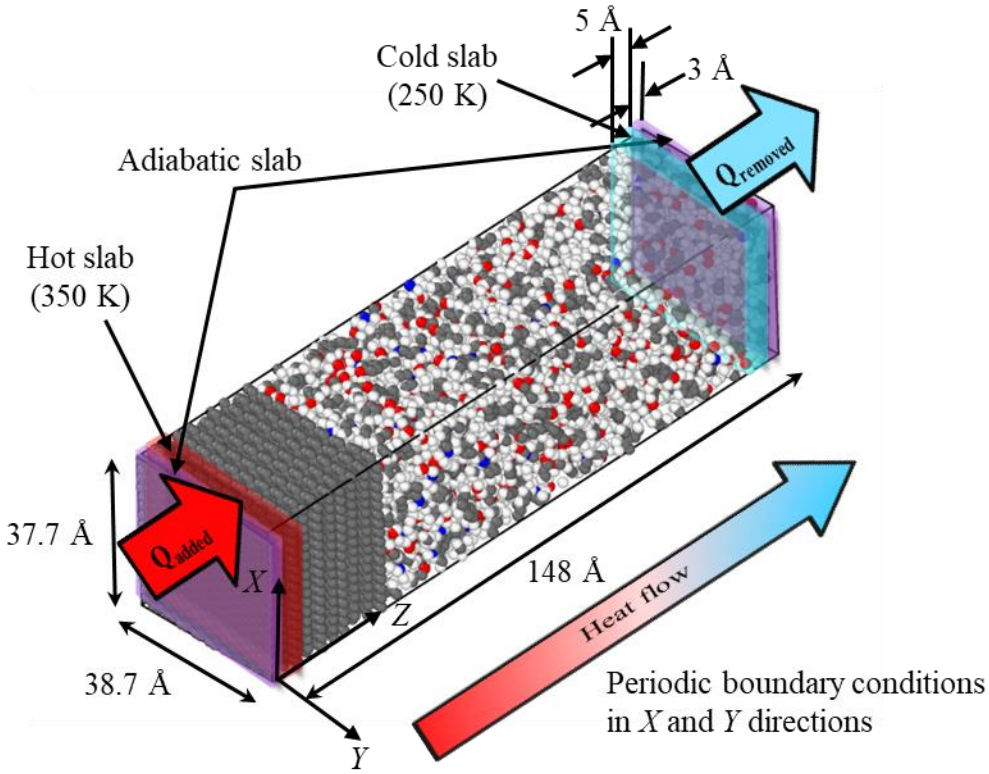

Figure 3.6. Schematic showing the method used to determine interfacial thermal conductivity between carbon fiber and epoxy in the MD simulations.

To monitor the variation of temperature across the length, the fully equilibrated MD simulation box is divided into slabs of equal thickness of 2 Å. The average temperature T_j of slab j is calculated as:

$$T_j = \frac{1}{3N_s k_B} \int_0^\tau \left(\sum_l^{N_s} m_l v_l^2 \right) dt \tag{3.2}$$

where, $\tau \approx 1$ ns. Also, N_s is the number of atoms in the slab j, k_B is the Boltzmann constant, m_l and v_l are the atomic mass and the instantaneous velocity of atom l.

For all cases, the initial simulation is run for 1 ns to obtain a steady-state temperature profile followed by 1 ns of production run to collect data for temperature gradient and heat flux. The interfacial thermal conductivity (K_{i}) between carbon fiber and epoxy is calculated using,

$$K_{\mathrm{i}} = -\frac{q_{\mathrm{z}}}{T_{23}/Z_{23}} \qquad 3.3$$

Here, T_{23}/Z_{23} is the temperature gradient across the carbon fiber/epoxy interface as shown in Fig. 3.7. We define, T_{23} and Z_{23} as $T_{23} = T_3 - T_2$ and $Z_{23} = Z_3 - Z_2$ respectively (see Fig. 3.7). The thermal conductivities of carbon fiber (K_{cf}) and epoxy (K_{ep}) are obtained by using T_{12} and T_{34} respectively (see Fig. 3.7).

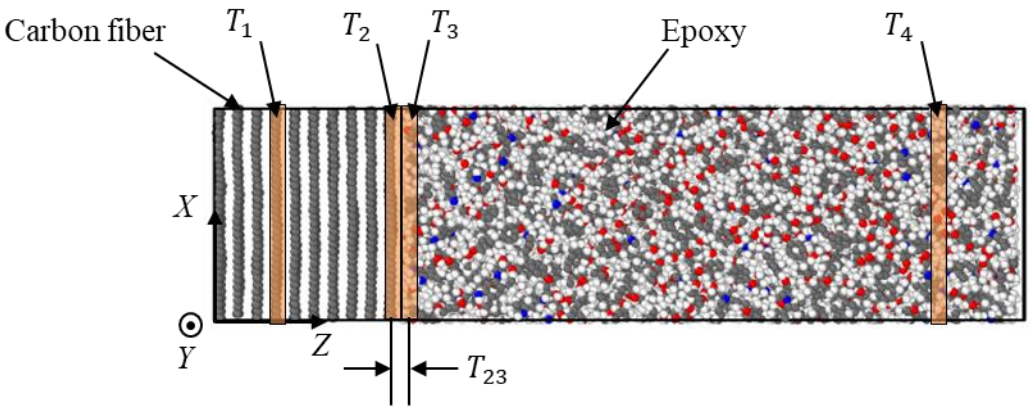

Figure 3.7. The MD sample indicating the locations at which temperatures are extracted in order to calculate thermal conductivities K_{cf}, K_{i} and K_{ep}.

3.3 Results and discussion

3.3.1 Validation of MD model

To validate the procedure followed for extracting thermal conductivity from MD simulations (discussed in Sec. 3.2.3), we modelled a pure 80% crosslinked epoxy system (i.e. without the graphite layers) of dimension 38.4 × 39.4 × 120 Å. Figure 3.8(a) shows that the energy added or subtracted from the hot and cold slabs is nearly same during the entire simulation time of 2000 ps. Figure 3.8(b) compares the temperature distribution along the length of the simulation box at different simulation times. It reveals that a steady-state is achieved at ~ 1000 ps. The MD simulations are allowed to run for a further 1 ns after which the conductivity of epoxy, K_{ep}, is extracted from the temperature profile. The thermal conductivity of pure epoxy evaluated is found to be 0.233 W/m.K. This is in good agreement with the reported values obtained from

experiments (0.15 – 0.25 W/m.K) [33,100,121,122] and simulations (0.197 – 0.31 W/m.K) [87,88,123,124]. The density of epoxy over 100 ps under the NPT ensemble is found to be around 1.099 ± 0.002 g/cm^3 which agrees reasonably well with simulated (1.12 – 1.18) [113,125,126] and experimental values (1.18 – 1.2) [113,126] reported in the literature. A close match between the thermal conductivity and density of pure epoxy predicted by MD simulations with those reported in the literature establishes the accuracy of procedures adopted and adequacy of the force field used in this work.

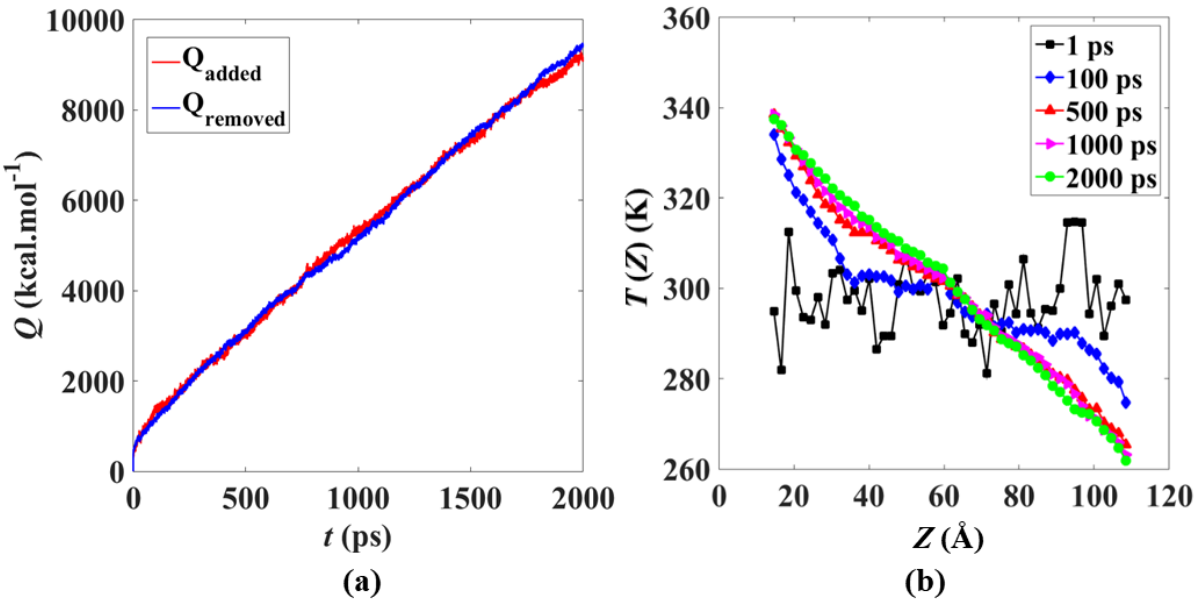

Figure 3.8. (a) Energy added to or removed from the hot and cold slabs respectively with simulation time in ps. (b) Temperature profiles T (Z) at various stages of the simulation.

3.3.2 Interfacial thermal conductivity

MD simulations are performed in this section to determine the interfacial thermal conductivity (K_i) of carbon fiber/epoxy composite following the same procedure described in Sec. 3.2.3 (see Fig. 3.9). Here, the temperature decreases gradually in fiber and epoxy region but shows a large jump across the carbon fiber/epoxy interface. The sudden drop characterizes the interfacial thermal conductivity with the general understanding that larger the jump, higher is the interfacial thermal resistance. Carbon fiber and epoxy interacts through weak non-bonded van der Waals interaction. This weak interaction is unable to reduce the vibrational mismatch between carbon fiber and epoxy [89]. Hence, a large temperature gradient between T_2 and T_3 is recorded at fiber/epoxy interface. For the case shown in Fig. 3.9, the K_i calculated using the jump in temperature of 15.1 ℃ across the interface is 0.026 W/m.K. This value obtained for the

carbon/epoxy system will be used as a benchmark for comparison with cases where the carbon is functionalized.

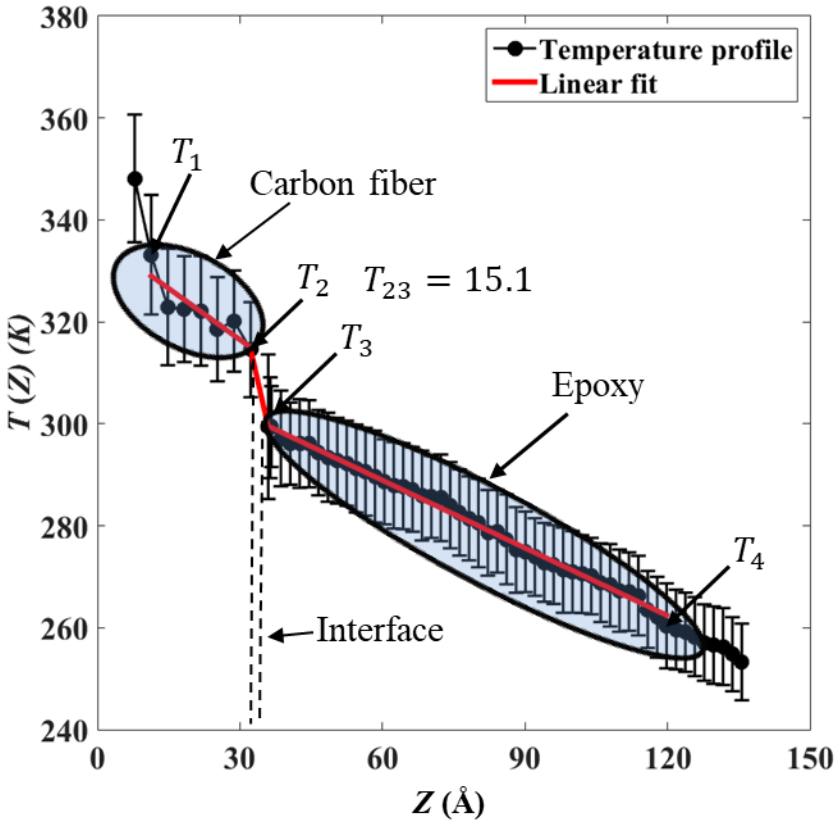

Figure 3.9. Typical temperature profile T (Z) in a carbon/epoxy system showing a large temperature jump across the interface.

Obviously, a typical commercial carbon fiber (approximately 7 μm in diameter) contains many more graphene layers [54,89,127] than can be realistically simulated in a MD protocol. A few words about the inevitable effect of the system size are in order here. The area i.e. $L_x \times L_y$ and number of graphene layers (N_g) used to represent a carbon fiber is expected to affect the values of K_{cf}, K_i and K_{ep}. We conducted number of simulations with different values of $L_x \times L_y$ and N_g (dimensions varying from 38.4 – 76.8 Å, and numbers from 5 – 20) as shown in Figs. 3.10.

We believe that in case of the epoxy, heat in the Z-direction is carried by diffusive modes with short propagation lengths --- much shorter than the sample length used. As a result, changing the sample length does not have an effect on the conductivity of epoxy. Note that, for a Z – dimension of 120 Å, K_{ep} is reasonably independent of the size and number of graphene layers (see, Fig. 3.10 (c)). Moreover, the value of K_{ep} obtained in the simulations is similar to that reported experimentally.

On the other hand, in graphene, K_{cf} increases marginally when cross sectional dimensions are doubled from 38.4 to 76.8 Å, but significantly with the number of layers (see, Fig. 3.10(a)). In the graphene layers, phonons are responsible for heat transport. The longest wavelength of phonons that can be excited in the simulations are limited by the dimensions of the stack of graphite layers. Mismatch between dominant long wavelength phonons in graphene and short propagation length diffusive modes in the epoxy are responsible for the interface conductivity [41].

From Fig. 3.10(b), it seems that, when the cross-sectional dimension is about 38.4 Å (the dimension used by us), and the number of layers is 10, all important long wavelength modes are already excited. Any further increase in cross sectional dimensions or number of layers, lead to only a marginal change in the interface conductivity. We have used cross sectional dimension of 38.4 Å and 10 graphene layers as a seemingly reasonable compromise.

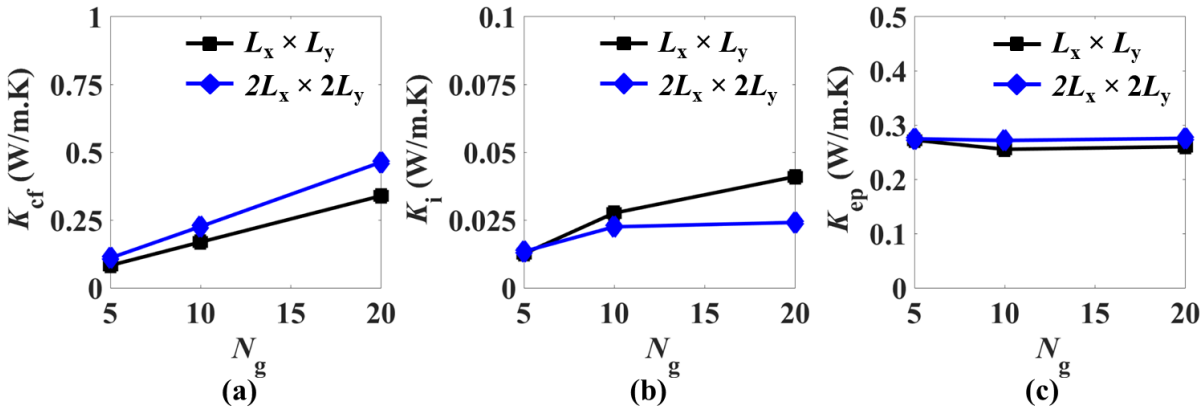

Figure 3.10. Effect of area and number of graphene layers (N_g) on thermal conductivity (K): (a) carbon fiber, (b) carbon fiber/epoxy interface, and (c) epoxy.

3.3.3. Effect of functionalization on the interfacial thermal conductivity in CFRP

In order to reduce the thermal resistance at the carbon epoxy interface (see, Fig. 3.11), different functional groups are used to bridge the carbon and the epoxy. To this end, we start with the functional groups attached at random locations on the graphene sheet in contact with the epoxy. One end of the functional groups (which can be carboxylic, amine, aniline, single-chain para-amine SGM, or double-chain meta-amine SGM) is covalently bonded to the graphene. The other end of the functional group (the R2 atom) connects to epoxy during crosslinking. As we achieve 80% crosslinking in our simulation, one end of some of the functional groups may be dangling. Both the nature of the functional group as well as the degree of functionalization (f) is expected to affect the extent to which the interfacial thermal resistance is reduced. We vary both in order

to select the most effective functional groups and the optimum value of *f*. To this end, the degree of functionalization is varied from 1 – 10 %. Specifically, *f* is defined as the ratio of the number of carbon atoms with an attached functional group, to the total number of carbon atoms present in a graphene sheet. The interfacial thermal conductivity for functionalized fiber (K_i^f) is evaluated using the same procedure as before, except that, for calculating Z_3 the average Z coordinate of the end reactive atoms of the functional group is used (see, Fig 3.11(b)).

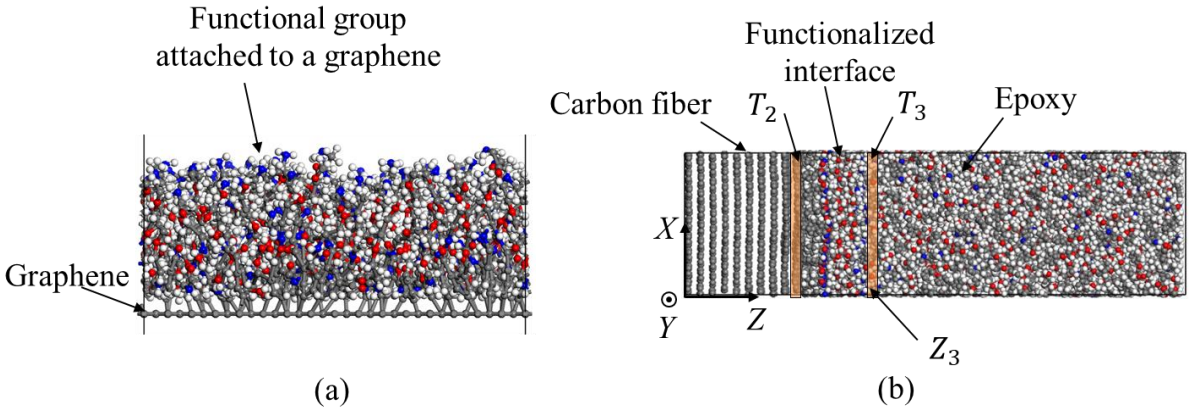

Figure 3.11. (a) A typical close – up of a 10% functionalized interface with double-chain meta-amine SGM. (b) Schematic of 10% functionalized double-chain meta-amine SGM interface indicating the location of Z_3.

For f = 5%, the temperature variation $T(Z)$ for all the functional groups are compared with the non-functionalized case in Fig. 3.12(a). It reveals that addition of functional groups on the fiber surface inevitably decreases the temperature jump across the interface. The functionalised interface has strong covalent bonds connecting the graphene with epoxy. These replace the weak van der Waals interaction between graphene and epoxy in a non-functionalised system. The strong covalent bonding reduces the vibrational mismatch between carbon and epoxy, promoting better heat transfer [47,48]. Moreover, the normalized interfacial thermal conductivity K_i^f/K_i for different functional groups with degree of functionalization f are compared in Fig. 3.12(b). It shows that while any functionalization improves the interfacial thermal conductivity, larger molecules (aniline, single-chain para-amine SGM, and double-chain meta-amine SGM) perform better at reducing the interfacial thermal resistance. Moreover, increasing the degree of functionalization from 5% to 10% does not have a significant effect on K_i^f except for single-chain para-amine SGM, which shows continuously improving performance with f. In fact, it performs better than the longest molecule, namely double-chain meta-amine SGM at f = 10%.

However, it is important to understand that why larger molecules perform better than shorter molecules in reducing the interfacial thermal resistance.

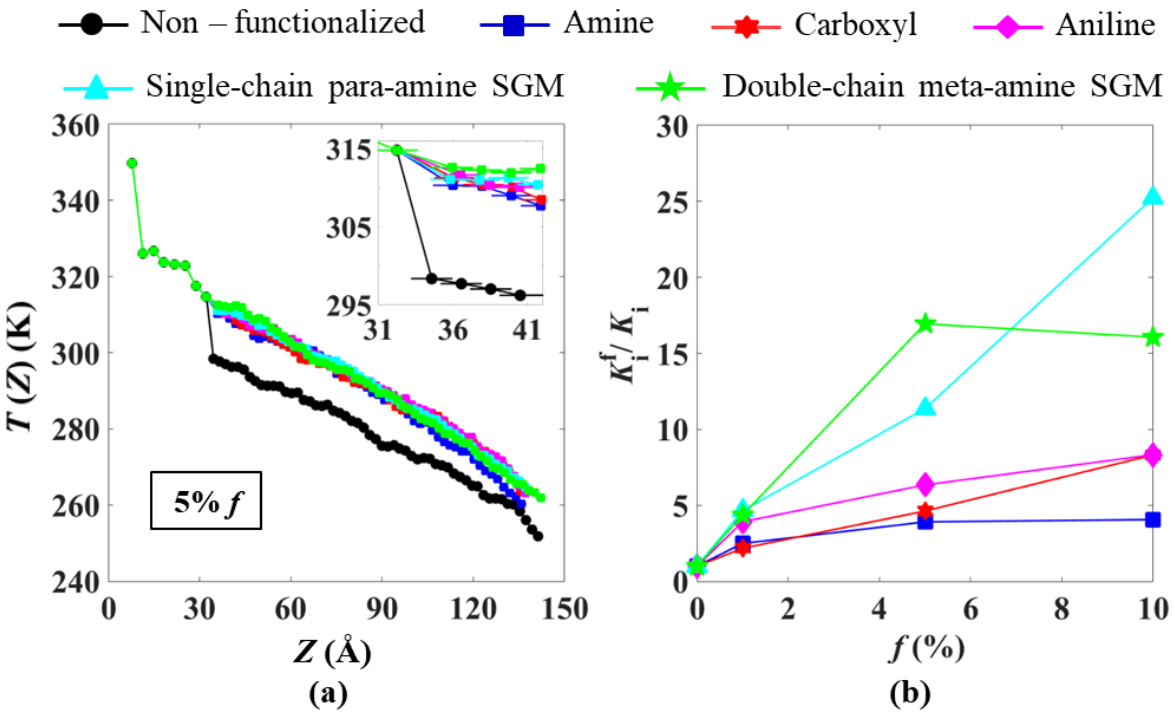

Figure 3.12. Effect of functionalization on (a) steady-state temperature profile $T(Z)$ corresponding to f = 5%. The inset shows the temperature variation at the interface. (b) Ratio of interfacial thermal conductivity with functionalization (K_i^f) and interfacial thermal conductivity without functionalization (K_i) with respect to f for different functional groups.

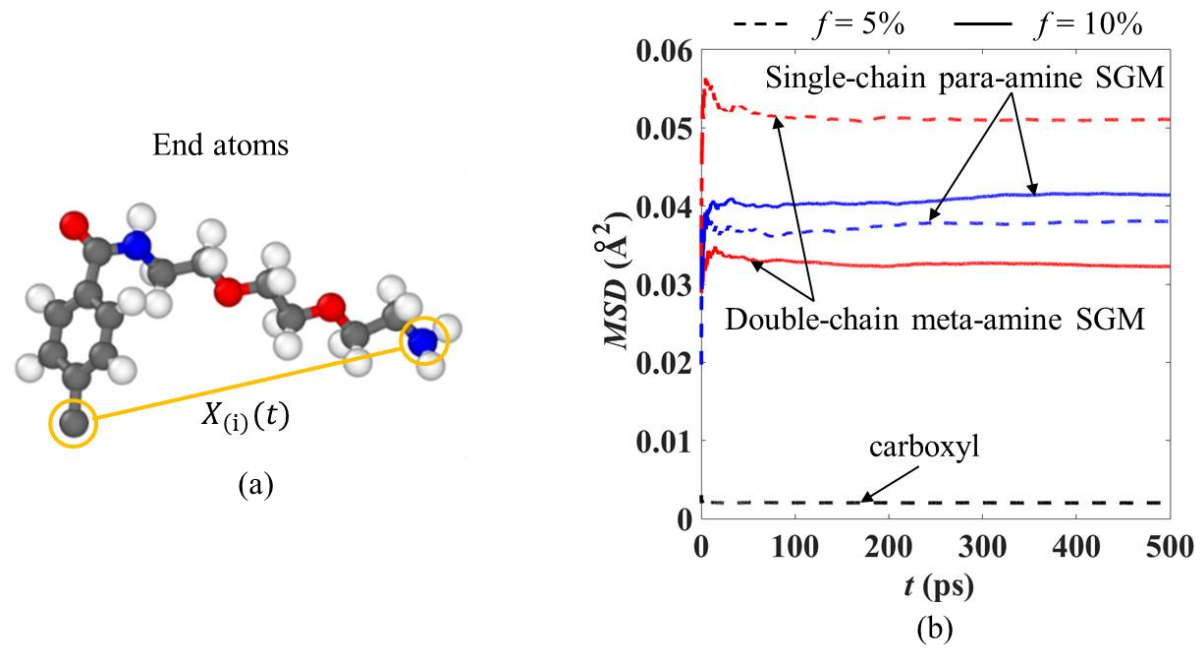

Figure 3.13. (a) End-to-end vector $X_{(i)}(t)$ of single-chain para-amine SGM. (b) *MSD* with time for a few groups at f = 5%.

To this end, the mean squared displacement (*MSD*), is defined as,

$$MSD(t) = \frac{1}{N}\sum_{i=1}^{N}\left|X_{(i)}(t) - X_{(i)}(0)\right|^2, \qquad 3.4$$

where $X_{(i)}$(t) is the end-to-end distance at time t of the ith functionalising molecule (see Fig. 3.13(a)), the ends of which are connected to the graphene layer and an epoxide ring. The molecules in these systems in the glassy state do not undergo large scale diffusive motions. Here, the MSD provides a measure of the average fluctuation in the end-to-end distance of a functionalizing molecule. As shown in Fig. 3.13(b), while carboxylic molecules exhibit very low fluctuations, both the single-chain para-amine SGM and double-chain meta-amine SGM fluctuate much more vigorously over time. Larger fluctuations facilitate better heat transfer. Consequently, while double-chain meta-amine SGM exhibits better K_i^f at 5% f, single-chain para-amine SGM performs better at f =10%.

It must be mentioned here that our observations stated above point to a relation between the stiffness and vibration modes of the functionalising molecule and its effectiveness decreasing interfacial thermal resistance. A better understanding of this relation merits a separate detailed study.

3.4 Conclusion

MD simulations are performed to investigate the effect of functionalization on the interfacial thermal conductivity (K_i) of carbon fiber/epoxy composites. Graphene layers are used to model the carbon fiber in MD simulations. The number of graphene layer and simulation box size is varied to minimize size effects. Different types of chemical groups with varying sizes and degrees of functionalization are attached to the graphene layer to study their effect on the interfacial thermal conductivity (K_i^f). Simulations show that functionalisation can increase interfacial conductivity by up to ~ 25 times. A relatively higher improvement in K_i^f is observed with larger functional groups. This is due to the fact that larger molecules exhibit more rigorous fluctuations in their end-to-end distances. Also, K_i^f does not seem to depend strongly on the degree of functionalization beyond 5% f in most cases. An exception is, single-chain para-amine SGM which shows increasing improvement with f. The present study suggests that improvement in K_i does not depend only on the type of a functional group but is also related to the structure and degree of functionalization. It is envisaged that the present study will be helpful towards tailoring interfaces in carbon fiber/epoxy composites with a view to improve their overall thermal conductivity.

Lastly, our MD simulations inevitably exhibit size effects so that the exact value of the interfacial thermal conductivity might be higher than what the simulations with 10 layers of graphene predict. This however, does not change the conclusion that properly tailoring the carbon epoxy interface can lead to significant reduction in its interfaces thermal resistance.

Chapter 4: Molecular dynamic study on modulating the interfacial interactions of carbon fiber/epoxy interfaces

Molecular dynamics (MD) simulations predict that larger functional groups are more effective as compared to smaller ones to increase the interfacial thermal conductivity of carbon fiber/epoxy interfaces. Is it possible that certain functional group may simultaneously enhance the interfacial thermal conductivity as well as interfacial shear strength? What is the optimum degree of functionalization (*f*)? To seek the answers, microbond MD simulations are performed in this chapter to study the interfacial interactions in carbon fiber/epoxy as a function of chemical ligand used to functionalize the carbon fiber. Further, how interfacial failure mechanisms depend on the chemistry at the interface is also explored.

4.1 Introduction

Carbon fiber reinforced plastics composites (CFRPs) are widely used in structural applications due to their superior properties such as high specific strength, high specific stiffness, good corrosion resistance, and low maintenance cost [20,128–130]. Interfacial adhesion in CFRPs affects the load transfer efficiency between carbon fiber (CF) and matrix. In fact, poor interfacial adhesion is often responsible for the somewhat low damage tolerance in these materials [49,131–133].

Various strategies such as sizing, dip coating, spray coating, chemical modifications, high-energy irradiation, plasma treatment [134–137], and thermal treatment have been used to improve the interfacial shear strength (IFSS) in composites [23,29,106,107]. Engineering the surface of the CF, without compromising its mechanical strength has emerged as a viable route to improve the interfacial adhesion between the CF and the matrix. For example, MXene nanosheets and NH_2 were grafted onto carbon fibers (eg. see, [73]), leading to about 33% increase in IFSS, as a result of an increase in the surface roughness of the fibers and their wettability with epoxy resin. Similarly, grafting of carbon nanotubes [55] and vertical graphene sheets [138] are viable ways of engineering the interface.

We focus on methods of functionalizing the CF surface with surface grafted molecules (SGM) that also covalently crosslink with the matrix. Chemical routes to grafting small molecules like amine (Fig. 4.1(a)) as well as longer bespoke molecules (Figs. 4.1(b), (c) and (d)) bearing a reactive amine group onto CF surfaces are now well established [66,67]. Extensive tests on single

fiber epoxy composites with functionalized CFs have demonstrated the efficacy of this strategy and, in some cases, resulted in ~172% increase in interfacial strength [66,92,93]. Further, molecular dynamics (MD) simulations on atomistic systems of CF and epoxy bridged by functionalizing molecules have elucidated the anchoring mechanisms at play [66,67].

Motivated by the analyses in [66,67], we have performed MD simulations on a single fiber-epoxy geometry that resembles a very small scale microbond test. Unlike in pull-out, fragmentation and push-out tests where the involvement of plastic dissipation in the bulk of the polymer enters the IFSS and undermines the influence of the interface [55]. Microbond tests allow us to focus on the strength of the interface more closely [139]. Moreover, we adopt a force field that allows bond scission to occur.

In the MD studies, we hope to gain insights into two aspects of the surface functionalisation process. Firstly, we seek to determine the role of grafting density on the IFSS. Our results show that, especially for longer molecules, an optimum areal density of grafting indeed exists, beyond which the IFSS starts to decrease. Secondly, we study the failure mechanisms at the interface and show that bond scission in longer molecules limit their effectiveness. Overall, in spite of the fact that our atomistic microbond test samples are unrealistically small, important insights about the functionalised interface can be obtained from the MD simulations.

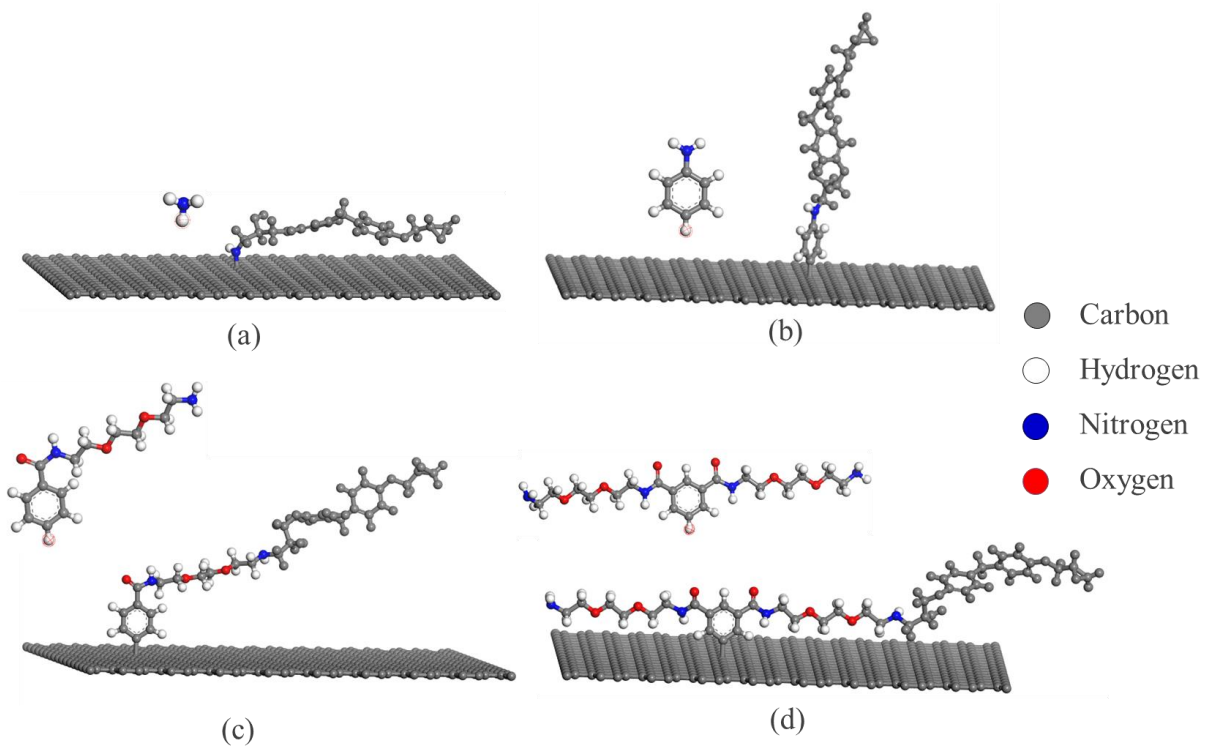

Figure 4.1. Chemical structure of functional groups connected between graphene and diglycidyl ether of bisphenol F (EPON862, all atoms are shown in grey color for clear visualization): (a)

amine, (b) aniline, (c) single-chain para-amine, and (d) double-chain meta-amine surface grafted molecules (SGM).

4.2 Computational details: the miniature microbond test

Figure 4.2(a) shows the experimental set-up of an actual microbond test to determine the IFSS. In this test, a single fiber with a cured polymer drop is pulled through a small opening between two knife edges. In the real test, the embedded length l_e is of the order of tens of micrometers.

Figure 4.2(b) shows the simulated miniature microbond test set-up. The atomistic model seeks to mimic the deformation in the region epoxy makes contact with knife edge to carbon fiber in Fig. 4.2(a). As shown in Fig. 4.2(b), the rigid carbon fiber (which typically has a diameter ~ 7 μm) is represented by ten graphene layers with interlayer separation of 3.35 Å [95,140]. The epoxy drop is of dimensions L_X = 38.4 Å and L_Y = 39.4 Å, with periodic boundary conditions (pbc) applied in the Y direction. The blue shaded part of the drop of thickness t_1 next to the fiber/matrix interface is allowed to deform while the yellow shaded part, with thickness t_2 is constrained, representing the part of the epoxy that sticks to the knife edge in the microbond test.

Diglycidyl ether of bisphenol F (EPON862) and diethyl toluene diamine (DETDA) are considered as epoxy resin and the crosslinker (curing agent) respectively. They are packed in a stoichiometric ratio of 2:1 in the simulation box with pbc in all three directions and equilibrated (in the commercial package Material Studio 18.1 [111], using the polymer consistent force field (PCFF) [114]) to produce a 80% crosslinked epoxy sample [140].

The temperature and pressure of the system are controlled via a Nose-Hoover thermostat [115,116] and a Berendsen barostat [117]. The cut-off for van der Waals interactions is kept at 10 Å [141]. A velocity-Verlet algorithm is used to integrate the equations of motion with a time step of 0.5 fs. Figure 4.2(c) shows the protocol followed to equilibrate the MD system. To reduce thermal fluctuations, the MD system is quenched from 300 K to 250 K with a rate of 10K/ps and allowed to equilibrate at 250 K for 25 ps using NVT ensemble, followed by NPT ensemble at 1 atm for 50 ps. The steps are repeated to equilibrate the MD system to 0 K shown in Fig. 4.2(c). After equilibration, the carbon atoms of graphene are moved to their mean positions in the *Z*-direction to avoid pull-out energy associated with the waviness of the graphene layers. All the graphene atoms are constrained to move along the *Z*-direction after this step. However, it may lead to the stretching of bonds. Therefore, the MD system is equilibrated again following the steps shown in Fig. 4.2(c) before performing microbond simulations.

Thereafter, the microbond MD simulations are performed with the open-source Large-scale Atomic/Molecular Massively Parallel Simulator (LAMMPS) [112] package. At this stage the atomic interactions are switched to the ReaxFF force field [126] to allow bond scissions. Also, pbc in the X and Z directions are removed. Instead, the top atoms of the graphene layers (see, Fig. 4.2(b)) are pulled in the X-direction with a constant velocity $\dot{u}_X$, which, is taken to be 1 m/s. So, the $X = 0, L_X$ surfaces are traction free while all atoms in the region $L_Z < Z < t_1$ are held fixed. The system is equilibrated for 100 timesteps after each displacement step ($\dot{u}_X \Delta t = 0.0005$ Å, $\Delta t = 0.5$ fs). The simulations are continued till the entire fiber of length L_X comes out of the epoxy.

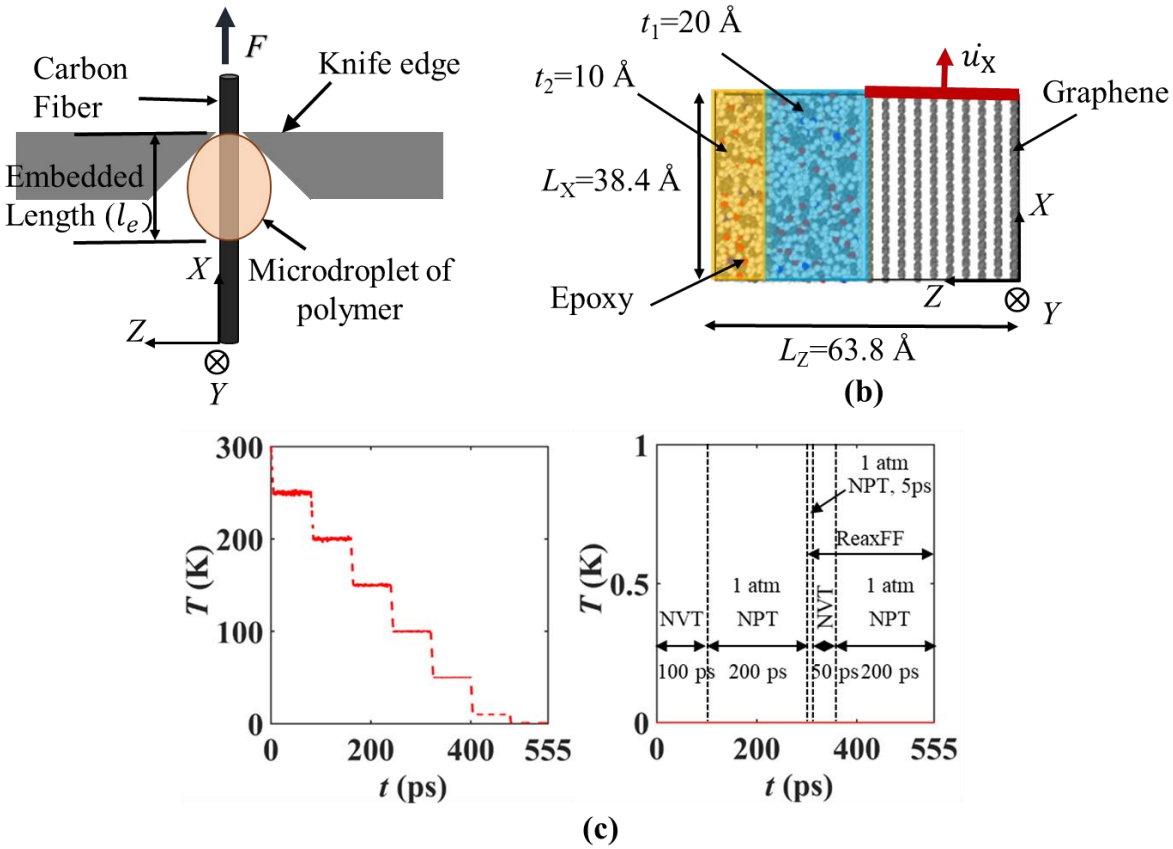

Figure 4.2. Schematic of a microbondbond test. (b) Atomistic model of the miniature microbond test. (c) Equilibration protocol for the crosslinked epoxy/graphene sample shown in (b).

Consider the situation depicted in Fig. 4.3(a), where the fibre has been pulled out by a distance u_X. The force required to pull the fibre out is given by,

$$F_X(u_X) = -\frac{\partial \Delta E}{\partial u_X}, \tag{4.1}$$

where, $\Delta E = E(u_X) - E(0)$, $E(u_X)$ being the total potential energy (sum of all bonded and non-bonded energies) of the system at the stage shown. The interfacial shear strength is then approximated as $\tau_{IFSS} = F_X(L_X)/L_X L_Y$.

Further, in a epoxy/graphene system without any functionalising molecules, the interaction between the epoxy and the graphene layers is purely van der Waals in nature. In Fig. 4.3(b), the van der Waals energy of interaction ΔE_{vdW} is plotted against u_X for two values of t_1, the thickness of the interfacial unconstrained epoxy layer. We see that the interaction energy does not change beyond $t_1 \simeq 10$ Å. We have used $t_1 = 20$ Å in all simulations reported herein.

As an example, the variation of $F_X(u_X)$ with u_X for the 'reference' case without any functionalisation at the interface is shown in Fig. 4.4. This force versus pullout displacement is typically obtained for all the simulations. The deformed configurations of our miniature microbond test are shown at the stages marked by solid circles. Initially, the pull-out force, which in this case is purely due to van der Waals interactions, increases and attains a first peak value of 0.48 nN at u_X of 2.4 Å. At this point debonding initiates and continues at an approximately constant force level of 0.51 nN. Beyond $u_X \simeq 33.6$ Å, the force drops as debonding progresses, reaching zero at complete pull-out [141,142].

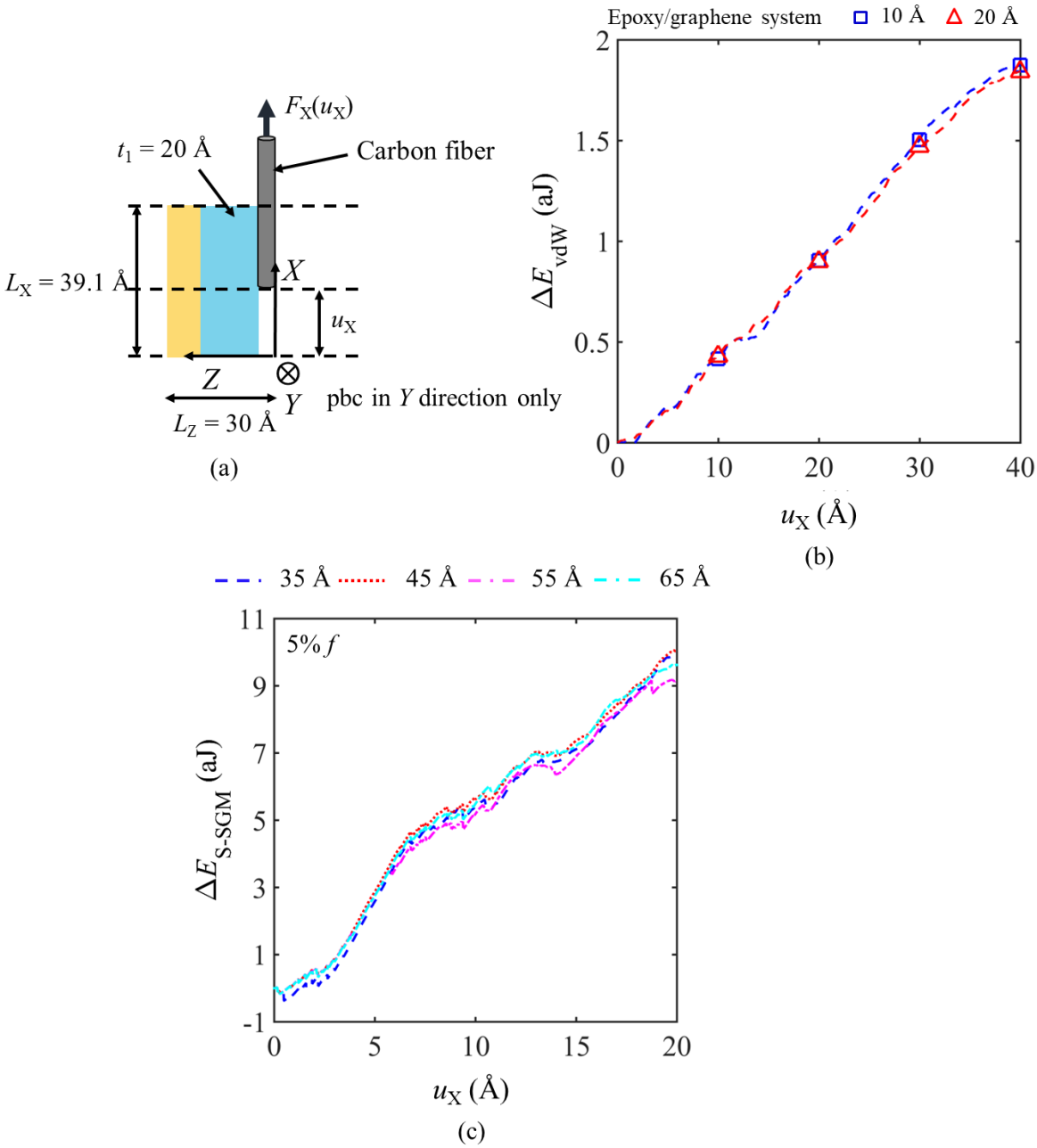

Figure 4.3. (a) Schematic showing the parameters involved in the microbond MD simulations. (b) Variation in van der Waals energy of interaction between epoxy and the graphene layer for $t_1 = 10$ and 20 Å. (c) Variation in potential energy during MD microbond simulation of 5% *f* S-SGM at different t_1.

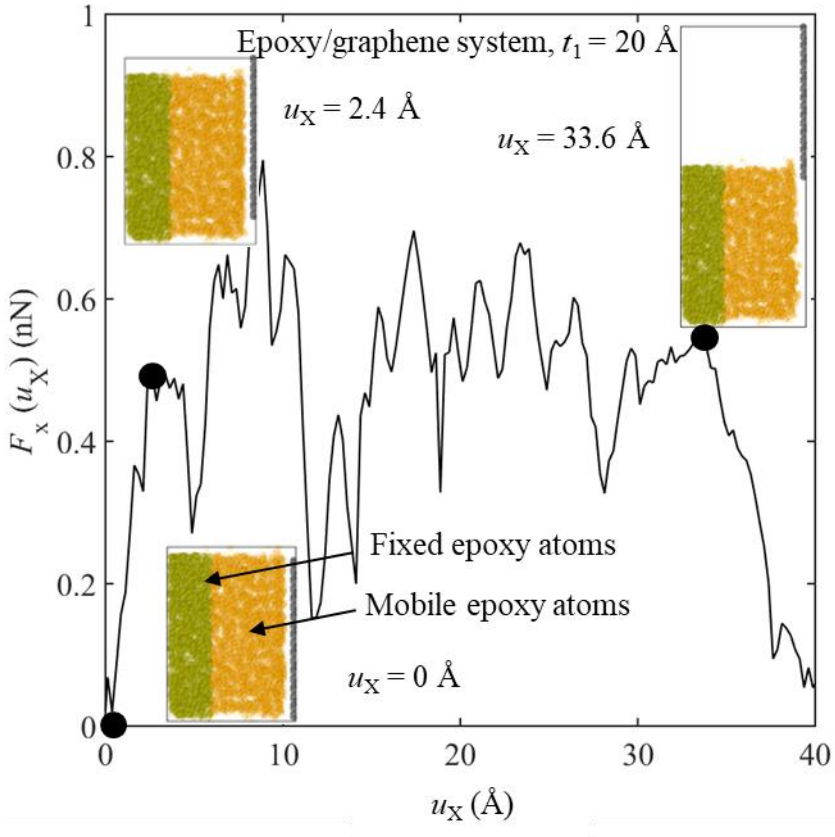

Figure 4.4. The pull-out force F_X (u_X) due to purely van der Waals interactions between the epoxy and the graphene for the reference case with no functionalization. The solid circles mark the deformation stages at which the deformed configurations are shown.

4.3 Results and Discussions

We have functionalized the graphene layer adjacent to the epoxy with 4 different chemical species, namely, amine, aniline, and surface grafted molecules single-chain para-amine (S-SGM) and double-chain meta-amine (D-SGM), as shown in Fig. 4.1. While $t_1 = 20$ Å is used for the reference case (see, Fig. 4.3(b)). The thickness of unconstrained dimension t_1 = 45 Å is identified for the length of the functionalising group (see, Fig 4.3(c)).

The degree of functionalization f is defined as the ratio of the number of randomly chosen sites on the graphene layer at which functionalizing molecules are actually grafted to the total number of possible sites. We have used f of 1, 5 and 10% for this study.

The pull-out energy for the reference case (epoxy/graphene system without functionalization) is denoted by ΔE_{ref}. For each of the 4 functionalising molecules, the pull-out energy is ΔE_{amine}, $\Delta E_{\text{aniline}}$, $\Delta E_{\text{S-SGM}}$, $\Delta E_{\text{D-SGM}}$. At each of the three degrees of functionalisation, the effectiveness

of the ligand is compared by recording the variation in relative pull-out energy of functionalized system with respect to unfunctionalized reference system ($\Delta E_{\mathrm{func}}/\Delta E_{\mathrm{ref}}$) in Fig. 4.5(a)-(d). As the graphene sheets are pulled out, the pull-out energy reaches a peak and then drops as the interaction between graphene and epoxy decreases. After the drop, the ratio of energies remains constant beyond $u_{\mathrm{X}} \simeq 20$ Å. This constant ratio indicates the average effectiveness of the functional group in improving the interfacial toughness with respect to reference case (unfunctionalized carbon fiber/epoxy interface). The energy required for complete debonding increases with f for all cases except D-SGM. At the degrees of functionalisation used, the effectiveness of functionalising molecules is very low for amine, moderate for aniline and significantly higher for the two longer surface grafted molecules as compared in Table 4.1 at $u_{\mathrm{X}} = 30$ Å. Moreover, the ratio is same for D-SGM on increasing the degree of functionalization from 5% to 10% *f*.

Accordingly, as shown in Fig. 4.6, the τ_{IFSS} is ordered as D-SGM>S-SGM>aniline>amine. However, as with the pull-out energy, the τ_{IFSS} for D-SGM peaks at $f = 5\%$ and drops thereafter. Two obvious conclusions emerge from these observations. Firstly, at the low degrees of functionalisation used in this work, longer molecules (in our case S-SGM and D-SGM) provide large increases in interfacial shear strength. Secondly, longer molecules begin losing their efficacy beyond a value of f. Thus, while at $f = 5\%$ D-SGM is about two times more effective than aniline, the latter almost catches up at 10%.

Let us now attempt to address why longer molecules are better at providing high interfacial shear strength? We assume, for the sake of this discussion, that all functionalising molecules are connected to epoxies in the bulk. This is indeed the situation upto $f = 5\%$. As shown in Fig. 4.7(a)-(d), the width of the interfacial region, quantified by b_1, is large for S-SGM and D-SGM. The non-bonded interactions between epoxy and the functional groups are consequently, higher than in cases of aniline and amine.

Moreover, the final separation between the graphene sheet and the epoxy occurs through large scale bond scission. As deformation proceeds, bond scissions occur at different locations. In case of amine, most scissions occur at the N-C bond (C is carbon atom belong to the graphene, see, Fig. 4.8(b)). These scissions require relatively low energy and occur very early in the deformation history (see, Table 4.2). In Fig. 4.7(e) and (i), this is evident from the numerous loose amine fragments embedded in the epoxy as deformation proceeds.

Aniline, S-SGM and D-SGM do not exhibit scission at the graphene end. Bond scission occurs primarily at the carbon-oxygen bonds on the backbones shown in Fig. 4.8 for S-SGM and D-SGM. Aniline does not have carbon-oxygen bonds on the backbone and therefore, scission occurs in epoxy at the location shown in Fig. 4.8(a). In all these cases, bond scission is more difficult and severe plastic deformation has to occur at the interface before separation can happen as bond scission starts at much later stage of pull-out test beyond 30 Å (see, Tables 4.3 – 4.5). The extent of plastic deformation at the interface is evident in Figs. 4.7(f-h) and (j-l). All these three are excellent functional groups that offer large increase in IFSS as f increases. However, the S-SGM and D-SGM perform marginally better due to the larger non-bonded interaction with the epoxy that they start with.

From the above discussion, it may seem that employing longer molecules like S-SGM and D-SGM are always more beneficial towards increasing IFSS. However, this is not necessarily the case. As mentioned earlier, beyond $f = 10\%$ aniline is expected to be more effective than D-SGM. Note that amine, aniline and S-SGM can link with two epoxy molecules (see, Fig. 4.1) while D-SGM can link with four. The search for available epoxide rings is limited to the region marked by b_1. The histogram in Fig. 4.9 shows the fraction of functional molecules that manage to bond with epoxy. At $f = 1\%$, all molecules get bonded or ~ 83% while at 5% close to 75% do. However, at 10%, the situation changes significantly. For amine, aniline and S-SGM, about 45% of the molecules get bonded to epoxy. For D-SGM however, only about 35% of the molecules link with epoxy. This implies that for D-SGM, the number of dangling functional groups becomes high, leading to a drop in the IFSS. A similar drop in IFSS is not expected for aniline, which will continue to show an increase in IFSS with f, surpassing the longer D-SGM.

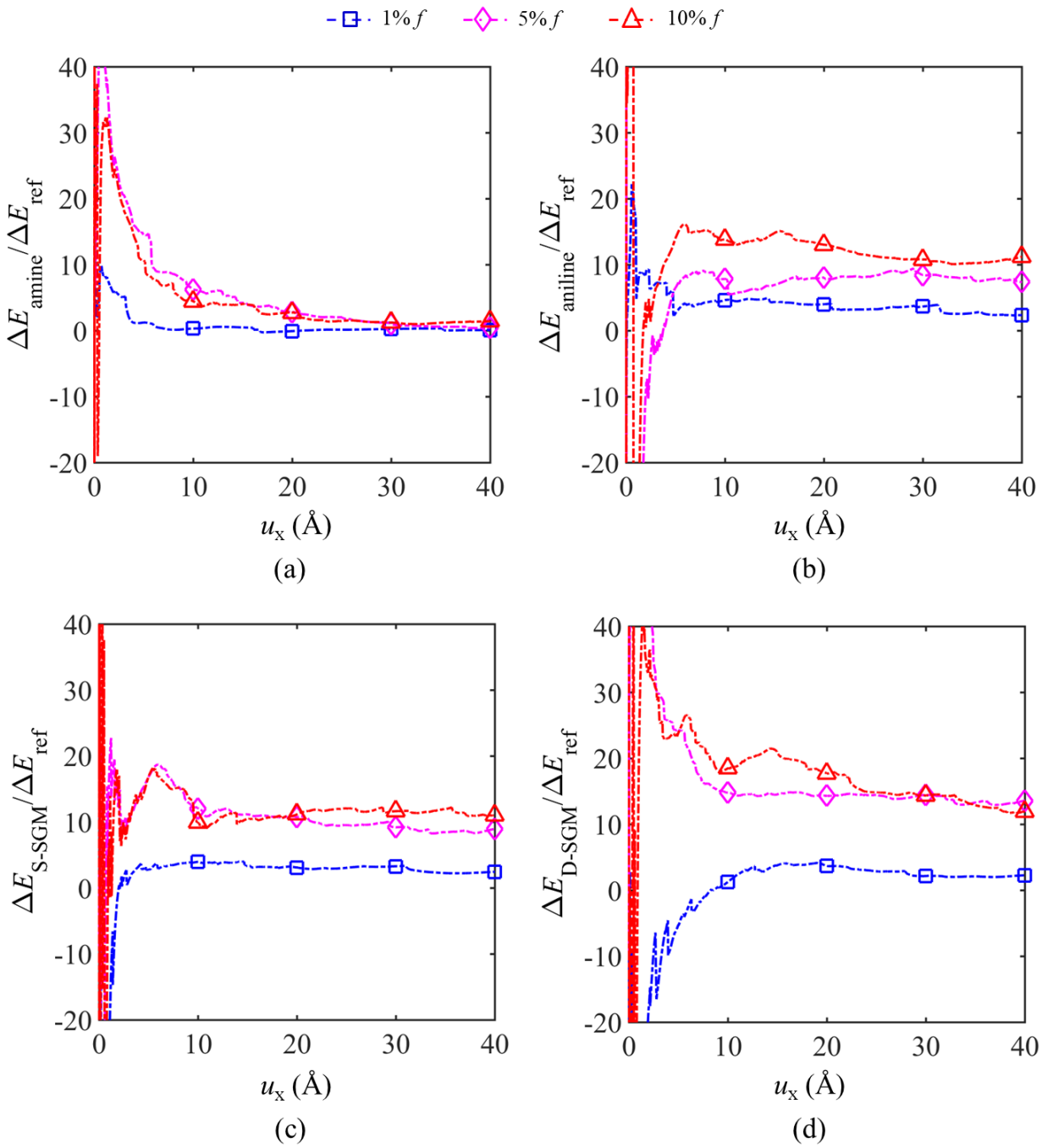

Figure 4.5. Pull-out energy for functionalizing molecules (a) amine, (b) aniline, (c) S-SGM and (d) D-SGM at $f = 1, 5, 10\%$.

Table 4.1. Effectiveness of functionalising molecules with respect to the reference case at u_X = 30 Å.

S. No.	Effectiveness	1% f	5% f	10% f
1	$\Delta E_{\text{amine}}/\Delta E_{\text{ref}}$	0.3	1.2	1.5

2	$\Delta E_{\text{aniline}}/\Delta E_{\text{ref}}$	4.3	9.8	12.6
3	$\Delta E_{\text{S-SGM}}/\Delta E_{\text{ref}}$	3.8	10.7	13.6
4	$\Delta E_{\text{D-SGM}}/\Delta E_{\text{ref}}$	2.5	16.9	16.8

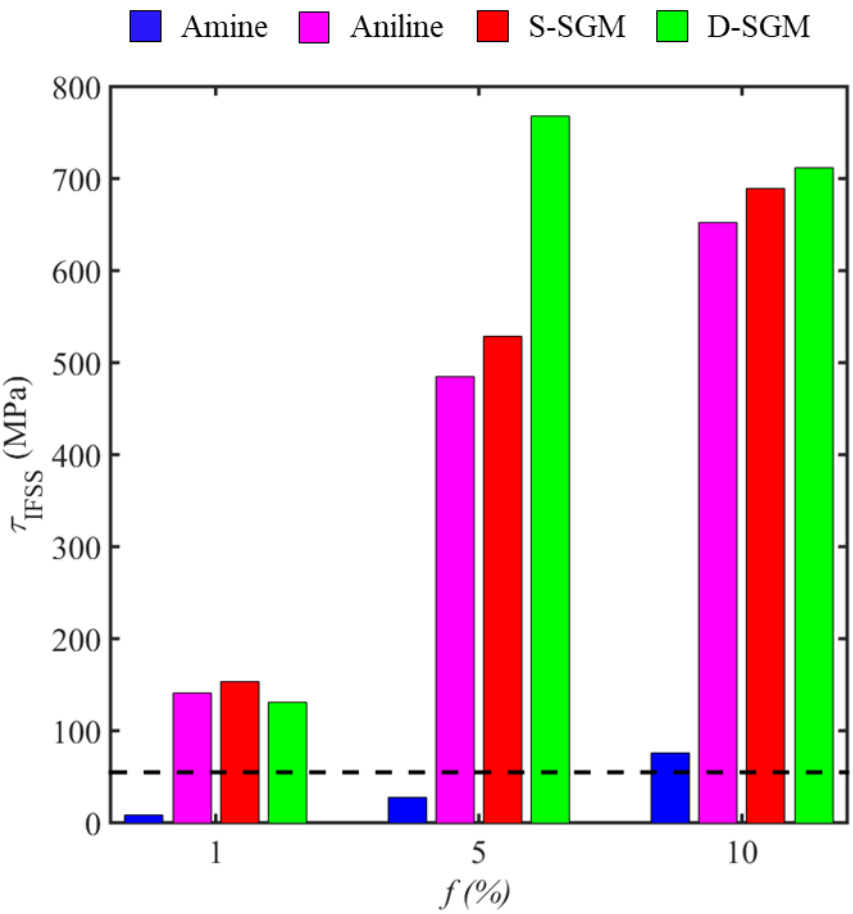

Figure 4.6. Histogram showing the change in the interfacial shear strength (τ_{IFSS}) for amine (blue), aniline (pink), S-SGM (red) and D-SGM (green). The IFSS for the reference case is shown with the dashed horizontal line.

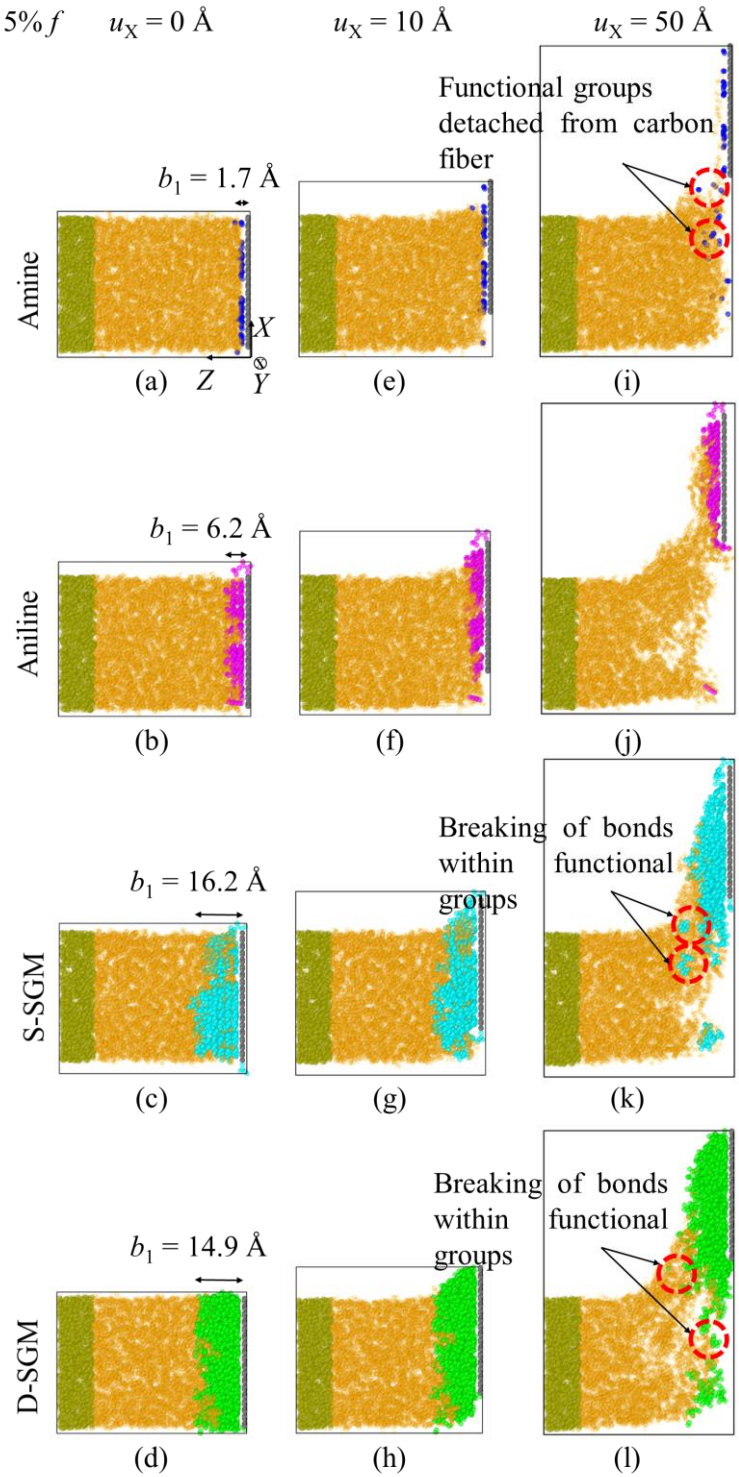

Figure 4.7. The initial samples with different functional groups are shown in (a)-(d). The thickness of the interface layer is marked in each. Deformed shapes of the corresponding samples at u_X =10 and u_X =50 Å are shown in (e)-(h) and (i)-(l) respectively. Locations of some broken bonds are indicated.

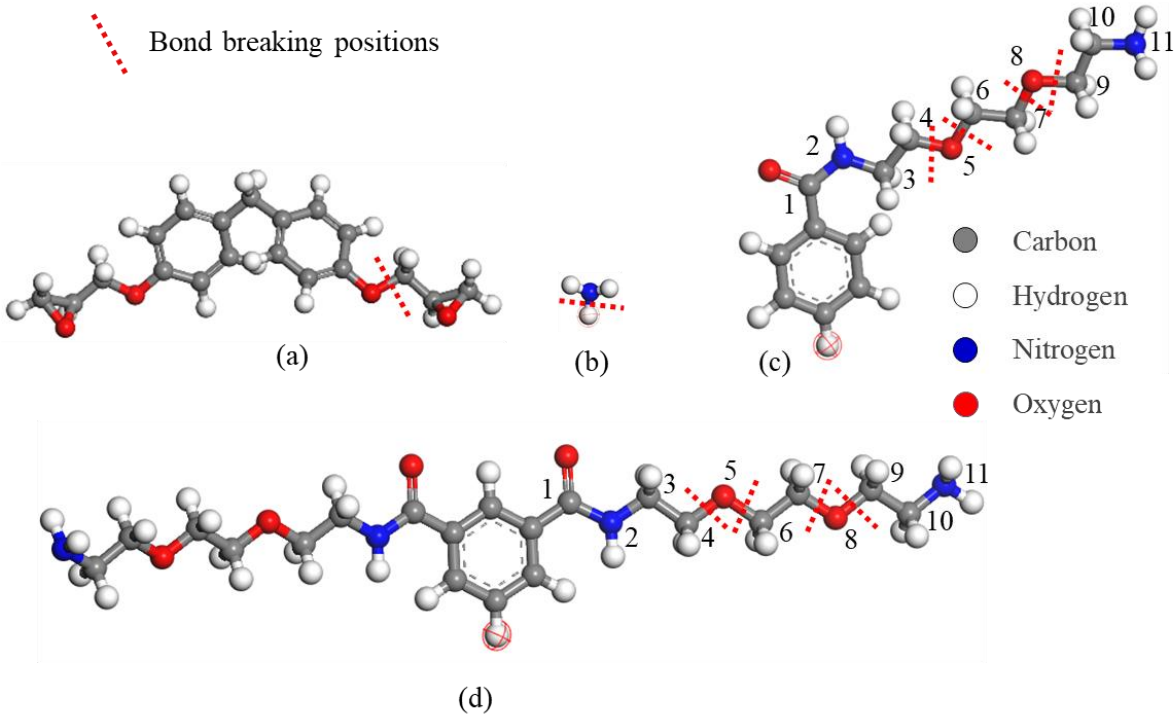

Figure 4.8. Common locations for bond scission in case of (a) aniline, where the scission occurs in EPON862, (b) amine, (c) S-SGM, and (c) D-SGM.

Table 4.2. Count and position of bond scission for amine functionalized graphene/epoxy system during MD microbond simulation fails mainly in attaching point of a functional group to graphene.

S. no.	1% *f*		5% *f*		10% *f*	
	positions	Pull-out distance (Å)	positions	Pull-out distance (Å)	positions	Pull-out distance (Å)
1	Attaching point	3.5	Attaching point	6	Attaching point	0.5
2	NA	NA	Attaching point	13	Attaching point	8.5
3	NA	NA	Attaching point	14	Attaching point	8.5
4	NA	NA	Attaching point	18	Attaching point	10.5
5	NA	NA	Attaching point	19	Attaching point	20.5

6	NA	NA	Attaching point	19	Attaching point	23.5
7	NA	NA	Attaching point	25.5	NA	NA
8	NA	NA	Attaching point	26	NA	NA
9	NA	NA	Attaching point	30	NA	NA
10	NA	NA	Attaching point	42.5	NA	NA

Table 4.3. Count and position of bond scission for aniline functionalized graphene/epoxy system during MD microbond simulation result cohesive failure in epoxy.

S. no.	1% *f*		5% *f*		10% *f*	
	positions	Pull-out distance (Å)	positions	Pull-out distance (Å)	positions	Pull-out distance (Å)
1	Epoxy	32	Epoxy	35	Epoxy	34
2	Epoxy	36	Epoxy	40.5	Epoxy	41
3	Epoxy	41.5	Epoxy	41.5	Epoxy	47.5
4	NA	NA	Epoxy	42	Epoxy	49
5	NA	NA	NA	NA	Epoxy	49.5

Table 4.4. Count and position of bond scission for single-chain para-amine SGM functionalized graphene/epoxy system during MD microbond simulation fails mainly in the functional group.

S. no.	1% *f*		5% *f*		10% *f*	
	positions	Pull-out distance (Å)	positions	Pull-out distance (Å)	positions	Pull-out distance (Å)
1	4 – 5	31.5	5 – 6	21.5	7 – 8	36
2	NA	NA	7 – 8	29.5	7 – 8	37
3	NA	NA	8 – 9	37.5	Epoxy	42.5
4	NA	NA	4 – 5	40.5	NA	NA
5	NA	NA	8 – 9	45	NA	NA

Table 4.5. Count and position of bond scission for double-chain meta-amine SGM functionalized graphene/epoxy system during MD microbond simulation fails mainly in the functional group.

S. no.	1% *f*		5% *f*		10% *f*	
	positions	Pull-out distance (Å)	positions	Pull-out distance (Å)	positions	Pull-out distance (Å)
1	4 – 5	28.8	7 – 8	33	Epoxy	24.5
2	7 – 8	46	8 – 9	37	7 – 8	33.5
3	NA	NA	8 – 9	42	4 – 5	34.5
4	NA	NA	4 – 5	44.5	5 – 6	37.5
5	NA	NA	4 – 5	44.5	Epoxy	42
6	NA	NA	5 – 6	47	7 – 8	45
7	NA	NA	7 – 8	48.5	NA	NA

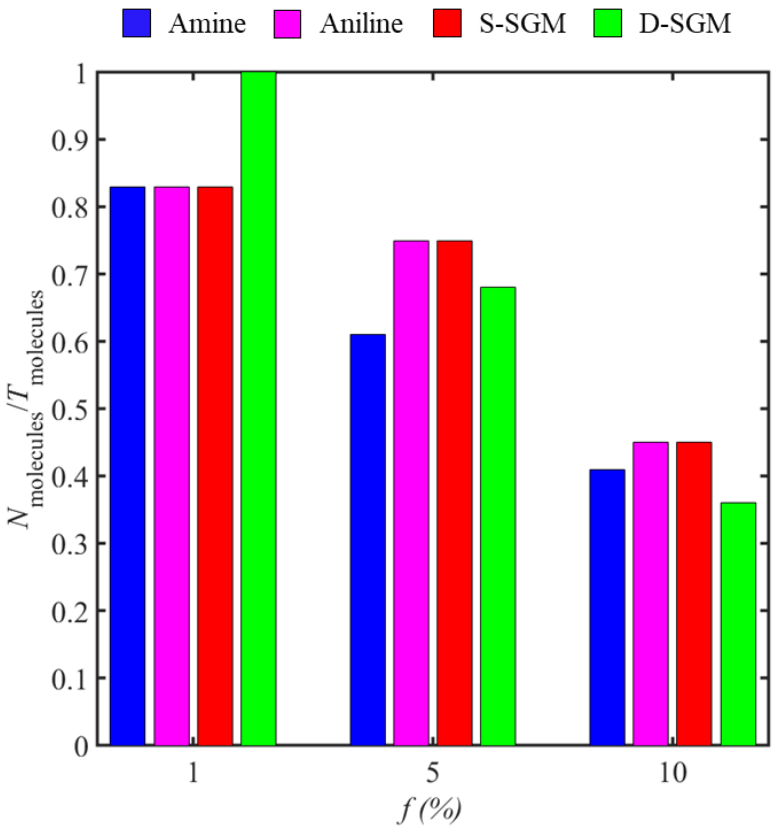

Figure 4.9. Histogram showing the ratio of the number of functionalizing molecules bonded to epoxy to the total number of functionalizing molecules.

4.4 Conclusion

Through carefully equilibrated molecular dynamics simulations, we have studied a miniature microbond test mimicking the pull-out of a carbon fiber embedded in an epoxy droplet. Functionalising molecules like amine, aniline, S-SGM and D-SGM are grafted onto the carbon fiber and allowed to crosslink with the bulk epoxy in order to study their relative effectiveness in enhancing the IFSS. All these molecules have amines at their ends and basically link with the epoxy in the same way.

We show that, at low grafting densities, given that all molecules link with epoxy, longer molecules provide higher IFSS. These molecules produce wider interfacial regions with high non-bonded interaction with epoxy. Moreover, during deformation, large plastic deformation of the epoxy ensues at the interface since bond scission in these cases are energetically expensive and occur at a large scale only after substantial deformation in the interface region. Thus, S-SGM and D-SGM are better candidates for functionalisation at low grafting densities.

The number of dangling D-SGM molecules, each of which is capable of linking with four epoxies, increases with grafting density. As a result, its efficacy as a functionalising molecule decreases beyond a critical grafting density.

Chapter 5: Study of electrical and mechanical properties of CNT/epoxy nanocomposites

Chapters 3 and 4 show the possibility of enhancing the interfacial thermal conductivity and shear stress at carbon fiber/epoxy interfaces with an optimum number and type of functional group predicted from the molecular dynamics (MD) simulations. The insulating nature of epoxy is another issue that needs to be addressed. An experimental study is performed in this chapter to improve the electrical conductivity of epoxy using carbon nanotubes (CNTs). The effect of CNT addition on the average mechanical properties of epoxy is also investigated.

5.1 Introduction

Epoxy is a thermosetting polymer that possesses high chemical resistance, thermal stability, strength, and modulus [143–145]. These excellent properties make epoxy suitable for reinforcement with fiber in the aerospace and automotive industries [146,147]. However, the insulating nature of epoxy limits its applicability in the areas of multifunctional composites. In advanced applications, the composites are needed to perform additional functions other than the structural requirements. Composites must be able to resist lightning strikes, harmful electromagnetic radiation, and dissipate thermal energy in various applications [12,14–18]. For example, in the aerospace industry, the current protection system consists of metal mesh attached to carbon fiber-reinforced plastics (CFRPs) which increases the overall weight of aircraft and decreases fuel efficiency. Also, these heavy metallic structures induce the stresses in composite and weaken the structure [19,20]. Therefore, a lot of efforts have been made to make the conductive carbon fiber polymer composite.

Various conductive nanofillers such as carbon black, graphene, graphite, carbon nanotubes (CNTs), and carbon nanofibers are added to improve the electrical conductivity of polymers [32–34]. Among them, the addition of CNTs is preferred due to their large aspect ratio, ability to form percolating conductive pathways at low concentrations, and excellent combination of mechanical, electrical, and thermal properties [148–151]. The load transfer capability from matrix to CNT improves mechanical property of CNT modified polymer [152,153]. However, adding CNT into the polymer increases viscosity of CNT modified polymer. Higher viscosity leads to poor infiltration in the fibres and thus degrades the overall performance of composites [129,154]. The CNTs at higher loading may also agglomerate and can substantially decrease the

fracture toughness of composites [149–151]. Therefore, a systematic study is carried out to identify the optimum loading of CNTs in the epoxy to enhance the electrical conductivity and fracture toughness.

To this end, various wt.% (0.05 – 3) CNTs are dispersed into the epoxy. Viscosity test is performed on the CNT modified epoxy (CNT/Ep) solution to determine the loading of CNTs into epoxy so that CNT/Ep can infiltrate and wet the carbon fibers effectively. Electrical percolation analysis is carried out to obtain a sudden jump in the electrical conductivity of CNT/Ep nanocomposites. Later, fracture toughness is evaluated for all the CNT/Ep nanocomposites to determine the optimum CNT concentration in epoxy.

5.2 Experimental

5.2.1 Materials

Multi-walled carbon nanotubes (MWCNTs) (Product specification, CAS 308068-56-6) are purchased from Nano Research Elements, India. Carbon nanotubes (CNTs) diameter is about 10 – 30 nm and 3 – 10 μm in length as per the supplier. Bisphenol-A Epofine 556 and Finehard 5200 (Fine Finish Organics Pvt. Ltd., India) are used as Ep resin and hardener respectively.

5.2.2 Processing of nanocomposites

Various concentrations of as-received CNTs i.e., 0.05, 0.1, 0.3, 0.5, 1, 1.5, 2, and 3 wt% are dispersed into epoxy resin and hardener in equal proportion of (100:24) using an ultrasonic probe sonicator (750 W, 20 kHz, probe tip 13mm, Cole-Parmer, USA) at 50% amplitude for 120 min. The maximum temperature of CNT modified Epoxy resin and hardener during sonication is kept at less than 70 ^{o}C [155]. After sonication, the CNT dispersed resin and hardener solutions are uniformly mixed in a 100:24 ratio by wt. and stirred with a glass rod followed by placing solution in a vacuum oven to remove bubbles. Then, the solution is poured into the mold. The processing steps are shown in Fig. 5.1. Later, CNT/Ep nanocomposites are cured at 80 ℃ for 6 hours, followed by 120 ℃ for 2 hours and 160 ℃ for 6 hours respectively. For neat epoxy (Ep) means no addition of CNTs into epoxy. Epoxy resin and hardener solutions are directly mixed in a 100:24 ratio by wt. to prepare Ep samples.

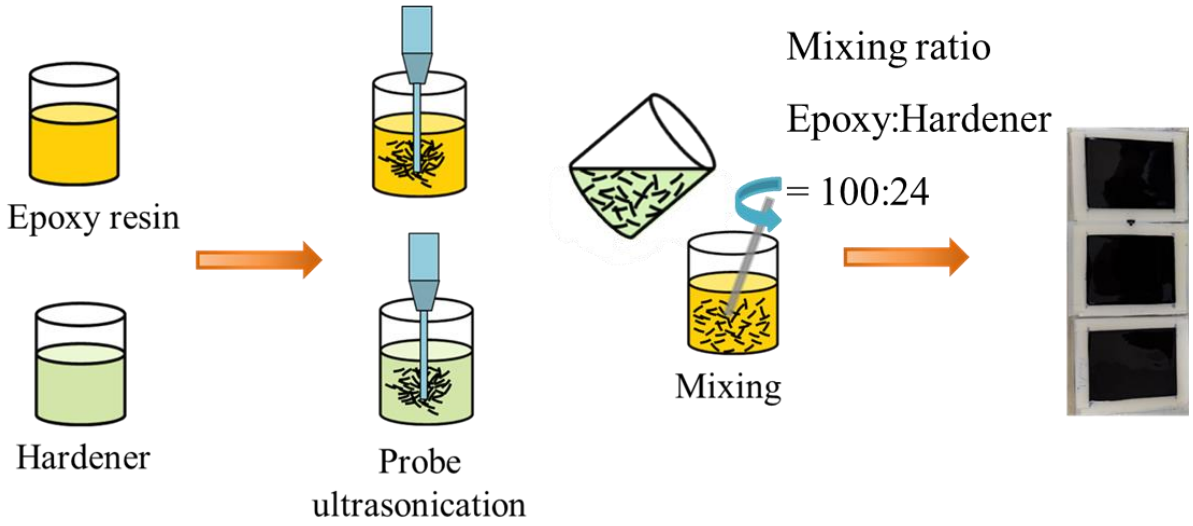

Figure 5.1. Schematic showing processing steps followed to fabricate nanocomposite samples.

5.2.3 Field emission scanning electron microscopy

Field emission scanning electron microscopy (FESEM, JEOL, JSM-7610F, Japan) is performed to study the dispersion of CNTs in the epoxy. The fractography analysis of failed fracture samples is carried out to understand the damage mechanisms in CNT/Ep and Ep nanocomposites.

5.2.4 Viscosity measurement

Viscosity test is performed using the rheometer (Anton Paar, MCR 702, Austria) to obtain the viscosity (η) behavior of Ep and CNT/Ep solution as shown in Fig. 5.2. Few drops of solution are dropped in the middle of the bottom plate and cone plate is moved down in such a way that a gap of 0.1 mm exists between the bottom plate and cone plate. Then, a cone plate with 1 degree and a diameter of 50 mm starts to rotate with increased torque to give a plot of viscosity at different shear rates ($\dot{\gamma}$) starting from 0.1 to 10^3 s^{-1}. The average viscosity of the solution is taken from the average value of three samples.

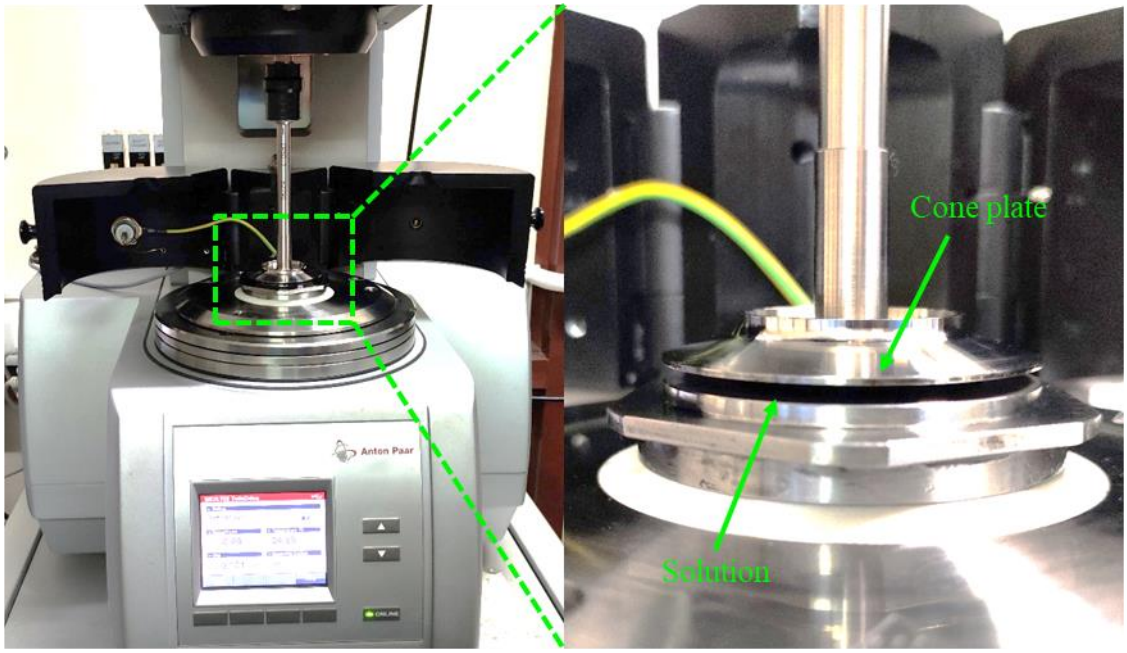

Figure 5.2. (a) Rheometer, and (b) zoom image of solution sandwiched between bottom (stationary) and cone plate (rotationary motion).

5.2.5 Electrical conductivity test

The variation in electrical conductivity of epoxy as a function of CNT concentration is obtained to determine the electrical percolation threshold in the CNT/Ep nanocomposite. The electrical resistance of each sample (25 × 25 × 3 mm) is measured on an IM3523 HIOKI LCR meter at constant voltage 2V using two electrode method as shown in Fig. 5.3.

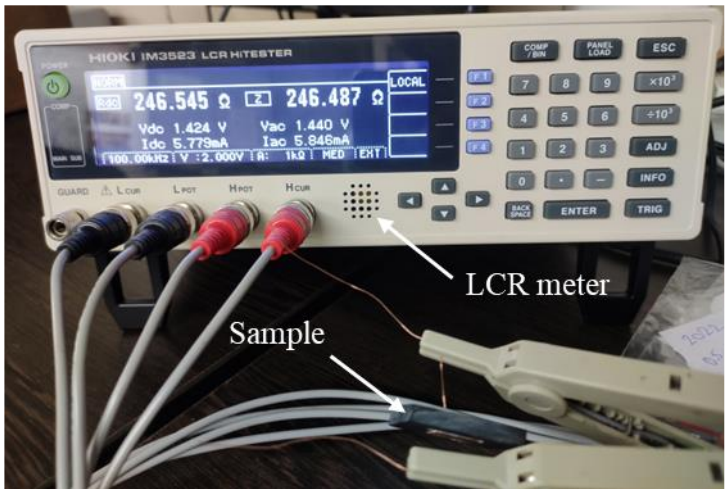

Figure 5.3. Experimental setup of electrical conductivity test.

The direct current electrical conductivity (σ_{DC}) is averaged over three samples and calculated using Eq.,

$$\sigma_{DC} = \frac{B}{A \times R} \quad 5.1$$

where R is the DC electrical resistance obtained from the LCR meter, and B is the thickness of the sample. A is the rectangular area of 10 × 10 mm^2 at the center of a sample upon which silver paste is applied to ensure good contact between the sample and connecting wires.

5.2.6 Fracture toughness test

To determine the ability of a material to resist crack propagation, the critical stress intensity factor (K_{IC}) is evaluated for all samples as per ASTM D5045-14 standard. Figure 5.4. (a) shows a schematic of a single-edge-notch bending (SENB) sample. The thickness of sample is 2.5 mm. The width of the sample, W, is 4B. L and S are the length and span length of the sample defined as $L = 4.4W$ and $S = 4W$. Initially, a notch (a_n) is created by machining (Fig. 5.4. (b)) and a natural sharp crack (a_r) (Fig. 5.4. (c)) is induced by tapping a fresh razor blade of 0.05 mm. The crack length a is monitored to satisfy the condition of $0.45 < a/W < 0.55$. Minimum three SENB samples for each type of CNT/Ep nanocomposites are tested on a universal testing machine (Shimadzu Corp., Japan) at a crosshead speed of 10 mm/min.

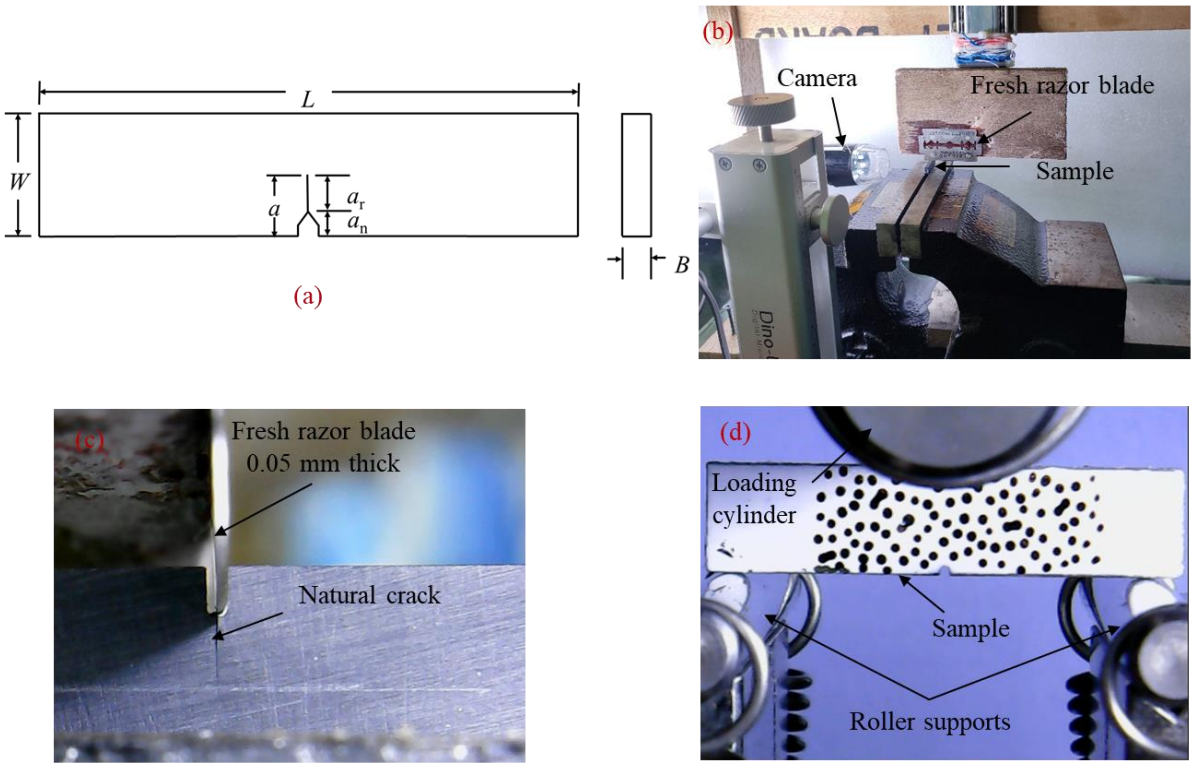

Figure 5.4. (a) Schematic of single-edge-notch bending (SENB) sample as per ASTM D5045-14. (b) Inserting a razor blade into the notch to generate a natural crack. (c) Natural crack obtained from tapping a fresh razor blade. (d) Experimental three-point bend setup.

The fracture toughness (K_{IC}) is given by Eq.,

$$K_{IC} = f(x)\left(\frac{F_Q}{BW^{1/2}}\right) \quad 5.2$$

Where $f(x)$ is defined as Eq.,

$$f(x) = \frac{6x^{\frac{1}{2}}[1.99 - x(1-x)(2.15 - 3.93x + 2.7x^2]}{(1+2x)(1-x)^{\frac{3}{2}}} \quad 5.3$$

Here x is the ratio of a/W, and F_Q is critical load.

5.3 Results and discussion

5.3.1 Effect of CNT dispersion on the viscosity of epoxy

The low viscosity of the solution is needed for proper mixing and wetting of fibers. Highly viscous epoxy may be unable to infiltrate through the fibers and can adversely affect the load

bearing capability of composites. Figure 5.5 shows the viscosity of CNT/Ep solutions at different wt. % of CNT measured at 25 ^{o}C. The viscosity of Ep at 0.1 shear strain rate is 6.96E+2 ± 2.2E+1 mPa.s lies within the value (5.90E+2 – 1.80E+4 mPa.s) reported in the literature [156–161]. The independent behavior of Ep with respect to shear strain rate shows the Newtonian behavior of the fluid. No increase in viscosity for 0.1 wt% of CNT/Ep suggests no hindrance to the flow of epoxy resin by CNT. Addition of CNT beyond 0.1 wt% makes the epoxy non-Newtonian. Higher viscosity suggests more interaction between CNT and polymer and resists the polymer flow [156,158]. Within shear strain rate (0.1 to 10^3), CNT/Ep shows shear thinning behavior with decreasing viscosity at shear strain rate. It may be due to rearrangement/alignment of CNTs in the polymer [156,162]. The viscosity of epoxy increases significantly beyond 1 wt% of CNTs. Moreover, while CNTs are well dispersed up to 1wt% loading (see, Figs. 5.6 (b), (c), and (d)), they tend to agglomerate at higher concentrations in the epoxy (see, Figs. 5.6 (e) and (f)). The increased viscosity and CNT agglomerate may make it difficult for the epoxy to wet the fiber fabric efficiently and hence may degrade the mechanical properties of composites prepared with CNT modified epoxy [163,164].

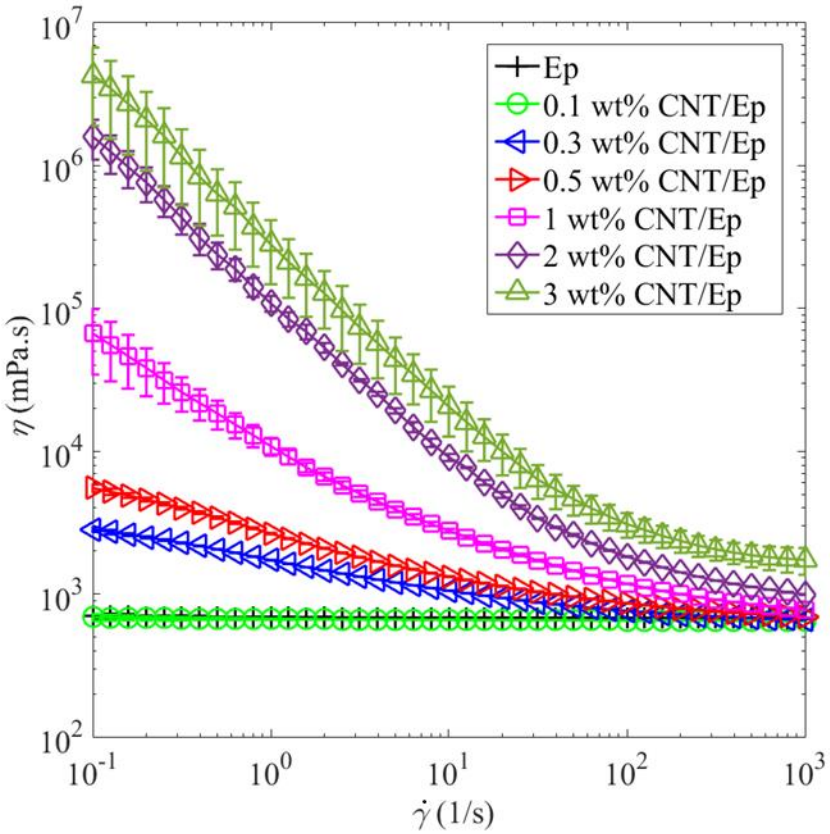

Figure 5.5. Effect of CNT addition on the viscosity of CNT/Ep solution.

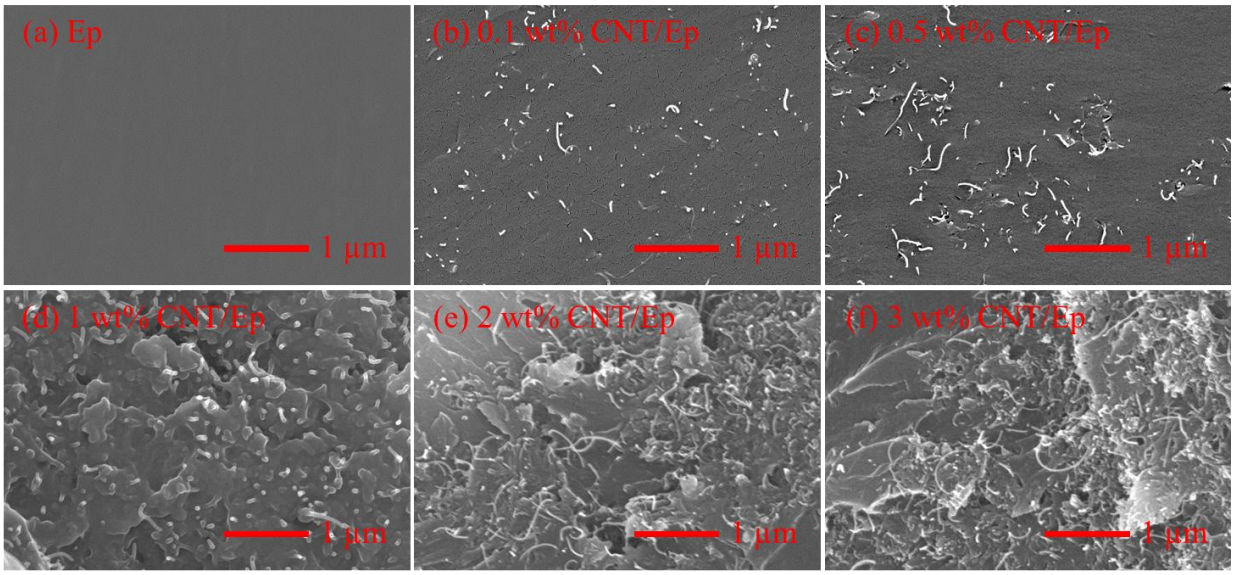

Figure 5.6. FESEM micrographs: (a) Neat epoxy, (b) 0.1, (c) 0.5, (d) 1, (e) 2, and (f) 3 wt% CNT/Ep.

5.3.2 Effect of CNT dispersion on the electrical conductivity of epoxy

Figure 5.7(a) compares the electrical conductivity of epoxy nanocomposites fabricated with varying concentration of CNTs. The electrical conductivity of Ep is found to be 2.9E-13 S/m agrees well with the reported value of Ep (1E-8 – 7.7E-13 S/m) [100,121,147,164–167]. The addition of CNT by 0.05 wt.% increases the electrical conductivity of epoxy by 1 order of magnitude. A sudden jump of electrical conductivity by a factor of ~ 10^9 is observed for 0.1 wt. % CNT/Ep nanocomposite (7.7E-5 S/m) as compared to Ep. This suggests the formation of electrically conductive network of CNTs have provided a path to flow charge through the nanocomposites. The minimum amount of CNTs required to form an electrically conductive path is defined as electrical percolation threshold concentration. It is marked by a sudden rise in electrical conductivity of base polymer. Figure 5.7(a) reveals that the percolation concentration for the epoxy is somewhere between 0.05 and 0.1 wt.% CNT/Ep. Beyond 0.1 wt%, the electrical conductivity of epoxy increases slowly and saturates around 0.5 wt% CNT concentration (9.2E-3 S/m). The maximum electrical conductivity of 0.1 S/m is calculated for 3 wt. % CNT/Ep. This study predicts 0.1 wt. % CNT is the optimum loading of CNT to form a conducting network into epoxy. Theoretically electrical percolation threshold can be obtained by using power-law model [168],

$$\sigma_{DC} = \sigma_0(\phi - \phi_c)^t \qquad 5.4$$

σ_0 is conductivity of CNTs and t is the critical exponent which defines the dimensionality of CNTs network within the polymer. ϕ and ϕ_c are the weight fraction and percolation threshold

weight fraction of CNTs respectively. In this model, ϕ_c varies until the best linear fit (see, Fig. 5.7(b)) is obtained for $\log_{10} \sigma_{DC}$ vs $\log_{10} (\phi - \phi_c)$ plot. The value of ϕ_c and σ_0 is found to be 0.098 and 0.18. The 2D dimensional network of CNTs is suggested within the epoxy as *t* is found to be 1.1 [168].

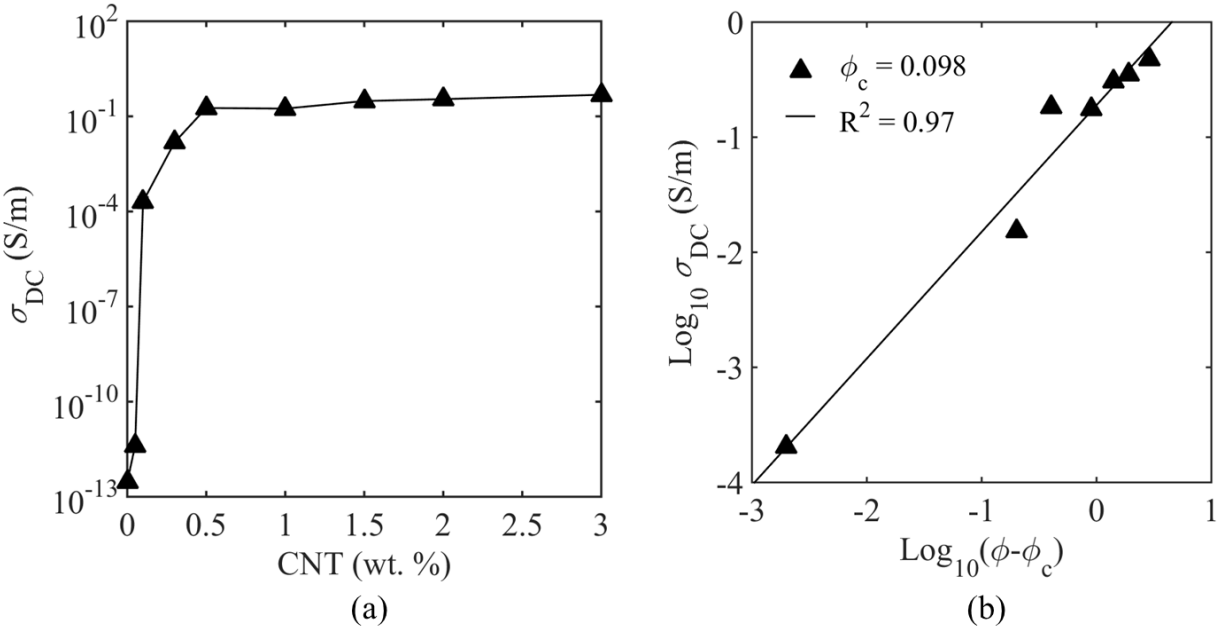

Figure 5.7. (a) Electrical conductivity of CNT/Ep nanocomposites at different wt. % of CNTs. (b) Powel law fitting to determine the electrical percolation threshold.

5.3.3 Effect of CNT dispersion on the fracture toughness of epoxy

Viscosity and electrical conductivity measurements show that the optimal loading of CNTs in epoxy is in the range of 0.1 and 1 wt%. Fracture tests are performed for all CNT/Ep nanocomposites to characterize the effect of CNT dispersion on the fracture toughness K_{IC} of epoxy in Fig 5.8. The K_{IC} 0.64 ± 0.04 MPa.m$^{1/2}$ obtained for Ep agrees well with the value reported in the literature (0.48 – 2.04) MPa. m$^{1/2}$ [169]. The lower K_{IC} obtained for Ep shows less resistance to crack growth. Adding CNT into epoxy shows steady enhancement in the K_{IC} up to 0.5 wt.% and reaches maximum improvement in fracture toughness by 61% at 1 wt. % CNT loading. This suggests 1 wt% may be the optimum loading of CNT needed to enhance both electrical conductivity and fracture toughness of the nanocomposite with minimum increase in viscosity. The enhanced fracture toughness is due to the huge surface area of dispersed CNT into epoxy that effectively transfers mechanical load from epoxy to CNT [170–173]. As the crack propagates, CNTs can hinder the growth of the crack or may deflect, and pull-out of CNTs (see Fig. 5.9 (b1-b2)) from epoxy may happen as compared to smooth growth of crack in epoxy (see

Fig. 5.9 (a1-a2)) resulting in higher toughness of nanocomposite [150,174]. CNT beyond optimum 1 wt. % may agglomerates (see, Figs 5.6(e) and (f)) and lead to a decrease in fracture toughness due to a lower effective surface area of CNTs. However, localized inelastic matrix deformation, void nucleation, and crack deflection at the agglomerates can contribute to the toughening mechanism in the nanocomposites [149] yet still higher K_{IC} than Ep.

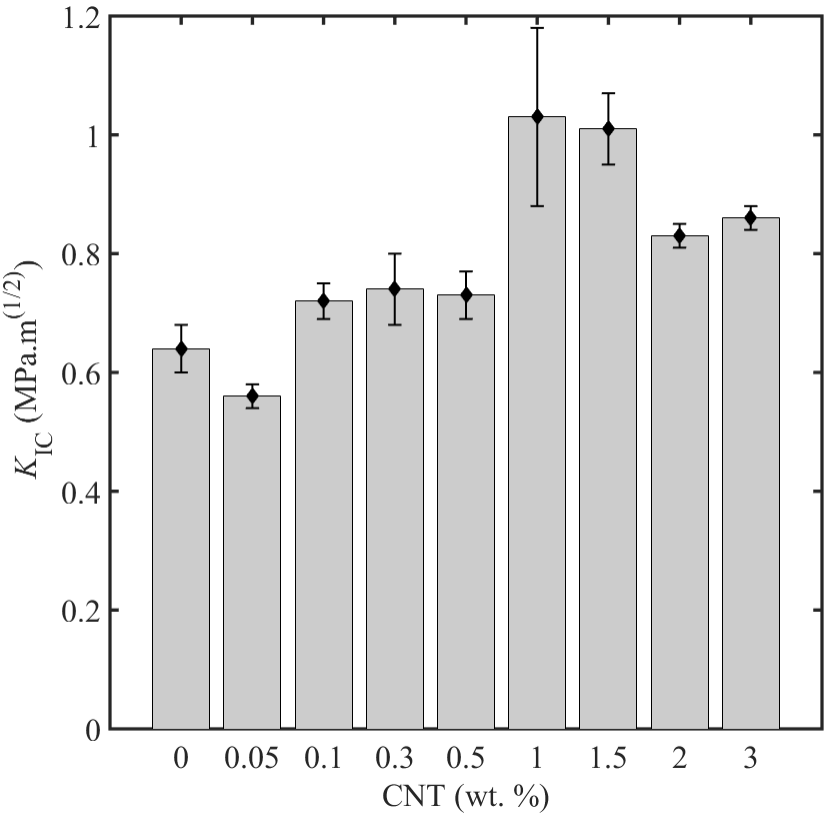

Figure 5.8. Effect of CNT loading on fracture toughness of CNT/Ep nanocomposites.

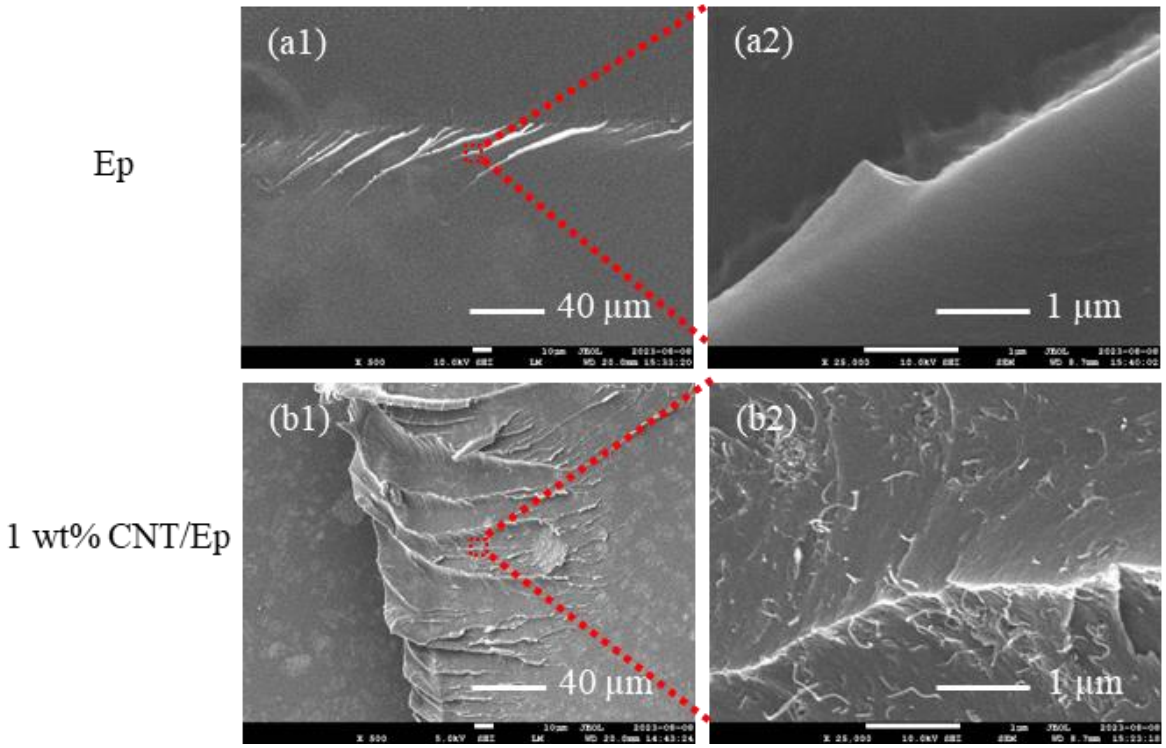

Figure 5.9. FESEM micrographs for Ep and optimum 1wt% CNT/Ep failed fracture samples.

5.4 Conclusion

Carbon nanotubes modified epoxy (CNT/Ep) nanocomposites with varying concentration of CNTs are prepared to determine the optimum loading of CNTs needed to improve the electrical conductivity and fracture toughness with minimum increment in viscosity. Adding CNT into epoxy increases the viscosity of CNT/Ep solution. The electrical percolation threshold lies between 0.05 and 0.1 wt% as a sudden jump of ~ 10^9 is observed in the magnitude of electrical conductivity. Beyond 0.1 wt%, enhancement in the electrical conductivity with the addition of CNT into epoxy is not much and it saturates around 0.5 wt% CNT loading. Moreover, the maximum improvement in fracture toughness by 61% is observed for 1 wt% CNT/Ep nanocomposites as compared to Ep. Thus, 1 wt% CNT is taken as the optimum loading to enhance the electrical conductivity and fracture toughness of epoxy.

Chapter 6: Synergetic effects of carbon fiber functionalization and CNT modified epoxy on the interfacial shear strength of carbon fiber/epoxy composites

Molecular dynamics (MD) simulations carried out in Chapters 3 and 4 suggest that modifying the carbon fiber surface with functional groups enhances the interfacial thermal conductivity and interfacial shear strength in carbon fiber/epoxy composites. Experimental work performed in Chapter 5 shows that 1wt% is the optimum loading of carbon nanotubes (CNTs) to enhance the electrical conductivity and fracture toughness of epoxy. Thus, functionalized carbon fiber reinforced with CNT modified epoxy (CNT/Ep) may improve the thermal conductivity, electrical conductivity, and mechanical properties of conventional carbon fiber/epoxy composites. An experimental verification of the MD simulation predictions is carried out in this chapter. Later, the possibility of harnessing the synergetic effects of carbon fiber functionalization and CNT modified epoxy to induce multifunctionality in conventional carbon fiber/epoxy composites is discussed.

6.1 Introduction

Carbon fiber reinforced plastics composites (CFRPs) are increasingly used in structural applications due to their superior properties such as high specific strength, high specific stiffness, good corrosion resistance, and low maintenance cost [20,128–130]. The mechanical properties of composites are governed by the fiber, matrix, and the interface between carbon fiber and matrix [23]. Matrix cracking, interfacial debonding, and delamination are common failure modes in composites [131–133]. The surface of carbon fiber is inert in nature and does not react or form any covalent bond with the matrix [44–46]. This results in the poor interfacial adhesion between the fiber and matrix which limits the overall load-carrying capabilities of composites [49]. It is the interface through which the applied load gets transferred from the matrix to the reinforcing fiber [175]. Such a transfer occurs in the form of interfacial shear stresses which are normally evaluated in terms of interfacial shear strength (IFSS) of the composite [90,91]. Thus, the stress transfer capability of an interface is a function of the interaction between the fiber and matrix, which can be controlled by the surface morphology of the fiber and the type of matrix used to process the composite [54].

Various strategies such as dip coating [51,52], nanoparticle grafting [53–55], thermal treatment [56,57], plasma treatment [58,59], high-energy irradiation [60,61], matrix modification [55,62–64], sizing [52,62,65] and chemical modification [66–74] have been implemented to increase the interfacial adhesion between fiber and matrix. Among these, chemical modifications have shown significant improvement in IFSS due to the mechanical interlocking and covalent bonding between functionalized fiber and polymer [61,66,70,71]. Pull-out, fragmentation, push-out, and microbond tests are commonly used experimental techniques to determine IFSS. However, a larger volume fraction of polymer undermines the influence of interface in these techniques [55]. Microbond test is more suited to characterize the interface [139]. Therefore, an experimental investigation is performed to characterize the synergetic effects of carbon fiber functionalization and CNT modified epoxy on the IFSS in carbon fiber/epoxy composites.

To this end, carbon fibers are functionalized with aniline molecule. Microbond test is performed to obtain the IFSS of functionalized and unfunctionalized carbon fiber/epoxy composites. Thereafter, IFSS of unfunctionalized and functionalized carbon fiber with CNT modified epoxy is evaluated. Fractography of tested samples is performed to gain interfacial failure mechanisms in different material combinations.

6.2 Experimental details

6.2.1 Materials

Carbon fibers (230 GSM, density 1.8 g/cc, average modulus 100 GPa) are purchased from Hindustan Technical Fabrics, India. Multi-walled carbon nanotubes (MWCNTs) (Product specification, CAS 308068-56-6) are procured from Nano Research Elements, India. Carbon nanotubes (CNTs) diameter is about 10 – 30 nm and 3 – 10 μm in length as per the supplier. Bisphenol-A Epofine 556 and Finehard 5200 (Fine Finish Organics Pvt. Ltd., India) are used as epoxy resin and hardener respectively.

6.2.2 Characterization

Thermogravimetric (TGA/DSC 1 STARe SYSTEM, Mettler Toledo) analysis is carried out from 25 ^{o}C to 1000 ^{o}C with a heating rate of 20 ^{o}C/min under air and nitrogen (inert gas). X-ray photoelectron spectroscopy (XPS, Escalab 250Xi, Thermo Fisher Scientific) is performed to detect the attachment of functional group on carbon fiber (analysis area of 0.3 mm × 0.3 mm) with a monochromated Al K_{α} source spot size of 600 μm and analysis depth may vary up to 10

nm. The fractography analysis of tested samples is done under field emission scanning electron microscopy (FESEM, JEOL, JSM-7610F, Japan) to understand the interfacial failure mechanisms of various fiber (unfunctionalized and functionalized) and matrix (neat epoxy and CNT modified epoxy) combinations. ^{1}H, ^{13}C, ^{19}F Nuclear magnetic resonance (NMR) spectra are recorded in $CDCl_3$ on JEOL JNM-ECS spectrometer, Japan at operating frequencies of 400 MHz {^{1}H} or 101MHz {13C} as indicated in the individual spectrum. Chemical shifts (δ) are given in parts per million (ppm) relative to residual solvent ($CDCl_3$, δ= 7.26 for ^{1}H NMR and 77.16 for ^{13}C NMR) and coupling constants (J) in Hz. Data for ^{1}H NMR spectra are reported as follows: chemical shift (multiplicity, coupling constants, number of hydrogens). Multiplicity is tabulated as *s* for singlet, *d* for doublet.

6.2.3 Unsized carbon fiber

Carbon fiber purchased from manufacturer has sizing layer which enables ease in handling of fiber named as received carbon fiber. Complete removal of sizing layer is a must to get graphitic surface of carbon fiber. Therefore, TGA is performed on as received carbon fiber. Fig. 6.1(a) shows thermal degradation of carbon fiber in air and nitrogen (inert gas) environment. The whole carbon fiber is decomposed in the air as shown in Fig. 6.1(a) while 6.5% loss of mass is observed in the presence of inert nitrogen gas and it gets stable from 600 K onwards suggest complete removal of sizing layer as shown in Fig. 6.1(b). Therefore, based on the results obtained from TGA. As received carbon fiber (3.8 g, 210 mm × 80 mm) is placed in the chemical vapour deposition at 650 ^{o}C for 15 minutes to ensure complete removing of sizing layer in the presence of argon (inert gas) named as unsized carbon fiber. The weight of unsized carbon fiber is measured as 3.55 g which results into the loss of 6.5% mass of as received carbon fiber same as obtained in TGA.

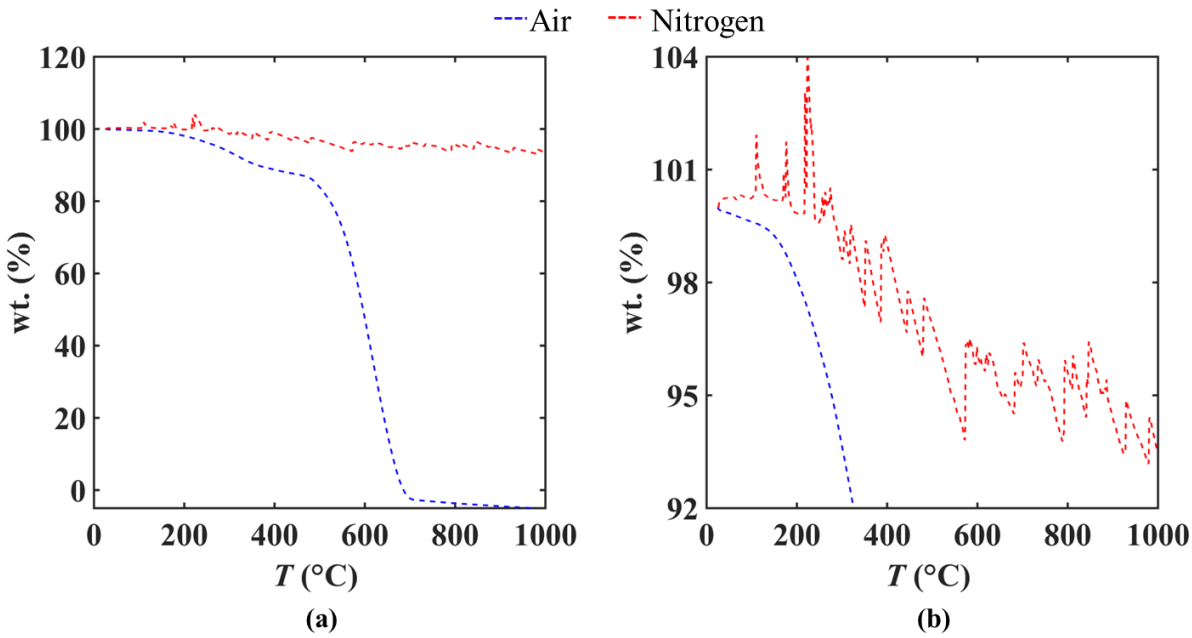

Figure 6.1. (a) Thermal degradation of as received carbon fiber under presence of air and nitrogen (inert gas), and (b) is zoom image of Fig. 6.1 (a).

6.2.4 Synthesis of aniline functionalized carbon fiber

6.2.4.1 Synthesis of N-(4-aminophenyl)-2,2-2-trifluoroacetamide

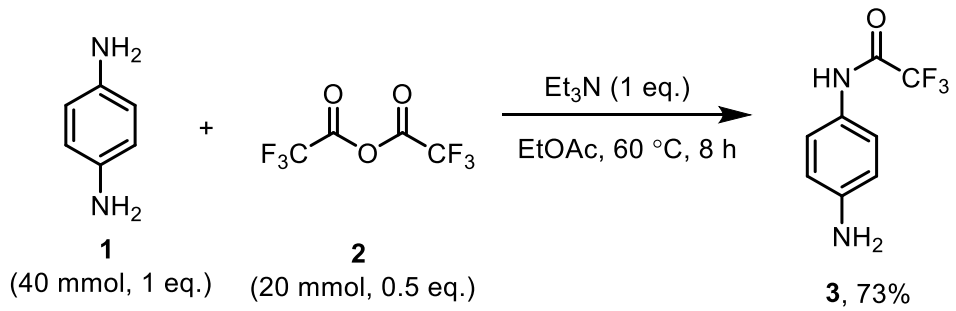

Figure 6.2. Scheme of chemical reactions to prepare N-(4-aminophenyl)-2,2,2-trifluoroacetamide.

Fig. 6.2 shows scheme adopted in the present work to prepare N-(4-aminophenyl)-2,2,2-trifluoroacetamide. Firstly 2,2,2-trifluoroacetic anhydride (4.37 mL, 20 mmol) is added to benzene-1,4-diamine (4.32g, 40 mmol) placed in round bottom flask under nitrogen inert gas to prepare the solution. Then, ethyl acetate anhydride is added to solution using syringe through septum followed by triethylamine (3.4 mL, 2.4 mmol). Then, solution is left for stirring at 60 ^{o}C for 8 hours to complete reaction. Thin layer chromatography is performed on obtained solution under 25% ethyl acetate-hexane and two spots are observed under ultraviolet ray lamp which

suggests the two possible end products of a reaction. Then, two end products are separated using column chromatography. Then, solvent in solution is evaporated using rotameter. Finally, N-(4-aminophenyl)-2,2,2-trifluoroacetamide (2g, brownish color) yield 46% is obtained.

Characterization data of N-(4-aminophenyl)-2,2,2-trifluoroacetamide (3): Yield: 2 g (46%); Color: Brown solid; ^{1}H NMR (400 MHz, $CDCl_3$) δ 10.31 (s (br), 2H), 7.26 (d, *J* = 1.3 Hz, 4H); ^{13}C NMR (101 MHz, $CDCl_3$) δ 154.54 (d, *J* = 37.1 Hz), 133.34, 120.83. ^{19}F NMR (376 MHz, $CDCl_3$) δ -74.34.

NMR Spectra's of N-(4-aminophenyl)-2,2,2-trifluoroacetamide (3):

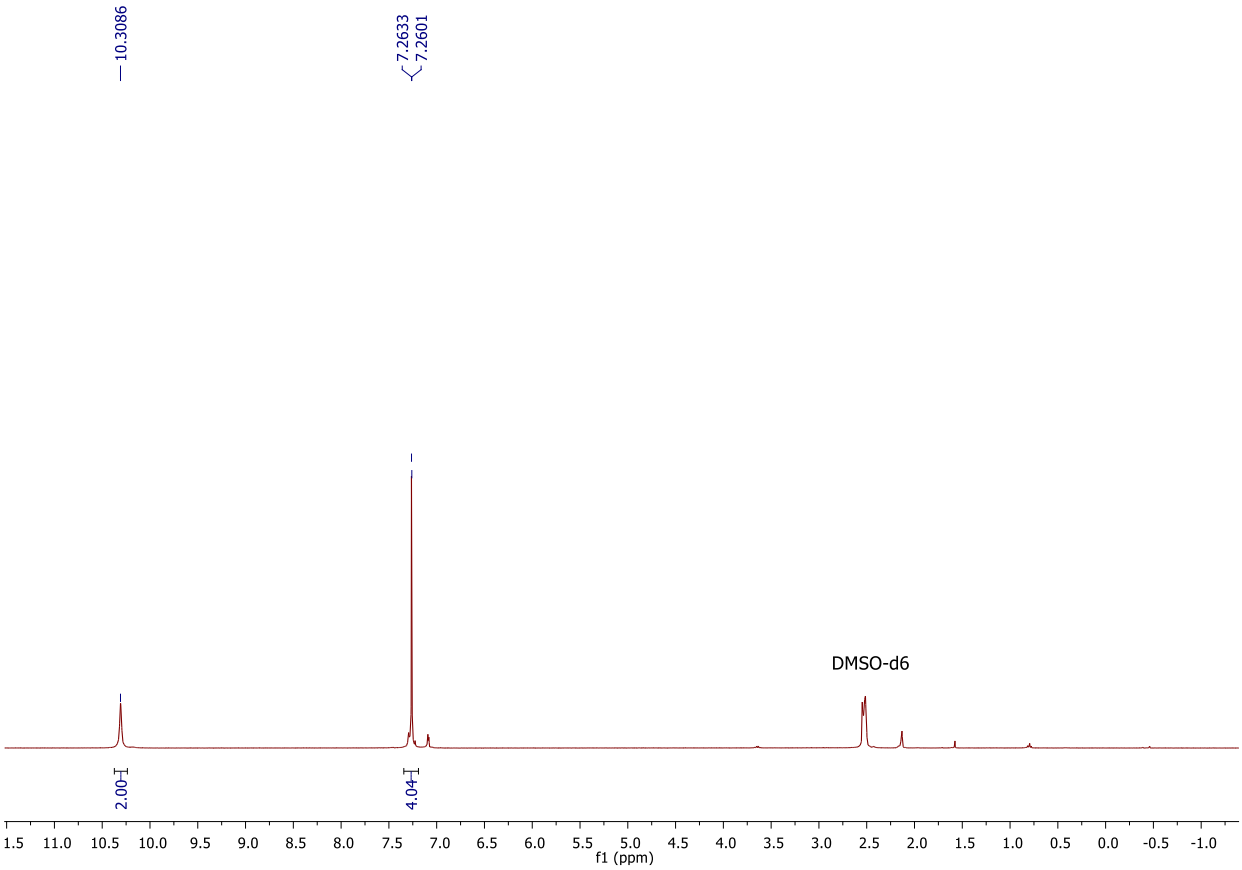

Figure 6.3. ^{1}H NMR, 400 MHz, $CDCl_3$ for N-(4-aminophenyl)-2,2,2-trifluoroacetamide.

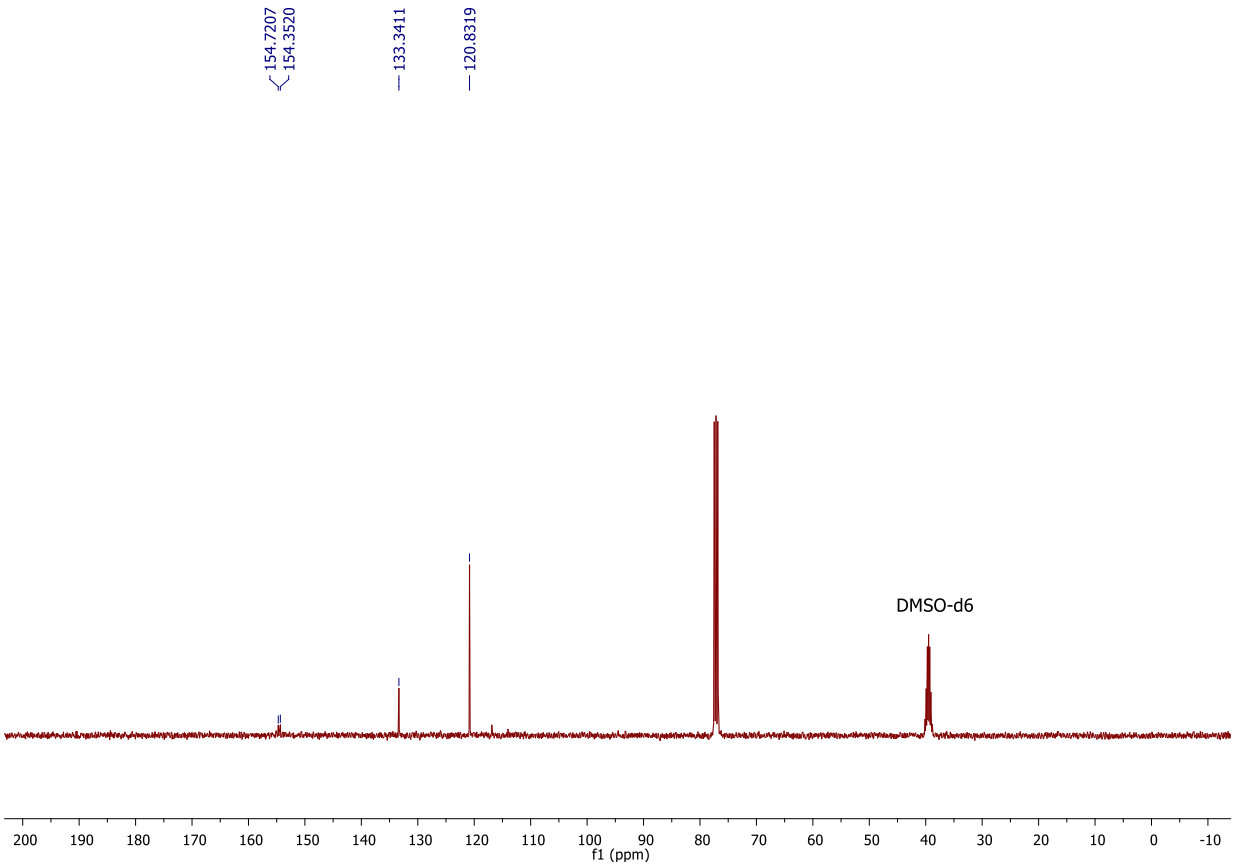

Figure 6.4. ^{13}C NMR, 101 MHz, $CDCl_3$ for N-(4-aminophenyl)-2,2,2-trifluoroacetamide.

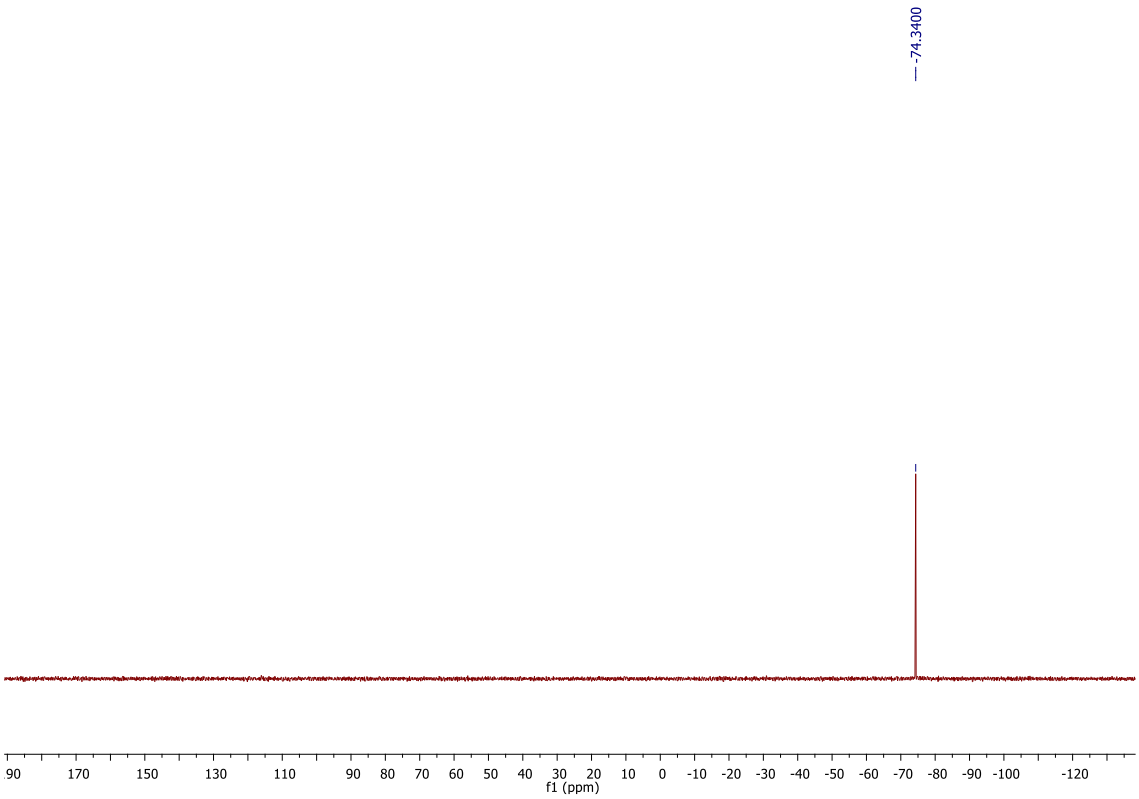

Figure 6.5. ^{19}F NMR, 376 MHz, $CDCl_3$ for N-(4-aminophenyl)-2,2,2-trifluoroacetamide.

6.2.4.2 Chemical attachment of aniline to carbon fiber

Functionalization of unsized carbon fiber with N-(4-aminophenyl)-2,2,2-trifluoroacetamide is done following the approach in the literature [92] and shown in Fig 6.6. Initially, solution of ortho-dichlorobenzene (20 mL), acetonitrile (10 mL) and N-(4-aminophenyl)-2,2,2-trifluoroacetamide (104 mg, 0.5 mmol) is degassed in a 250 mL round bottom flask in inert nitrogen gas for 1 hour. Then, unsized carbon fiber (233 mg) is submerged in the solution, followed by addition of tert-butyl nitrile (111 µL, 0.93 mmol) and heated at 50 ^{o}C by placing reaction vessel in an oil bath. The reaction is carried out for 24 hours with a reflux condenser under nitrogen atmosphere. After that, solution is decanted and resuspended followed by manual agitation in chloroform until solution becomes clear. Then carbon fibers are placed in a buchner funnel and rinsed with equal proportions of dichloromethane, ethanol and acetone (200 mL) under vacuum filtration which is followed by drying under reduced pressure for 24 hours to yield aniline-flourine tag functionalized carbon fibers. Boc group is removed from aniline-flourine tag functionalized carbon fiber using acidic wash to give free amine so that it can react with epoxy molecules named as aniline-carbon fiber.

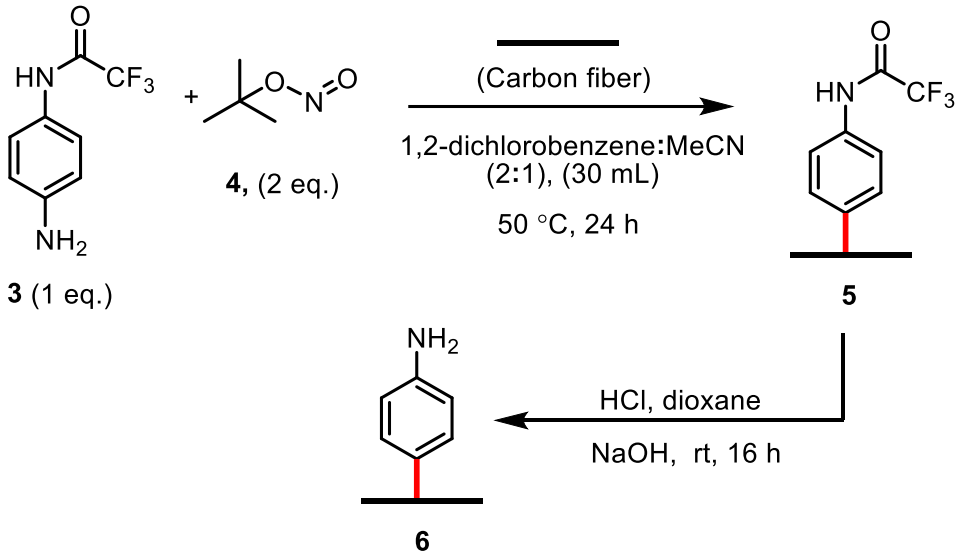

Figure 6.6. Scheme to prepare aniline functionalized carbon fiber.

6.2.5 Composite preparation

Individual fiber filaments are carefully extracted from a fiber tow (see, Fig. 6.7(a)) and attached to a hollow rectangular frame (see, Fig. 6.7(b)). Neat epoxy (Ep) is prepared by mixing of epoxy resin and hardener solutions in a 100:24 ratio by wt. Then a drop of the matrix is poured over the fiber filament, and as soon as the drop makes contact with the fiber it disintegrates into multiple

micro-sized droplets as shown in Fig. 6.7(c). The single fiber/epoxy composite samples are cured under vacuum oven at 80 ℃ for 6 hours, followed by 120 ℃ for 2 hours and 160 ℃ for 6 hours respectively. 1wt% CNT in the epoxy is chosen to make CNT modified epoxy (CNT/Ep) as it gives enhanced electrical conductivity with improved fracture toughness, and keeping the minimum viscosity observed in chapter 5. 1 wt% are dispersed into epoxy resin and hardener in equal proportion of (100:24) using an ultrasonic probe sonicator (750 W, 20 kHz, probe tip 13mm, Cole-Parmer, USA) at 50% amplitude for 120 min. The maximum temperature of CNT modified Ep resin and hardener during sonication is kept at less than 70 ^{o}C [155]. After sonication, the CNT dispersed resin and hardener solutions are uniformly mixed in a 100:24 ratio by wt. and stirred with a glass rod. Then a drop of matrix (CNT/Ep) is poured over a fiber filament followed the same procedure as done for fiber/epoxy composite. In this way, various combinations of (unfunctionalized and functionalized) carbon fiber and (Ep and CNT/Ep) matrix are prepared.

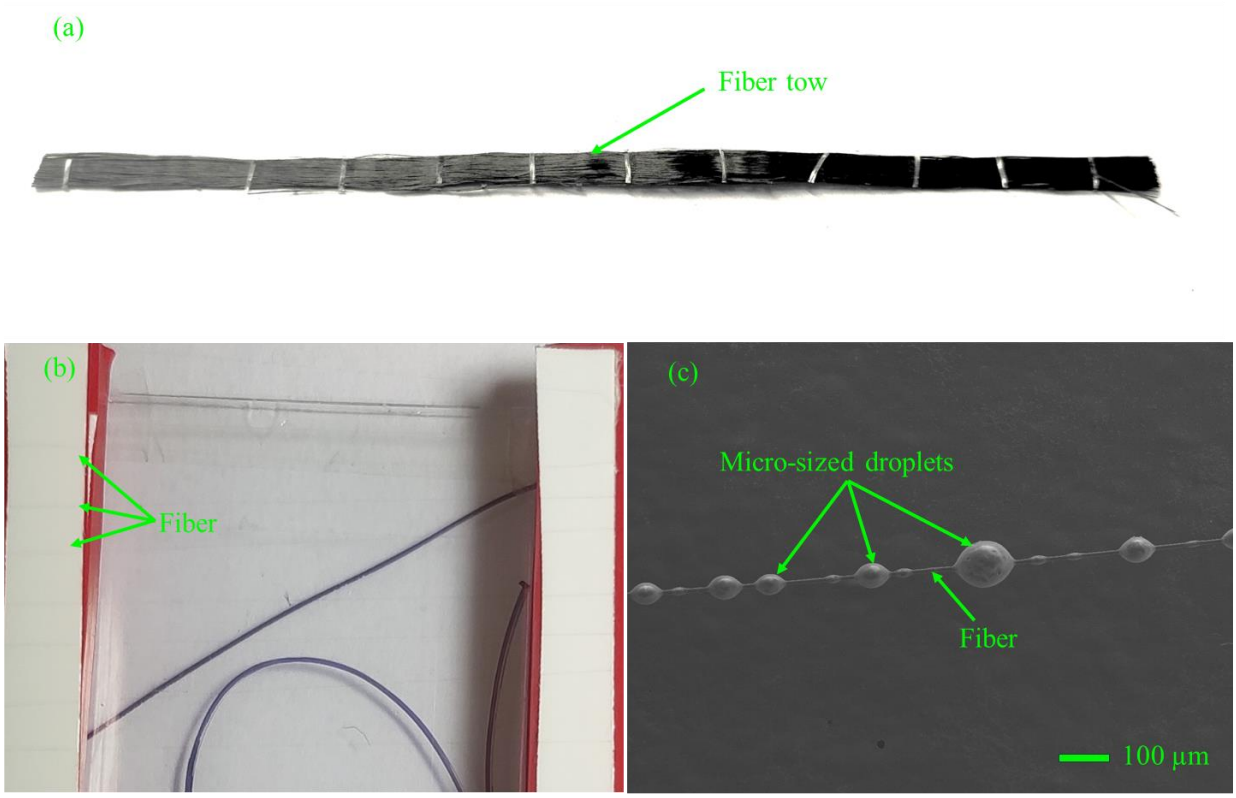

Figure 6.7. (a) Fiber tow. (b) Individual fiber filaments on a rectangular frame. (c) Multiple micro-sized droplets on a single carbon fiber.

6.2.6 Microbond test

Fig. 6.8(a) illustrates the experimental set-up consisting of a single carbon fiber held in a grip. Microdroplets of matrix on carbon fiber is visible in the zoomed view (see, Fig. 6.8(b)) of Fig.

6.8(a). A Dino-Lite optical camera is installed for live recording of the test. To evaluate the IFSS of the fiber/matrix interface in each sample, microbond tests are performed on a universal testing machine (Shimadzu, Japan) at a crosshead speed of 0.005 mm/min. Microdroplet get stuck in the vice edge and fiber is pulled until fiber/epoxy interface fails. From the recorded load versus displacement data, the maximum debond force (F_{max}) is extracted and plotted as a function of the embedded length l_e of the microdroplet. A linear curve is fitted to the experimental data points and the slope of the fit is calculated to find the IFSS as per Eq. [55],

$$\tau_{IFSS} = \frac{F_{max}}{\pi d l_e} \qquad 6.1$$

where, F_{max} is the maximum force obtained during the microbond test, d is the diameter of carbon fiber (7 μm), and l_e is the embedded length of the microdroplet.

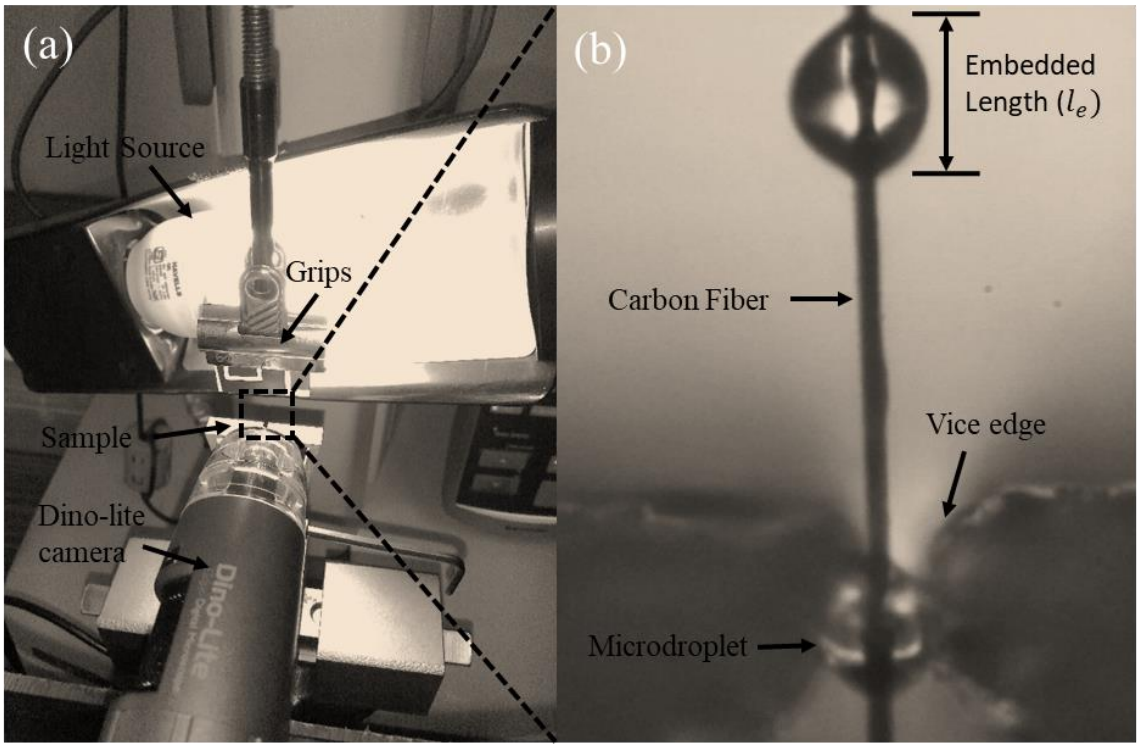

Figure 6.8. (a) Experimental setup of the microbond test. (b) Optical image of microdroplets present on a single carbon fiber filament.

6.3 Results and discussion

6.3.1 XPS analysis of functionalized fiber

To decide whether carbon fibers are functionalized or not functionalized, XPS is performed systematically on as received carbon fibers, unsized carbon fibers, functionalized aniline-fluorine tag carbon fiber and aniline-carbon fiber. Figure 6.9 shows XPS spectrum for all the samples. Figure 6.9(a) shows C1s spectrum, two peaks are obtained for as received carbon fibers at 284.6 eV and 285.9 eV corresponds to C=C (sp^2 graphitic structure) and C-O bonds [78,150]. As received carbon fiber have similar elemental composition as unsized carbon fiber and consists of carbon, oxygen, and nitrogen element in Fig 6.9(b) and (c). Therefore, an element fluorine atom is chosen to help us in identifying the attachment of functional group to carbon fiber. It also provide free amine after acidic washing to form covalent bond with epoxy molecules. Figure 6.9(d) shows peak corresponds to aniline-flourine tag carbon fiber which is absent in rest of fibers and confirms the attachment of aniline-flourine tag to carbon fiber. To make aniline reaction with epoxy molecules, aniline-fluorine tag carbon fiber is washed in acidic medium to release free amine named as aniline-carbon fiber. No fluorine peak is observed in Fig. 6.9(d) after this step. Once, it is understood that aniline is attached to the carbon fiber. It is necessary to quantify the numbers of aniline that are attached with carbon fiber.

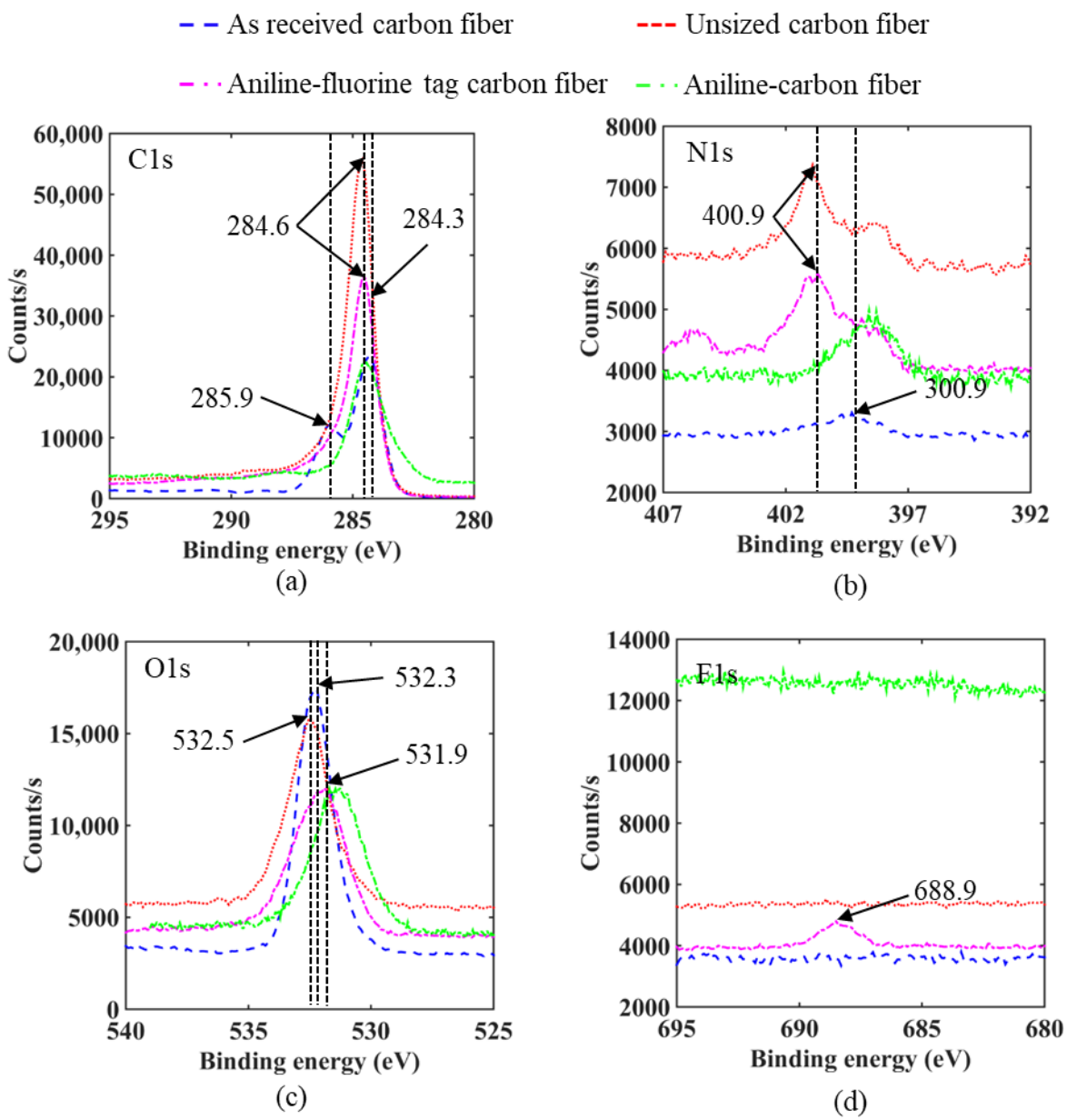

Figure 6.9. XPS spectrum obtained for all samples (a) C1s , (b) N1s, (c) O1s and (d) F1s.

Table 6.1 shows atomic % concentrations obtained for samples. Once as received carbon fiber is heated to get unsized carbon fiber. It is observed that the heating of fibers under inert gas reduces the oxygen concentrations and increases nitrogen as well as carbon content. Functionalized aniline-fluorine tag carbon fiber shows presence of 1.1% of atomic concentrations of fluorine. Atomic concentration also increases by 1.35% and 2.03% for oxygen and nitrogen for unsized carbon fiber. Acidic washing of aniline-flourine tag carbon fiber give aniline-carbon fiber. Nitrogen content for both aniline-flourine tag carbon fiber and aniline-carbon fiber are similar. The increase in oxygen elemental composition suggest some oxidation reaction in fiber.

Tabel 6.1. Atomic % concentrations detected by XPS survey for all types of carbon fibers.

S. no.	System	C1s	N1s	O1s	F1s
1	As received carbon fiber	80.49	1.22	18.29	NA
2	Unsized carbon fiber	87.73	3.36	8.9	NA
3	Aniline-flourine tag carbon fiber	83.25	5.39	10.25	1.10
4	Aniline-carbon fiber	78.27	5.22	16.51	NA

In MD simulations, degree of functionalization (*f*) is defined as the ratio of number of carbon atoms that are attached to a functional group to the total number of carbon atoms present in a graphene sheet [140]. However, Atomic concentrations obtained from XPS can have atomic concentrations up to depth of 10 nm. Consider interlayer distance of graphene 3.35 Å gives equivalent data of ~ 30 graphene. Normalized atomic ratio in Table 6.2 obtained for aniline-flourine tag carbon fiber equivalent to 1.3% *f* are underestimated compared to the MD simulations.

Tabel 6.2. XPS normalized atomic ratio obtained for aniline-fluorine tag carbon fiber.

Element	Normalized Atomic ratio
C	1
N	.065
O	.123
F	.013

6.3.2 Effect of functionalization and CNT/Ep on the IFSS of carbon fiber/epoxy composites

The mechanical properties of CFRPs are influenced by the interfacial adhesion of fiber-matrix interface. The higher interfacial adhesion of composites signifies better stress transfer from matrix to reinforcing filler that makes optimal use of reinforcement in composites. From the linear fits in Fig. 6.10(a1-a2), the IFSS is calculated and presented in Fig. 6.10(b1-b2). Functionalization of carbon fiber with anilines shows IFSS of 37.6 MPa which is 149% higher as compared to unfunctionalized unsized carbon fiber. This suggests better adhesion between

carbon fiber and epoxy which is evident by the presence of chunks of polymer on debonded aniline-carbon fiber/Ep composite (see Fig. 6.11(b)) as compared to the clean fiber observed in unsized carbon fiber/Ep composite (see Fig. 6.11(a)). Comparing Table 6.3 and 6.4, direct comparison of findings obtained in the experiments and MD simulations seems unfair due to constraint on pull-out velocity but trends in results can be compared. Similar improvement is observed in MD simulations for 1% *f* aniline-carbon fiber/Ep composite. Unsized carbon fiber/CNT/Ep shows the improvement in IFSS by 58% as compared to unsized carbon fiber/Ep composite. This suggests better interfacial adhesion as observed in Fig. 6.11(c). Moreover, aniline-carbon fiber/CNT/Ep shows the maximum improvement in the IFSS by 227% as compared to unsized carbon fiber/Ep composite. FESEM micrographs shows a large chunk of matrix in case of debonded aniline-carbon fiber/CNT/Ep composite (see Fig. 6.11(d)). This suggests that harnessing the synergetic effects of aniline-carbon fiber and CNT modified epoxy are beneficial to increase the IFSS. Thus, it is expected to provide multifunctionality with improving interfacial thermal conductivity of carbon fiber/epoxy interfaces along with better electrical, mechanical properties of CNT/Ep over the conventional carbon fiber/Ep composites.

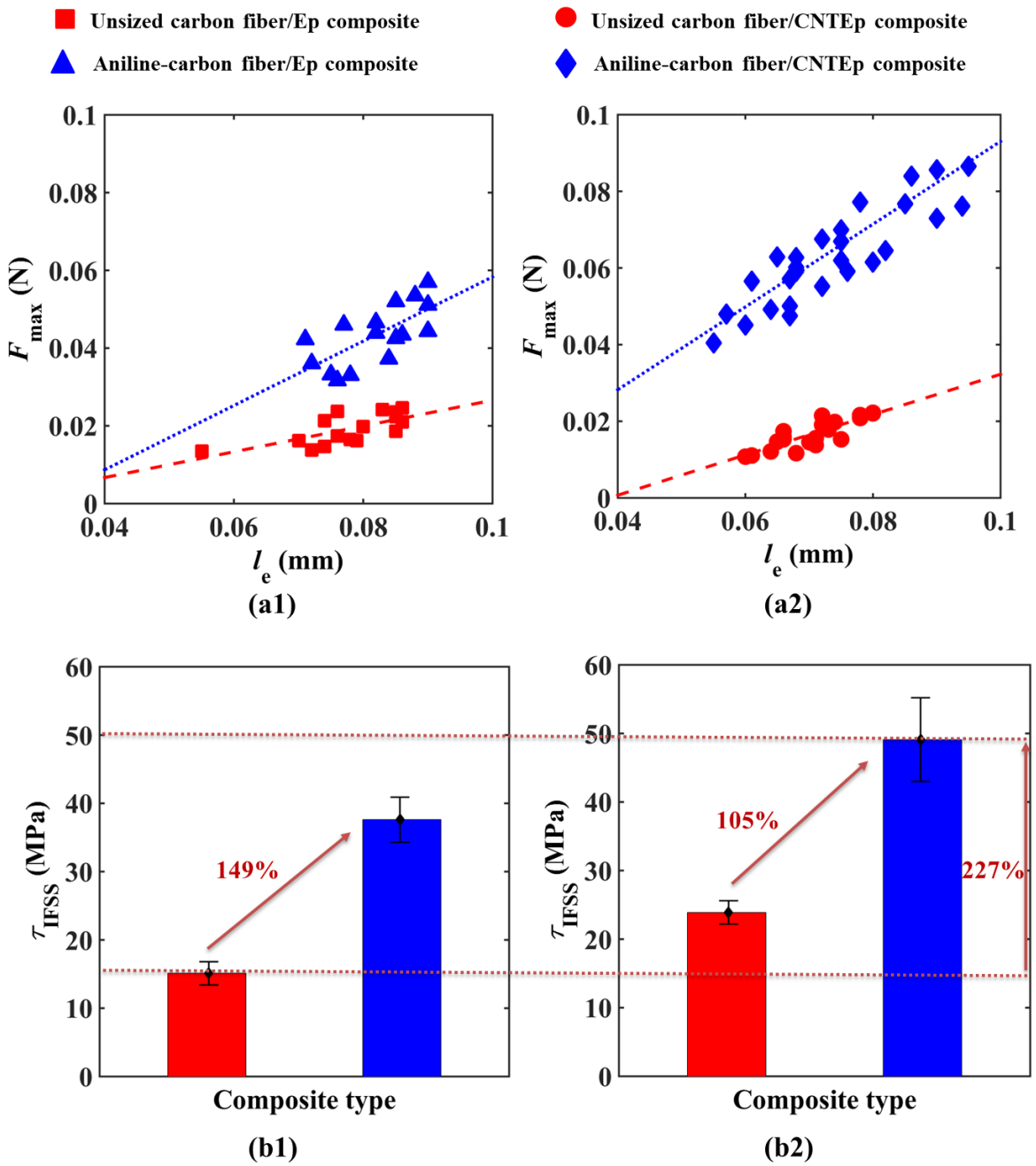

Figure 6.10. Maximum debond force (F_{max}) with respect to the embedded length (l_e) of microdroplets for (a1) unsized and aniline-carbon fiber/Ep and (a2) unsized and aniline-carbon fiber/CNTEp composite. IFSS obtained for unsized and aniline-carbon fiber with (b1) Ep and (b2) CNT/Ep. The markers correspond to the experimental results, while the lines represent linear fits to the experimental data (a1 – a2).

Table 6.3. Experimental IFSS obtained for composites.

Composite type	IFSS (MPa)		% change
	Ep	CNT/Ep	

Unsized carbon fiber	15.1 ± 1.7	23.9 ± 1.7	58%
Aniline-carbon fiber	37.6 ± 3.3	49.1 ± 6.1	30%
% change	149%	105%	

Table 6.4. MD results predicted IFSS obtained for composites.

MD system	1% *f*	5% *f*	10% *f*
	IFSS (MPa)	IFSS (MPa)	IFSS (MPa)
Unsized carbon fiber/Ep	54.8	54.8	54.8
Aniline-carbon fiber/Ep (% change)	141.5 (158.2%)	485.2 (785.4%)	652.3 (1090.3%)

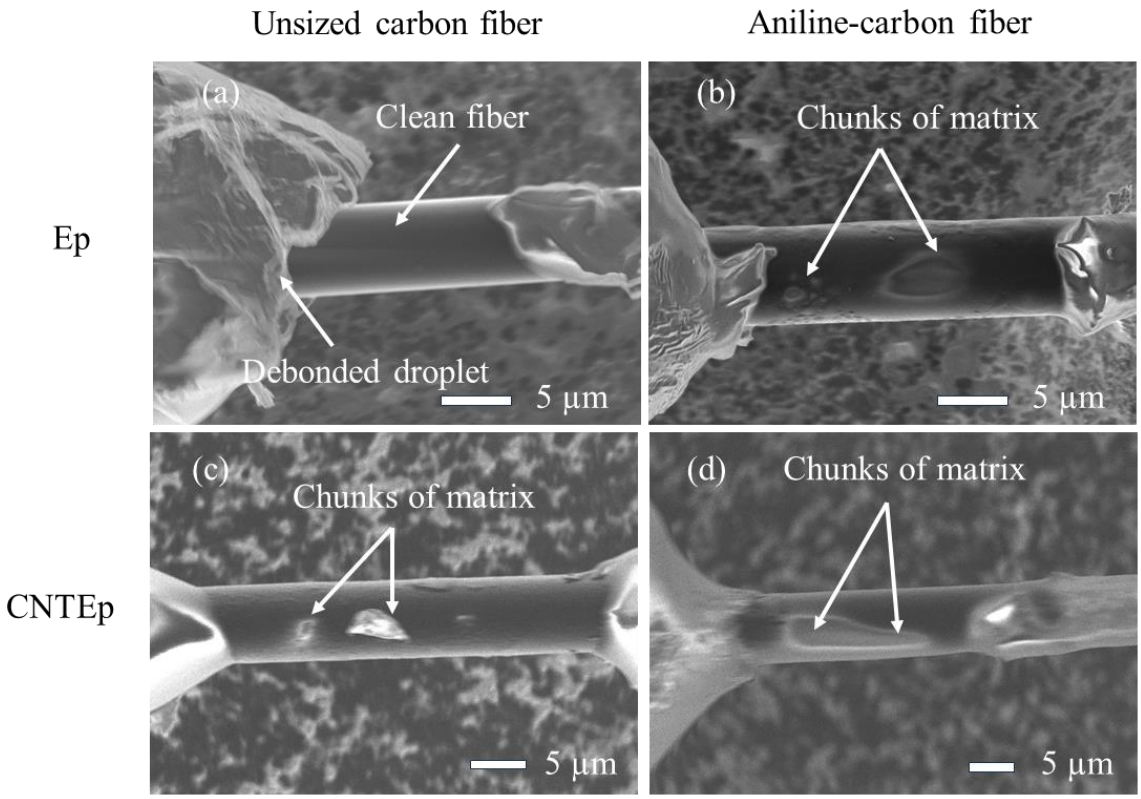

Figure 6.11. FESEM micrograph of: (a) unsized carbon fiber/Ep, (b) aniline-carbon fiber/Ep, (c) unsized carbon fiber/CNT/Ep, (a) aniline-carbon fiber/CNT/Ep deboned samples.

6.4 Conclusion

Synergetic effects of carbon fiber functionalization and CNT modified epoxy on the interfacial shear strength (IFSS) of carbon fiber/epoxy composites is explored. Single fiber/matrix composites of various combination of fiber (unfunctionalized and functionalized) and matrix (neat epoxy and CNT modified Epoxy) are prepared. Firstly, aniline-carbon fiber is synthesized and attachment of aniline to carbon fiber is confirmed by NMR and XPS. Microbond test is performed to evaluate the IFSS of various type of composites. Aniline-carbon fiber/Ep shows the improvement in IFSS by 149% as compared to unsized carbon fiber/Ep closer to MD predictions for 1% *f* aniline-carbon fiber/Ep system. Large chunks of polymer on debonded aniline-carbon fiber/Ep suggest better adhesion between functionalized carbon fiber and epoxy. Moreover, the aniline-carbon fiber/CNT/Ep shows the maximum improvement in the IFSS by 227% as compared to unsized carbon fiber/Ep among all combinations. This suggests harnessing synergetic effects of aniline-carbon fiber and CNT modified epoxy is suitable engineering strategy that can be adopted to induce multifunctionality over conventional carbon fiber/epoxy composites.

Chapter 7: Conclusions and future scope

7.1 Summary of the work

The present study aims to identify suitable strategies to optimally functionalize the carbon fiber/epoxy interface. Molecular dynamics (MD) simulations are performed to optimize the type and number of functional groups to modulate the interfacial thermal conductivity and interfacial interactions of carbon fiber/epoxy interfaces. An experimental investigation is carried out to optimize the loading of carbon nanotubes (CNTs) in epoxy to improve the electrical and mechanical properties of CNT modified epoxy (CNT/Ep) nanocomposites. The synergetic effects of carbon fiber functionalization and optimized CNT/Ep is explored experimentally. The salient features of this thesis are described below.

- MD simulations predict that when carbon fiber is functionalized with different types of small (amine and carboxylic) and large (aniline, single-chain para-amine surface grafted molecules (SGM), and double-chain meta-amine SGM) functional groups, larger functional groups are more effective as compared to small ones to increase interfacial thermal conductivity of carbon fiber/epoxy composites. It is observed that large molecules exhibit more vigorous fluctuations in their end-to-end distances.
- MD microbond simulations suggest the improvement in interfacial shear strength (IFSS) is relatively higher for larger functional groups as compared to small ones. IFSS seems to saturate at a 5% degree of functionalization (*f*) possibly due to saturation of interactions between functional groups and epoxy molecules. Interfacial failure mechanism at functionalized carbon fiber/epoxy strongly depends on the type of functional groups.
- It is concluded that 1 wt% CNT is the optimum loading in epoxy to enhance electrical conductivity with improved fracture toughness, keeping the viscosity at its minimum.
- An experimental study using microbond test shows that aniline-carbon fiber//Ep can enhance the IFSS by 149% as compared to unfunctionalized carbon fiber/Ep found to be closer to MD IFSS results for 1% *f* aniline-carbon fiber/epoxy MD system. Moreover, the synergetic effects of carbon fiber functionalization and CNT modified Ep show the maximum improvement in IFSS of 227% as compared to unfunctionalized carbon fiber/Ep.

In summary, it can be concluded that the interfacial properties of carbon fiber/epoxy composites strongly depend on the type of functional groups, and do not increase much once 5% *f* is reached.

Harnessing the synergetic effects of carbon fiber functionalization and CNT modified epoxy can be an effective strategy to induce multifunctionality in conventional carbon fiber/epoxy composites.

7.2 Future scope

1. Thermal conductivity tests on aniline-carbon fiber/epoxy laminates to verify how the improvement in interfacial thermal conductivity predicted from MD simulations manifest at the bulk level.
2. To study the thermal, electrical, and mechanical properties of aniline-carbon fiber/CNT modified epoxy laminate and compare it with conventional carbon fiber/epoxy composite.
3. Composites are exposed to outdoor conditions during their service life, effects of environmental outdoor conditions should be studied on fabricated composites.
4. Different interfacial failure mechanisms associated with the type of functional groups observed in MD microbond simulations should be implemented through a broad range of functional groups using machine learning to identify the more suitable functional groups.

Publications

Refereed Journals

1. Chauhan, A., Agnihotri, P. K., & Basu, S. (2023). Molecular dynamic study on modulating the interfacial thermal conductivity of carbon fiber/epoxy interfaces. *Computational Materials Science*, *217*, 111914.

2. Chauhan, A., Agnihotri, P. K., & Basu, S. Molecular dynamic study on modulating the interfacial interactions of carbon fiber/epoxy interfaces. (*under review – Composites part B*).

3. Gupta, H., Chauhan, A., Srivastav, M., Agnihotri, P. K., Basu, S., & Gupta, N. A comprehensive investigation of the interplay between electrical, thermal, and mechanical properties of CNT-filled epoxy resin. (*in – preparation*).

4. Chauhan, A., Singh, P. R., Goswami, A., & Agnihotri, P. K., Synergetic effects of carbon fiber functionalization and CNT modified epoxy on the interfacial shear strength of carbon fiber/epoxy composites. (*in – preparation*).

Other Journals

1. Surana, I., Bedi, H. S., Bhinder, J., Ghai, V., Chauhan, A., & Agnihotri, P. K. (2020). Compression and fracture behavior of leather particulate reinforced polymer composites. *Materials Research Express*, *7*(5).

2. Ghai, V., Bedi, H. S., Bhinder, J., Chauhan, A., Singh, H., & Agnihotri, P. K. (2020). Catalytic-free growth of VACNTs for energy harvesting. *Fullerenes Nanotubes and Carbon Nanostructures*, *28*(11), 907–912.

3. Chauhan, A., Bedi, H. S., & Agnihotri, P. K. (2022). Enhancing aging resistance of glass fiber/epoxy composites using carbon nanotubes. *Materials Chemistry and Physics*, *291*, 126740.

Conference Proceedings

1. Gupta, H., Chauhan, A., Agnihotri, P. K., Basu, S., & Gupta, N., Study of EMI Shielding performance of CNT-filled Epoxy Resin. 4th International Conference on High Voltage Engineering and Power Systems 2023 (ICHVEPS 2023), August 6 – 10, 2023, Bali, Indonesia.

Presentations in Conferences

1. Chauhan, A., Bedi, H. S., & Agnihotri, P. K., Interfacial properties of different grades of epoxy reinforced with carbon fiber. 2nd International Conference on Nanoscience and Nanotechnology (ICNAN-2019), November 29 – December 01, 2019, Vellore Institute of Technology, Tamil Nadu, India.

2. Chauhan, A., Bedi, H. S., & Agnihotri, P. K., Effect of carbon nanotubes on the environmental assisted degradation and damage sensing abilities of glass fiber/epoxy composites. 7th International Conference on Mechanics of Composites (MECHCOMP7), September 1 – 3, 2021, University of Porto, Porto, Portugal.

3. Chauhan, A., & Agnihotri, P. K., Molecular dynamic study on investigating the effect of crosslinked networks on thermal conductivity of thermoset epoxy polymer. International Hybrid Conference on Nano Structured Materials and Polymers (ICNP-2023), May 12 – 14, 2023, Mahatma Gandhi University, Kerala, India.

4. Chauhan, A., Molecular dynamic study on investigating the effect of interatomic potentials on mechanical properties of graphene. 3rd International Conference on Recent Advances in Materials & Manufacturing Technologies (IMMT-2023), Nov 20 – 23, 2023, Birla Institute of Technology & Science Pilani, Dubai Campus, Dubai, UAE.

References

[1] J. Baur, E. Silverman, Challenges and structures for aerospace, MRS Bull. 32 (2007) 328–334.

[2] S.L. Gao, R.C. Zhuang, J. Zhang, J.W. Liu, E. Mäder, Glass fibers with carbon nanotube networks as multifunctional sensors, Adv. Funct. Mater. 20 (2010) 1885–1893.

[3] R.F. Gibson, A review of recent research on mechanics of multifunctional composite materials and structures, Compos. Struct. 92 (2010) 2793–2810.

[4] H. Qian, A.R. Kucernak, E.S. Greenhalgh, A. Bismarck, M.S.P. Shaffer, Multifunctional structural supercapacitor composites based on carbon aerogel modified high performance carbon fiber fabric, ACS Appl. Mater. Interfaces. 5 (2013) 6113–6122.

[5] C. González, J.J. Vilatela, J.M. Molina-Aldareguía, C.S. Lopes, J. LLorca, Structural composites for multifunctional applications: Current challenges and future trends, Prog. Mater. Sci. 89 (2017) 194–251.

[6] K.J. Narayana, R.G. Burela, A review of recent research on multifunctional composite materials and structures with their applications, Mater. Today Proc. 5 (2018) 5580–5590.

[7] P. Hung, K. Lau, B. Fox, N. Hameed, J.H. Lee, D. Hui, Surface modification of carbon fibre using graphene-related materials for multifunctional composites, Compos. Part B Eng. 133 (2018) 240–257.

[8] N. Forintos, T. Czigany, Multifunctional application of carbon fiber reinforced polymer composites: Electrical properties of the reinforcing carbon fibers – A short review, Compos. Part B Eng. 162 (2019) 331–343.

[9] C. Robert, I. Pillin, M. Castro, J.-F. Feller, Multifunctional carbon nanotubes enhanced structural composites with improved toughness and damage monitoring, J. Compos. Sci. 3 (2019) 109.

[10] D.D.L. Chung, A review of multifunctional polymer-matrix structural composites, Compos. Part B Eng. 160 (2019) 644–660.

[11] P.K. Mallick, Fiber-reinforced composites: materials, manufacturing, and design, CRC press, 2007.

[12] Q. Zhao, K. Zhang, S. Zhu, H. Xu, D. Cao, L. Zhao, R. Zhang, W. Yin, Review on the electrical resistance/conductivity of carbon fiber reinforced polymer, Appl. Sci. 9 (2019) 2390.

[13] J. Zhang, G. Lin, U. Vaidya, H. Wang, Past, present and future prospective of global carbon fibre composite developments and applications, Compos. Part B Eng. 250 (2023) 110463.

[14] N. Yamamoto, R. Guzman de Villoria, B.L. Wardle, Electrical and thermal property enhancement of fiber-reinforced polymer laminate composites through controlled implementation of multi-walled carbon nanotubes, Compos. Sci. Technol. 72 (2012) 2009–2015.

[15] G.C. Yu, L.Z. Wu, L.J. Feng, Enhancing the thermal conductivity of carbon fiber reinforced polymer composite laminates by coating highly oriented graphite films, Mater. Des. 88 (2015) 1063–1070.

[16] F.S. Wang, Y.Y. Ji, X.S. Yu, H. Chen, Z.F. Yue, Ablation damage assessment of aircraft carbon fiber/epoxy composite and its protection structures suffered from lightning strike, Compos. Struct. 145 (2016) 226–241.

[17] L. Guadagno, L. Vertuccio, C. Naddeo, M. Raimondo, G. Barra, F. De Nicola, R. Volponi, P. Lamberti, G. Spinelli, V. Tucci, Electrical current map and bulk conductivity of carbon fiber-reinforced nanocomposites, Polymers (Basel). 11 (2019) 1865.

[18] E.C. Senis, I.O. Golosnoy, J.M. Dulieu-Barton, O.T. Thomsen, Enhancement of the electrical and thermal properties of unidirectional carbon fibre/epoxy laminates through the addition of graphene oxide, J. Mater. Sci. 54 (2019) 8955–8970.

[19] M. Gagné, D. Therriault, Lightning strike protection of composites, Prog. Aerosp. Sci. 64 (2014) 1–16.

[20] T.R. Pozegic, J. V. Anguita, I. Hamerton, K.D.G.I. Jayawardena, J.S. Chen, V. Stolojan, P. Ballocchi, R. Walsh, S.R.P. Silva, Multi-Functional Carbon Fibre Composites using Carbon Nanotubes as an Alternative to Polymer Sizing, Sci. Rep. 6 (2016) 37334.

[21] S. Torquato, S. Hyun, A. Donev, Multifunctional Composites: Optimizing Microstructures for Simultaneous Transport of Heat and Electricity, Phys. Rev. Lett. 89 (2002) 266601.

[22] K.K. Sairajan, G.S. Aglietti, K.M. Mani, A review of multifunctional structure technology

for aerospace applications, Acta Astronaut. 120 (2016) 30–42.

[23] P. Zinck, H.D. Wagner, L. Salmon, J.F. Gerard, Are microcomposites realistic models of the fibre/matrix interface? II. Physico-chemical approach, Polymer (Guildf). 42 (2001) 6641–6650.

[24] E. Bekyarova, E.T. Thostenson, A. Yu, H. Kim, J. Gao, J. Tang, H.T. Hahn, T.W. Chou, M.E. Itkis, R.C. Haddon, Multiscale carbon nanotube-carbon fiber reinforcement for advanced epoxy composites, Langmuir. 23 (2007) 3970–3974.

[25] S.B. Lee, O. Choi, W. Lee, J.W. Yi, B.S. Kim, J.H. Byun, M.K. Yoon, H. Fong, E.T. Thostenson, T.W. Chou, Processing and characterization of multi-scale hybrid composites reinforced with nanoscale carbon reinforcements and carbon fibers, Compos. Part A Appl. Sci. Manuf. 42 (2011) 337–344.

[26] V. Shukla, Review of electromagnetic interference shielding materials fabricated by iron ingredients, Nanoscale Adv. 1 (2019) 1640–1671.

[27] S.A. Grammatikos, E.Z. Kordatos, T.E. Matikas, A.S. Paipetis, Real-time debonding monitoring of composite repaired materials via electrical, acoustic, and thermographic methods, J. Mater. Eng. Perform. 23 (2014) 169–180.

[28] I. Gaztelumendi, M. Chapartegui, R. Seddon, S. Flórez, F. Pons, J. Cinquin, Enhancement of electrical conductivity of composite structures by integration of carbon nanotubes via bulk resin and/or buckypaper films, Compos. Part B Eng. 122 (2017) 31–40.

[29] Y.J. Kwon, Y. Kim, H. Jeon, S. Cho, W. Lee, J.U. Lee, Graphene/carbon nanotube hybrid as a multi-functional interfacial reinforcement for carbon fiber-reinforced composites, Compos. Part B Eng. 122 (2017) 23–30.

[30] V. Kostopoulos, A. Vavouliotis, P. Karapappas, P. Tsotra, A. Paipetis, Damage monitoring of carbon fiber reinforced laminates using resistance measurements. Improving sensitivity using carbon nanotube doped epoxy matrix system, J. Intell. Mater. Syst. Struct. 20 (2009) 1025–1034.

[31] S. Han, D.D.L. Chung, Increasing the through-thickness thermal conductivity of carbon fiber polymer-matrix composite by curing pressure increase and filler incorporation, Compos. Sci. Technol. 71 (2011) 1944–1952.

[32] S. Mondal, S. Ghosh, S. Ganguly, P. Das, R. Ravindren, S. Sit, G. Chakraborty, N.C. Das, Highly conductive and flexible nano-structured carbon-based polymer nanocomposites

with improved electromagnetic-interference-shielding performance, Mater. Res. Express. 4 (2017) 105039.

[33] S. Liu, V.S. Chevali, Z. Xu, D. Hui, H. Wang, A review of extending performance of epoxy resins using carbon nanomaterials, Compos. Part B Eng. 136 (2018) 197–214.

[34] S.A. Mirmohammadi, S. Sadjadi, N. Bahri-Laleh, Electrical and electromagnetic properties of CNT/polymer composites, in: Carbon Nanotub. Polym., Elsevier, 2018: pp. 233–258.

[35] H. Zhang, M. Kuwata, E. Bilotti, T. Peijs, Integrated damage sensing in fibre-reinforced composites with extremely low carbon nanotube loadings, J. Nanomater. 16 (2015) 243–423.

[36] D. He, B. Fan, H. Zhao, X. Lu, M. Yang, Y. Liu, J. Bai, Design of electrically conductive structural composites by modulating aligned CVD-grown carbon nanotube length on glass fibers, ACS Appl. Mater. Interfaces. 9 (2017) 2948–2958.

[37] H. Zhang, Y. Liu, M. Kuwata, E. Bilotti, T. Peijs, Improved fracture toughness and integrated damage sensing capability by spray coated CNTs on carbon fibre prepreg, Compos. Part A Appl. Sci. Manuf. 70 (2015) 102–110.

[38] S.A. Grammatikos, A.S. Paipetis, On the electrical properties of multi scale reinforced composites for damage accumulation monitoring, Compos. Part B Eng. 43 (2012) 2687–2696.

[39] B. Wang, X. Zhou, J. Yin, L. Wang, Investigation on some matrix-dominated properties of hybrid multiscale composites based on carbon fiber/carbon nanotube modified epoxy, J. Appl. Polym. Sci. 128 (2013) 990–996.

[40] M. Yoonessi, M. Lebroín-Coloín, D. Scheiman, M.A. Meador, Carbon nanotube epoxy nanocomposites: The effects of interfacial modifications on the dynamic mechanical properties of the nanocomposites, ACS Appl. Mater. Interfaces. 6 (2014) 16621–16630.

[41] H.W. Zhou, L. Mishnaevsky, H.Y. Yi, Y.Q. Liu, X. Hu, A. Warrier, G.M. Dai, Carbon fiber/carbon nanotube reinforced hierarchical composites: Effect of CNT distribution on shearing strength, Compos. Part B Eng. 88 (2016) 201–211.

[42] B. Wang, Y. Liu, Y. Gao, Comparison of two different carbon nanotubes-based hybrid multiscale composites with respect to mechanical and electrical properties, Plast. Rubber Compos. 46 (2017) 231–237.

[43] G. Lee, K.D. Ko, Y.C. Yu, J. Lee, W.R. Yu, J.H. Youk, A facile method for preparing CNT-grafted carbon fibers and improved tensile strength of their composites, Compos. Part A Appl. Sci. Manuf. 69 (2015) 132–138.

[44] T. Oldham, K. Simon, D.R. Ferriell, M.A. Belcher, A. Rubin, E. Thimsen, Highly Uniform Activation of Carbon Fiber Reinforced Thermoplastics by Low-Temperature Plasma, ACS Appl. Polym. Mater. 1 (2019) 2638–2648.

[45] H. Li, M. Liebscher, D. Zhao, B. Yin, Y. Du, J. Yang, M. Kaliske, V. Mechtcherine, A review of carbon fiber surface modification methods for tailor-made bond behavior with cementitious matrices, Prog. Mater. Sci. 132 (2023) 101040.

[46] W. Hu, L. Yang, F. Wang, J. Zhi, H. He, C. Hu, F. Wei, S. Liu, Y. Li, Y. Cang, B. Yang, Insight into the enhanced interfacial adhesion of carbon fiber reinforced composites: A facile ferric ion and tannic acid self-assembly strategy, Compos. Part A Appl. Sci. Manuf. 177 (2024) 107926.

[47] M.D. Losego, M.E. Grady, N.R. Sottos, D.G. Cahill, P. V Braun, Effects of chemical bonding on heat transport across interfaces, Nat. Mater. 11 (2012) 502–506.

[48] F. Sun, T. Zhang, M.M. Jobbins, Z. Guo, X. Zhang, Z. Zheng, D. Tang, S. Ptasinska, T. Luo, Molecular Bridge Enables Anomalous Enhancement in Thermal Transport across Hard-Soft Material Interfaces, Adv. Mater. 26 (2014) 6093–6099.

[49] F. Teklal, A. Djebbar, S. Allaoui, G. Hivet, Y. Joliff, B. Kacimi, A review of analytical models to describe pull-out behavior – Fiber/matrix adhesion, Compos. Struct. 201 (2018) 791–815.

[50] M. Hao, Z. Hu, Y. Huang, X. Qian, Z. Wen, X. Wang, L. Liu, F. Lu, Y. Zhang, Enhanced both in-plane and through-thickness thermal conductivity of carbon fiber/epoxy composites by fabricating high thermal conductive coaxial PAN/PBO carbon fibers, Compos. Part B Eng. 229 (2022) 109468.

[51] M. Li, Y. Gu, Y. Liu, Y. Li, Z. Zhang, Interfacial improvement of carbon fiber/epoxy composites using a simple process for depositing commercially functionalized carbon nanotubes on the fibers, Carbon N. Y. 52 (2013) 109–121.

[52] Q. Wu, H. Bai, R. Zhao, A. Gao, H. Deng, Z. Ye, J. Zhu, Core-shell ZrO2@GO hybrid for effective interfacial adhesion improvement of carbon fiber/epoxy composites, Surfaces and Interfaces. 40 (2023) 103070.

[53] P. Lv, Y.Y. Feng, P. Zhang, H.M. Chen, N. Zhao, W. Feng, Increasing the interfacial strength in carbon fiber/epoxy composites by controlling the orientation and length of carbon nanotubes grown on the fibers, Carbon N. Y. 49 (2011) 4665–4673.

[54] H.S. Bedi, M. Tiwari, P.K. Agnihotri, Quantitative determination of size and properties of interphases in carbon nanotube-based multiscale composites, Carbon N. Y. 132 (2018) 181–190.

[55] H.S. Bedi, B.K. Billing, P.K. Agnihotri, Interphase engineering in carbon fiber/epoxy composites: Rate sensitivity of interfacial shear strength and interfacial fracture toughness, Polym. Compos. 41 (2020) 2803–2815.

[56] A. Bismarck, C. Wuertz, J. Springer, Basic surface oxides on carbon fibers, Carbon N. Y. 37 (1999) 1019–1027.

[57] T. Ramanathan, A. Bismarck, E. Schulz, K. Subramanian, The use of a single-fibre pull-out test to investigate the influence of acidic and basic surface groups on carbon fibres on the adhesion to poly(phenylene sulfide) and matrix-morphology-dependent fracture behaviour, Compos. Sci. Technol. 61 (2001) 1703–1710.

[58] J. Sun, F. Zhao, Y. Yao, Z. Jin, X. Liu, Y. Huang, High efficient and continuous surface modification of carbon fibers with improved tensile strength and interfacial adhesion, Appl. Surf. Sci. 412 (2017) 424–435.

[59] D.J. Eyckens, K. Jarvis, A.J. Barlow, Y. Yin, L.C. Soulsby, Y.A. Wickramasingha, F. Stojcevski, G. Andersson, P.S. Francis, C. Henderson, Improving the effects of plasma polymerization on carbon fiber using a surface modification pretreatment, Compos. Part A Appl. Sci. Manuf. 143 (2021) 106319.

[60] Z. Xu, Y. Huang, C. Zhang, L. Liu, Y. Zhang, L. Wang, Effect of γ-ray irradiation grafting on the carbon fibers and interfacial adhesion of epoxy composites, Compos. Sci. Technol. 67 (2007) 3261–3270.

[61] S. Wettmarshausen, J.F. Friedrich, A. Meyer-Plath, G. Kalinka, G. Hidde, S. Weidner, Coating of carbon fibers with adhesion-promoting thin poly(acrylic acid) and poly(hydroxyethylmethacrylate) layers using electrospray ionization, J. Adhes. Sci. Technol. 29 (2015) 1628–1650.

[62] A. Godara, L. Gorbatikh, G. Kalinka, A. Warrier, O. Rochez, L. Mezzo, F. Luizi, A.W. van Vuure, S. V. Lomov, I. Verpoest, Interfacial shear strength of a glass fiber/epoxy bonding in composites modified with carbon nanotubes, Compos. Sci. Technol. 70 (2010)

1346–1352.

[63] Y. Tian, H. Zhang, Z. Zhang, Influence of nanoparticles on the interfacial properties of fiber-reinforced-epoxy composites, Compos. Part A Appl. Sci. Manuf. 98 (2017) 1–8.

[64] H. Pu, Y.L. Hou, J.Z. Chen, D.L. Zhao, Graphene with different groups on the interfacial properties of carbon fiber/epoxy composites, Polymer (Guildf). 290 (2024) 126512.

[65] W. Liu, S. Zhang, B. Li, F. Yang, W. Jiao, L. Hao, R. Wang, Improvement in interfacial shear strength and fracture toughness for carbon fiber reinforced epoxy composite by fiber sizing, Polym. Compos. 35 (2014) 482–488.

[66] L. Servinis, K.M. Beggs, C. Scheffler, E. Wolfel, J.D. Randall, T.R. Gengenbach, B. Demir, T.R. Walsh, E.H. Doeven, P.S. Francis, L.C. Henderson, Electrochemical surface modification of carbon fibres by grafting of amine, carboxylic and lipophilic amide groups, Carbon N. Y. 118 (2017) 393–403.

[67] B. Demir, K.M. Beggs, B.L. Fox, L. Servinis, L.C. Henderson, T.R. Walsh, A predictive model of interfacial interactions between functionalised carbon fibre surfaces cross-linked with epoxy resin, Compos. Sci. Technol. 159 (2018) 127–134.

[68] X. Zhang, G. Wu, Grafting halloysite nanotubes with amino or carboxyl groups onto carbon fiber surface for excellent interfacial properties of silicone resin composites, Polymers (Basel). 10 (2018) 1171.

[69] J. Chen, H. Xu, C. Liu, L. Mi, C. Shen, The effect of double grafted interface layer on the properties of carbon fiber reinforced polyamide 66 composites, Compos. Sci. Technol. 168 (2018) 20–27.

[70] D.J. Eyckens, C.L. Arnold, J.D. Randall, F. Stojcevski, A. Hendlmeier, M.K. Stanfield, J. Pinson, T.R. Gengenbach, R. Alexander, L.C. Soulsby, P.S. Francis, L.C. Henderson, Fiber with Butterfly Wings: Creating Colored Carbon Fibers with Increased Strength, Adhesion, and Reversible Malleability, ACS Appl. Mater. Interfaces. 11 (2019) 41617–41625.

[71] H. Wang, K. Jin, J. Tao, Improving the interfacial shear strength of carbon fibre and epoxy via mechanical interlocking effect, Compos. Sci. Technol. 200 (2020) 108423.

[72] T. Kim, J. Shin, K. Lee, Y. Jung, S.B. Lee, S.J. Yang, A universal surface modification method of carbon nanotube fibers with enhanced tensile strength, Compos. Part A Appl. Sci. Manuf. 140 (2021) 106182.

[73] J. Chen, Y. Zhao, M. Sun, Z. Liu, H. Liu, S. Xiong, S. Li, J. Song, K. Wang, Functionalized carbon fibers with MXene via electrochemistry aryl diazonium salt reaction to improve the interfacial properties of carbon fiber/epoxy composites, J. Mater. Res. Technol. 19 (2022) 3699–3712.

[74] S. Hu, P. Han, C. Meng, Y. Yu, S. Han, H. Wang, G. Wei, Z. Gu, Comparative study of different bonding interactions on the interfacial adhesion and mechanical properties of MXene-decorated carbon fiber/epoxy resin composites, Compos. Sci. Technol. 245 (2024) 110352.

[75] S. Mondal, P. Das, S. Ganguly, R. Ravindren, S. Remanan, P. Bhawal, T.K. Das, N.C. Das, Thermal-air ageing treatment on mechanical, electrical, and electromagnetic interference shielding properties of lightweight carbon nanotube based polymer nanocomposites, Compos. Part A Appl. Sci. Manuf. 107 (2018) 447–460.

[76] H. Abbasi, M. Antunes, J.I. Velasco, Recent advances in carbon-based polymer nanocomposites for electromagnetic interference shielding, Prog. Mater. Sci. 103 (2019) 319–373.

[77] K. Sushmita, G. Madras, S. Bose, Polymer nanocomposites containing semiconductors as advanced materials for EMI shielding, ACS Omega. 5 (2020) 4705–4718.

[78] W. Lee, J.U. Lee, H.J. Cha, J.H. Byun, Partially reduced graphene oxide as a multi-functional sizing agent for carbon fiber composites by electrophoretic deposition, RSC Adv. 3 (2013) 25609–25613.

[79] A. Caradonna, C. Badini, E. Padovano, M. Pietroluongo, Electrical and thermal conductivity of epoxy-carbon filler composites processed by calendaring, Materials (Basel). 12 (2019) 1522.

[80] Y. Gao, M. Zhang, X. Chen, Y. Zhu, H. Wang, S. Yuan, F. Xu, Y. Cui, D. Bao, X. Shen, Y. Sun, J. Peng, Y. Zhou, M. Zhang, A high-performance thermal conductive and outstanding electrical insulating composite based on robust neuron-like microstructure, Chem. Eng. J. 426 (2021) 131280.

[81] X. Zhang, H. Zhang, D. Li, H. Xu, Y. Huang, Y. Liu, D. Wu, J. Sun, Highly thermally conductive and electrically insulating polydimethylsiloxane composites prepared by ultrasonic-assisted forced infiltration for thermal management applications, Compos. Part B Eng. 224 (2021) 109207.

[82] A. Karakassides, A. Ganguly, C.E. Salmas, P.K. Sharma, P. Papakonstantinou, Improving

the Through-Thickness Thermal Conductivity of Carbon Fiber/Epoxy Laminates by Direct Growth of SiC/Graphene Heterostructures on Carbon Fibers, ACS Omega. 8 (2023) 24406–24417.

[83] K. Dong, K. Liu, Q. Zhang, B. Gu, B. Sun, Experimental and numerical analyses on the thermal conductive behaviors of carbon fiber/epoxy plain woven composites, Int. J. Heat Mass Transf. 102 (2016) 501–517.

[84] V. Varshney, A.K. Roy, T.J. Michalak, J. Lee, B.L. Farmer, Effect of Curing and Functionalization on the Interface Thermal Conductance in Carbon Nanotube – Epoxy Composites, J. Miner. Met. Mater. Soc. 65 (2013) 140–146.

[85] K.S. Khare, F. Khabaz, R. Khare, Effect of Carbon Nanotube Functionalization on Mechanical and Thermal Properties of Cross-Linked Epoxy − Carbon Nanotube Nanocomposites : Role of Strengthening the Interfacial Interactions, Appl. Mater. Interfaces. 6 (2014) 6098–6110.

[86] Y. Wang, H.F. Zhan, Y. Xiang, C. Yang, C.M. Wang, Y.Y. Zhang, Effect of Covalent Functionalization on Thermal Transport across Graphene-Polymer Interfaces, J. Phys. Chem. C. 119 (2015) 12731–12738.

[87] X. Shen, Z. Wang, Y. Wu, X. Liu, J.K. Kim, Effect of functionalization on thermal conductivities of graphene/epoxy composites, Carbon N. Y. 108 (2016) 412–422.

[88] Y. Wang, C. Yang, Q.X. Pei, Y. Zhang, Some Aspects of Thermal Transport across the Interface between Graphene and Epoxy in Nanocomposites, ACS Appl. Mater. Interfaces. 8 (2016) 8272–8279.

[89] V. Varshney, A.K. Roy, J.W. Baur, Modeling the Role of Bulk and Surface Characteristics of Carbon Fiber on Thermal Conductance across the Carbon-Fiber/Matrix Interface, ACS Appl. Mater. Interfaces. 7 (2015) 26674–26683.

[90] M. Zu, Q. Li, Y. Zhu, M. Dey, G. Wang, W. Lu, J.M. Deitzel, J.W. Gillespie, J.H. Byun, T.W. Chou, The effective interfacial shear strength of carbon nanotube fibers in an epoxy matrix characterized by a microdroplet test, Carbon N. Y. 50 (2012) 1271–1279.

[91] C. Zhi, H. Long, M. Miao, Influence of microbond test parameters on interfacial shear strength of fiber reinforced polymer-matrix composites, Compos. Part A Appl. Sci. Manuf. 100 (2017) 55–63.

[92] L. Servinis, L.C. Henderson, L.M. Andrighetto, M.G. Huson, T.R. Gengenbach, B.L. Fox,

A novel approach to functionalise pristine unsized carbon fibre using in situ generated diazonium species to enhance interfacial shear strength, J. Mater. Chem. A. 3 (2015) 3360–3371.

[93] K.M. Beggs, M.D. Perus, L. Servinis, L.A. O'Dell, B.L. Fox, T.R. Gengenbach, L.C. Henderson, Rapid surface functionalization of carbon fibres using microwave irradiation in an ionic liquid, RSC Adv. 6 (2016) 32480–32483.

[94] L.S. Melro, R. Pyrz, L.R. Jensen, A molecular dynamics study on the interaction between epoxy and functionalized graphene sheets, IOP Conf. Ser. Mater. Sci. Eng. 139 (2016) 012036.

[95] B. Demir, L.C. Henderson, T.R. Walsh, Design Rules for Enhanced Interfacial Shear Response in Functionalized Carbon Fiber Epoxy Composites, ACS Appl. Mater. Interfaces. 9 (2017) 11846–11857.

[96] C. Park, G.J. Yun, Characterization of interfacial properties of graphene-reinforced polymer nanocomposites by molecular dynamics-shear deformation model, J. Appl. Mech. 85 (2018) 091007.

[97] H. Wang, K. Jin, C. Wang, X. Guo, Z. Chen, J. Tao, Effect of fiber surface functionalization on shear behavior at carbon fiber/epoxy interface through molecular dynamics analysis, Compos. Part A Appl. Sci. Manuf. 126 (2019) 105611.

[98] J. Fan, J. Yang, L. Wang, H. Li, J. Tian, J. Ye, Y. Zhao, Enhanced mechanical properties of epoxy nanocomposites with mildly surface-functionalized graphene oxide by tuned amine species, Appl. Surf. Sci. 558 (2021) 149964.

[99] R. Gulotty, M. Castellino, P. Jagdale, A. Tagliaferro, A.A. Balandin, Effects of functionalization on thermal properties of single-wall and multi-wall carbon nanotube-polymer nanocomposites, ACS Nano. 7 (2013) 5114–5121.

[100] J. Chen, J. Han, D. Xu, Thermal and electrical properties of the epoxy nanocomposites reinforced with purified carbon nanotubes, Mater. Lett. 246 (2019) 20–23.

[101] M. Tiwari, B.K. Billing, H.S. Bedi, P.K. Agnihotri, Quantification of carbon nanotube dispersion and its correlation with mechanical and thermal properties of epoxy nanocomposites, J. Appl. Polym. Sci. 137 (2020) 1–11.

[102] Z. He, X. Zhang, M. Chen, M. Li, Y. Gu, Z. Zhang, Q. Li, Effect of the filler structure of carbon nanomaterials on the electrical, thermal, and rheological properties of epoxy

composites, J. Appl. Polym. Sci. 129 (2013) 3366–3372.

[103] L. Ren, Q. Li, J. Lu, X. Zeng, R. Sun, J. Wu, J. Bin Xu, C.P. Wong, Enhanced thermal conductivity for Ag-deposited alumina sphere/epoxy resin composites through manipulating interfacial thermal resistance, Compos. Part A Appl. Sci. Manuf. 107 (2018) 561–569.

[104] N.S. Majeed, S.M. Salih, B.A. Abdulmajeed, Effect of nanoparticles on thermal conductivity of epoxy resin system, IOP Conf. Ser. Mater. Sci. Eng. 518 (2019) 062006.

[105] H. Wang, L. Li, Y. Chen, M. Li, H. Fu, X. Hou, X. Wu, C. Te Lin, N. Jiang, J. Yu, Efficient Thermal Transport Highway Construction within Epoxy Matrix via Hybrid Carbon Fibers and Alumina Particles, ACS Omega. 5 (2020) 1170–1177.

[106] M. Sharma, S. Gao, E. Mäder, H. Sharma, L.Y. Wei, J. Bijwe, Carbon fiber surfaces and composite interphases, Compos. Sci. Technol. 102 (2014) 35–50.

[107] C. Wang, X. Ji, A. Roy, V. V. Silberschmidt, Z. Chen, Shear strength and fracture toughness of carbon fibre/epoxy interface: effect of surface treatment, Mater. Des. 85 (2015) 800–807.

[108] S. Chen, J. Feng, Epoxy laminated composites reinforced with polyethyleneimine functionalized carbon fiber fabric: Mechanical and thermal properties, Compos. Sci. Technol. 101 (2014) 145–151.

[109] K. Sharma, K. Sen Kaushalyayan, M. Shukla, Pull-out simulations of interfacial properties of amine functionalized multi-walled carbon nanotube epoxy composites, Comput. Mater. Sci. 99 (2015) 232–241.

[110] H. Chen, V. V. Ginzburg, J. Yang, Y. Yang, W. Liu, Y. Huang, L. Du, B. Chen, Thermal conductivity of polymer-based composites: Fundamentals and applications, Prog. Polym. Sci. 59 (2016) 41–85.

[111] BIOVIA, Dassault Systemes, [Materials Studio] [2018], San Diego: Dassault systemes, (2018).

[112] A.P. Thompson, H.M. Aktulga, R. Berger, D.S. Bolintineanu, W.M. Brown, P.S. Crozier, P.J. in 't Veld, A. Kohlmeyer, S.G. Moore, T.D. Nguyen, R. Shan, M.J. Stevens, J. Tranchida, C. Trott, S.J. Plimpton, LAMMPS - a flexible simulation tool for particle-based materials modeling at the atomic, meso, and continuum scales, Comput. Phys. Commun. 271 (2022) 108171.

[113] B. Demir, T.R. Walsh, A robust and reproducible procedure for cross-linking thermoset polymers using molecular simulation, Soft Matter. 12 (2016) 2453–2464.

[114] H. Sun, S.J. Mumby, J.R. Maple, A.T. Hagler, An ab Initio CFF93 All-Atom Force Field for Polycarbonates, J. Am. Chem. Soc. 116 (1994) 2978–2987.

[115] S. Nosé, A unified formulation of the constant temperature molecular dynamics methods, J. Chem. Phys. 81 (1984) 511–519.

[116] W.G. Hoover, Canonical dynamics: Equilibrium phase-space distributions, Phys. Rev. A. 31 (1985) 1695.

[117] H.J.C. Berendsen, J.P.M. Postma, W.F. Van Gunsteren, A. Dinola, J.R. Haak, Molecular dynamics with coupling to an external bath, J. Chem. Phys. 81 (1984) 3684–3690.

[118] T. Luo, J.R. Lloyd, Enhancement of thermal energy transport across graphene/graphite and polymer interfaces: A molecular dynamics study, Adv. Funct. Mater. 22 (2012) 2495–2502.

[119] W. Jiao, W. Liu, F. Yang, L. Jiang, W. Jiao, R. Wang, Improving the interfacial strength of carbon fiber/vinyl ester resin composite by self-migration of acrylamide: A molecular dynamics simulation, Appl. Surf. Sci. 454 (2018) 74–81.

[120] A. Vashisth, C. Ashraf, C.E. Bakis, A.C.T. van Duin, Effect of chemical structure on thermo-mechanical properties of epoxy polymers: Comparison of accelerated ReaxFF simulations and experiments, Polymer (Guildf). 158 (2018) 354–363.

[121] J. He, H. Wang, Z. Su, Y. Guo, X. Tian, Q. Qu, Y.L. Lin, Thermal conductivity and electrical insulation of epoxy composites with graphene-SiC nanowires and BaTiO3, Compos. Part A Appl. Sci. Manuf. 117 (2019) 287–298.

[122] M. Martins, R. Gomes, L. Pina, C. Pereira, O. Reichmann, D. Teti, N. Correia, N. Rocha, Highly conductive carbon fiber-reinforced polymer composite electronic box: Out-of-autoclave manufacturing for space applications, Fibers. 6 (2018) 1–23.

[123] A. Kumar, V. Sundararaghavan, A.R. Browning, Study of temperature dependence of thermal conductivity in cross-linked epoxies using molecular dynamics simulations with long range interactions, Model. Simul. Mater. Sci. Eng. 22 (2014) 025013.

[124] V. Varshney, S.S. Patnaik, A.K. Roy, B.L. Farmer, Heat transport in epoxy networks: A molecular dynamics study, Polymer (Guildf). 50 (2009) 3378–3385.

[125] V. Varshney, S.S. Patnaik, A.K. Roy, B.L. Farmer, A molecular dynamics study of epoxy-

based networks: Cross-linking procedure and prediction of molecular and material properties, Macromolecules. 41 (2008) 6837–6842.

[126] A. Vashisth, C. Ashraf, W. Zhang, C.E. Bakis, A.C.T. Van Duin, Accelerated ReaxFF Simulations for Describing the Reactive Cross-Linking of Polymers, J. Phys. Chem. A. 122 (2018) 6633–6642.

[127] W.D. Bascom, L.T. Drzal, The Surface Properties of Carbon Fibers and Their Adhesion to Organic Polymers., 1987.

[128] Z.N. Azwa, B.F. Yousif, A.C. Manalo, W. Karunasena, A review on the degradability of polymeric composites based on natural fibres, Mater. Des. 47 (2013) 424–442.

[129] W. Nsengiyumva, S. Zhong, J. Lin, Q. Zhang, J. Zhong, Y. Huang, Advances, limitations and prospects of nondestructive testing and evaluation of thick composites and sandwich structures: A state-of-the-art review, Compos. Struct. 256 (2021) 112951.

[130] C.-B. Qu, H.-M. Xiao, G.-W. Huang, N. Li, M. Li, F. Li, Y.-Q. Li, Y. Liu, S.-Y. Fu, Effects of cryo-thermal cycling on interlaminar shear strength and thermal expansion coefficient of carbon fiber/graphene oxide-modified epoxy composites, Compos. Commun. 32 (2022) 101180.

[131] E.T. Thostenson, T.W. Chou, Carbon nanotube networks: sensing of distributed strain and damage for life prediction and self healing, Adv. Mater. 18 (2006) 2837–2841.

[132] L. Gao, E.T. Thostenson, Z. Zhang, T.W. Chou, Coupled carbon nanotube network and acoustic emission monitoring for sensing of damage development in composites, Carbon N. Y. 47 (2009) 1381–1388.

[133] H. Zhang, E. Bilotti, T. Peijs, The use of carbon nanotubes for damage sensing and structural health monitoring in laminated composites: a review, Nanocomposites. 1 (2015) 167–184.

[134] S. Mujin, H. Baorong, W. Yisheng, T. Ying, H. Weiqiu, D. Youxian, The surface of carbon fibres continuously treated by cold plasma, Compos. Sci. Technol. 34 (1989) 353–364.

[135] M.A. Montes-Morán, R.J. Young, Raman spectroscopy study of high-modulus carbon fibres: effect of plasma-treatment on the interfacial properties of single-fibre-epoxy composites: Part II - Characterisation of the fibre-matrix interface, Carbon N. Y. 40 (2002) 857–875.

[136] K.Y. Rhee, S.J. Park, D. Hui, Y. Qiu, Effect of oxygen plasma-treated carbon fibers on

the tribological behavior of oil-absorbed carbon/epoxy woven composites, Compos. Part B Eng. 43 (2012) 2395–2399.

[137] Y. Liang, X. Li, D. Semitekolos, C.A. Charitidis, H. Dong, Enhanced properties of PAN-derived carbon fibres and resulting composites by active screen plasma surface functionalisation, Plasma Process. Polym. 17 (2020) 1900252.

[138] Z. Sha, Z. Han, S. Wu, F. Zhang, M.S. Islam, S.A. Brown, C. Wang, Low-temperature plasma assisted growth of vertical graphene for enhancing carbon fibre/epoxy interfacial strength, Compos. Sci. Technol. 184 (2019) 107867.

[139] R.D. Dsouza, D. Di Vito, J. Jokinen, M. Kanerva, Mutual dependence of experimental and data analysis features in characterization of fiber-matrix interface via microdroplets, Polym. Compos. (2023) 1–20.

[140] A. Chauhan, P.K. Agnihotri, S. Basu, Molecular dynamic study on modulating the interfacial thermal conductivity of carbon fiber/epoxy interfaces, Comput. Mater. Sci. 217 (2023) 111914.

[141] M. Li, H. Zhou, Y. Zhang, Y. Liao, H. Zhou, The effect of defects on the interfacial mechanical properties of graphene/epoxy composites, RSC Adv. 7 (2017) 46101–46108.

[142] A.A. Sahraei, A.H. Mokarizadeh, M. Foroutan, D. George, D. Rodrigue, M. Baniassadi, Atomistic simulation of interfacial properties and damage mechanism in graphene nanoplatelet/epoxy composites, Comput. Mater. Sci. 184 (2020) 109888.

[143] S. Kesavan Pillai, S.S. Ray, Epoxy-based carbon nanotubes reinforced composites, in: Adv. Nanocomposites Synth. Charact. Ind. Appl., IntechOpen, 2011: pp. 727–792.

[144] G. Gkikas, N.M. Barkoula, A.S. Paipetis, Effect of dispersion conditions on the thermo-mechanical and toughness properties of multi walled carbon nanotubes-reinforced epoxy, Compos. Part B Eng. 43 (2012) 2697–2705.

[145] S.A. Hawkins, H. Yao, H. Wang, H.J. Sue, Tensile properties and electrical conductivity of epoxy composite thin films containing zinc oxide quantum dots and multi-walled carbon nanotubes, Carbon N. Y. 115 (2017) 18–27.

[146] P.K. Ghosh, K. Kumar, N. Chaudhary, Influence of ultrasonic dual mixing on thermal and tensile properties of MWCNTs-epoxy composite, Compos. Part B Eng. 77 (2015) 139–144.

[147] S. Roy, R.S. Petrova, S. Mitra, Effect of carbon nanotube (CNT) functionalization in

epoxy-CNT composites, Nanotechnol. Rev. 7 (2018) 475–485.

[148] J. Sandler, M. Shaffer, T. Prasse, W. Bauhofer, K. Schulte, A. Windle, Development of a dispersion process for carbon nanotubes in an epoxy matrix and the resulting electrical properties, Polymer (Guildf). 40 (1999) 5967–5971.

[149] F.H. Gojny, M.H.G. Wichmann, B. Fiedler, K. Schulte, Influence of different carbon nanotubes on the mechanical properties of epoxy matrix composites - A comparative study, Compos. Sci. Technol. 65 (2005) 2300–2313.

[150] J. Cha, G.H. Jun, J.K. Park, J.C. Kim, H.J. Ryu, S.H. Hong, Improvement of modulus, strength and fracture toughness of CNT/Epoxy nanocomposites through the functionalization of carbon nanotubes, Compos. Part B Eng. 129 (2017) 169–179.

[151] R. Vijayan, A. Ghazinezami, S.R. Taklimi, M.Y. Khan, D. Askari, The geometrical advantages of helical carbon nanotubes for high-performance multifunctional polymeric nanocomposites, Compos. Part B Eng. 156 (2019) 28–42.

[152] L.S. Schadler, S.C. Giannaris, P.M. Ajayan, Load transfer in carbon nanotube epoxy composites, Appl. Phys. Lett. 73 (1998) 3842–3844.

[153] P.M. Ajayan, L.S. Schadler, C. Giannaris, A. Rubio, Single-walled carbon nanotube--polymer composites: strength and weakness, Adv. Mater. 12 (2000) 750–753.

[154] A. Mirabedini, A. Ang, M. Nikzad, B. Fox, K.T. Lau, N. Hameed, Evolving Strategies for Producing Multiscale Graphene-Enhanced Fiber-Reinforced Polymer Composites for Smart Structural Applications, Adv. Sci. 7 (2020).

[155] A. Chauhan, H.S. Bedi, P.K. Agnihotri, Enhancing aging resistance of glass fiber/epoxy composites using carbon nanotubes, Mater. Chem. Phys. 291 (2022) 126740.

[156] Z. Fan, S.G. Advani, Rheology of multiwall carbon nanotube suspensions, J. Rheol. (N. Y. N. Y). 51 (2007) 585–604.

[157] A. Allaoui, N. Bounia, Rheological and Electrical Transitions in Carbon Nanotube/Epoxy Suspensions, Curr. Nanosci. 6 (2010) 158–162.

[158] A. Jiménez-Suárez, M. Campo, M. Sánchez, C. Romón, A. Ureña, Influence of the functionalization of carbon nanotubes on calendering dispersion effectiveness in a low viscosity resin for VARIM processes, Compos. Part B Eng. 43 (2012) 3482–3490.

[159] R. Pilawka, S. Paszkiewicz, Z. Rosłaniec, Epoxy composites with carbon nanotubes, Adv. Manuf. Sci. Technol. 36 (2012) 67–79.

[160] D.J. Kwon, Z.J. Wang, J.Y. Choi, P.S. Shin, K.L. DeVries, J.M. Park, Interfacial and mechanical properties of epoxy composites containing carbon nanotubes grafted with alkyl chains of different length, Compos. Part A Appl. Sci. Manuf. 82 (2016) 190–197.

[161] M.H. Al-Saleh, M.R. Irshidat, Effect of viscosity reducing agent on the properties of CNT/epoxy nanocomposites, J. Polym. Eng. 36 (2016) 407–412.

[162] R. Meier, C. Kirdar, N. Rudolph, S. Zaremba, K. Drechsler, Investigation of the shear thinning behavior of epoxy resins for utilization in vibration assisted liquid composite molding processes, AIP Conf. Proc. 1593 (2014) 458–462.

[163] L. Vaisman, G. Marom, H.D. Wagner, Dispersions of surface-modified carbon nanotubes in water-soluble and water-insoluble polymers, Adv. Funct. Mater. 16 (2006) 357–363.

[164] Y. Geng, M.Y. Liu, J. Li, X.M. Shi, J.K. Kim, Effects of surfactant treatment on mechanical and electrical properties of CNT/epoxy nanocomposites, Compos. Part A Appl. Sci. Manuf. 39 (2008) 1876–1883.

[165] C.F. Pitt, B.P. Barth, B.E. Godard, Electrical Properties of Epoxy Resins, IRE Trans. Compon. Parts. 4 (1957) 110–113.

[166] A. Martone, C. Formicola, M. Giordano, M. Zarrelli, Reinforcement efficiency of multi-walled carbon nanotube/epoxy nano composites, Compos. Sci. Technol. 70 (2010) 1154–1160.

[167] S. Bellucci, L. Coderoni, F. Micciulla, G. Rinaldi, I. Sacco, The electrical properties of epoxy resin composites filled with cnts and carbon black, J. Nanosci. Nanotechnol. 11 (2011) 9110–9117.

[168] F. Stan, R.T. Rosculet, C. Fetecau, Direct Current method with reversal polarity for electrical conductivity measurement of TPU/MWCNT composites, Meas. J. Int. Meas. Confed. 136 (2019) 345–355.

[169] N. Domun, H. Hadavinia, T. Zhang, T. Sainsbury, G.H. Liaghat, S. Vahid, Improving the fracture toughness and the strength of epoxy using nanomaterials-a review of the current status, Nanoscale. 7 (2015) 10294–10329.

[170] O. Lourie, H.D. Wagner, Evidence of stress transfer and formation of fracture clusters in carbon nanotube-based composites, Compos. Sci. Technol. 59 (1999) 975–977.

[171] O. Lourie, H.D. Wagner, Y. Zhang, S. Iijima, Dependence of elastic properties on morphology in single-wall carbon nanotubes, Adv. Mater. 11 (1999) 931–934.

[172] A. De la Vega, I.A. Kinloch, R.J. Young, W. Bauhofer, K. Schulte, Simultaneous global and local strain sensing in SWCNT-epoxy composites by Raman and impedance spectroscopy, Compos. Sci. Technol. 71 (2011) 160–166.

[173] P.C. Ma, Q. Bin Zheng, E. Mäder, J.K. Kim, Behavior of load transfer in functionalized carbon nanotube/epoxy nanocomposites, Polymer (Guildf). 53 (2012) 6081–6088.

[174] F.H. Gojny, M.H.G. Wichmann, U. Köpke, B. Fiedler, K. Schulte, Carbon nanotube-reinforced epoxy-composites: Enhanced stiffness and fracture toughness at low nanotube content, Compos. Sci. Technol. 64 (2004) 2363–2371.

[175] R.F. Minty, L. Yang, J.L. Thomason, The influence of hardener-to-epoxy ratio on the interfacial strength in glass fibre reinforced epoxy composites, Compos. Part A Appl. Sci. Manuf. 112 (2018) 64–70.